1-1-2017

Change In Processing Speed And Its Associations With Cerebral White Matter Microstructure

Muzamil Arshad
Wayne State University,

CHANGE IN PROCESSING SPEED AND ITS ASSOCIATIONS WITH CEREBRAL WHITE MATTER MICROSTRUCTURE

by

MUZAMIL ARSHAD

DISSERTATION

Submitted to the Graduate School

of Wayne State University,

Detroit, Michigan

in partial fulfillment of the requirements

for the degree of

DOCTOR OF PHILOSOPHY

2017

MAJOR: TRANSLATIONAL NEUROSCIENCE

Approved By:

_____

Advisor Date

_____

Advisor Date

_____

_____

_____

DEDICATION

This work is dedicated to my loving family for all their help and support. My mom Naheed and my dad Arshad who have made great sacrifices to allow me to pursue my dreams. Words cannot describe how grateful I am to have such loving and supportive parents. This journey is as much yours as it is mine. To my uncle Shamim who has been like a grandfather and with whom I have interesting discussions on life, science, and politics. To my siblings Mohsin, Moiz, and Mariam who have provided their love and support. I am proud of you three. Finally, to my nephew, Ismaeel who always puts a smile on my face and my new niece Nusaybha Zainab (as you wished Mariam I included her middle name!) who has reminded me that there is more to life than just work and in doing so has helped me to the end of this journey.

ACKNOWLEDGMENTS

I would like to acknowledge the many individuals who have helped me through this project and without whom I would not be here. First to my advisors, Dr. Jeffrey Stanley and Dr. Naftali Raz, for your guidance and unwavering support which has provided me with confidence needed to overcome the many obstacles and challenges. To the members of my committee: Dr. Gow, Dr. Kuhn, and Dr. Baltes, for your generous support and guidance. I would like to thank Cheryl without who we would not have any participants. To Caroline for all the things she has done, including constantly reminding me and for our morning discussions. To Dalal who made it possible for me to test the MR sequences used in this project and for all her words of support. Indeed, Dalal you have been like an older sister for me. To the MRI techs Pavan, Zahid, and Yang, who not only scanned our participants but provided interesting conversations. I am also thankful for my fellow TNP, MD/PhD students and lab members, past and present, for all your guidance, wisdom, new ideas and support. It's truly been an honor and privilege to have worked with such caring individuals.

Finally, this journey would not have been possible without the support of my loving family, especially my parents, who have encouraged me and make me want to better myself. *This is for you*.

TABLE OF CONTENTS

LIST OF TABLES

LIST OF FIGURES

CHAPTER 1: MOTIVATIONS FOR INVESTIGATING NEURAL CORRELATES OF INFORMATION PROCESSING SPEED

1.1 Introduction

Aging, even in its benign form, is associated with a decline in cognitive function and, along with the associated loss of independence, it is one of the most feared aspects of aging (Daffner, 2010; Deary, et al., 2009; Williams & Kemper, 2010). Indeed, cognitive impairment is a predictor of disability in Activities of Daily Living (ADL) and Instrumental Activities of Daily Living (IADL) tasks (Dodge et al., 2005). Long-term care for individuals who need assistance with IADLs or ADLs was estimated at $120 billion in 2000 by the Congressional Budget Office (Knickman & Snell, 2002) and is expected to rise as the number of individuals over 65 continues to increase. The significant financial costs and personal burden of cognitive impairment makes research on early identification and possible prevention of age related cognitive decline a rising public health challenge (Sing-Manoux & Kivimaki, 2010).

Multiple cognitive domains show age related decline, which, in part may, be explained by age differences in a more fundamental aspect of cognition: information processing speed. Salthouse (Salthouse, 1996) has described six variables which can be used to assess processing speed, with reaction time (RT) being the most commonly used measure. Reaction time is defined as the interval between the stimulus presentation and the initiation of a response (Pachella, 1974).

Reduced processing speed is considered one of the most reliable markers of psychological aging (Birren & Fisher, 1995), with an estimated effect size for age differences in various measures of processing speed, estimated at $r = -.52$ (Verhaeghen & Salthouse, 1997). The processing speed hypothesis (Salthouse, 1996) posits that effects of age on various cognitive functions is mediated, in part, through slowing of information processing. Consistent with this hypothesis, cross-sectional studies have found that after adjusting for measures of perceptual speed, associations between age

and measures of intelligence (Hertzog, 1989) and memory are reduced (Salthouse, 1992, 1993). Although longitudinal investigations of processing speed and cognitive functions have produced mixed results (Robitaille, et al., 2013), some studies have found, nonetheless, within-person change in processing speed is associated with changes in other cognitive domains (Finkel et al., 2005; Robitaille et al., 2013; Zimprich & Martin, 2002). Finally, in a study of 2,039 community dwelling older adults, training on tasks designed to improve processing speed showed transfer to improvements in the instrumental activity of daily living and safer driving (Ball et al., 2013). Given the hypothesized central role of processing speed to cognitive aging, and the need for interventions to mitigate its effects, elucidating the neural substrates of age related slowing is a high priority.

1.2 Search for the neural substrates of processing speed

Investigations of slow RT in persons affected by a degenerative white-matter disease, multiple sclerosis (MS), have provided insights into potential mechanisms of age related slowing. Multiple sclerosis involves neuropathology that disrupts cerebral white matter. White matter contains both myelinated and unmyelinated axons that enable the reliable transmission of information across both the cerebral cortex and subcortical structures. It is plausible that myelin loss, a characteristic of multiple sclerosis (Haines, et al., 2011), would disrupt the flow of information in the central nervous system (CNS). Indeed, myelination of axons is hypothesized as a neural substrate of increased processing speed during childhood development (Chevalier et al., 2015) and age related loss of myelin is hypothesized as a substrate of age related slowing in processing speed (Lu et al., 2011).

The myelin sheath that wraps around an axon is not continuous along its length, rather there are periodic gaps where no myelin is present. These gaps, along the axon, are referred to as the nodes of Ranvier and contain voltage gated Na^+ and K^+ channels necessary to propagate an action

potential. By limiting depolarization only to the nodes of Ranvier, myelin greatly increases the conduction velocity of action potentials through saltatory conduction. In contrast, unmyelinated axons have ion channels distributed along the length of the axon and must propagate the action potential along its length. Before discussing the structural variables, which influence conduction velocity, a brief discussion of the role of Na^+ and K^+ channels is warranted.

While action potentials, and saltatory conduction, are largely a voltage gated Na^+ channel process, voltage gated K+ channels are critical in shaping the action potential, determining the window over which synaptic inputs can be integrated, minimizing the jitter in action potentials, and increasing the precision of action potential timing (Gittelman & Tempel, 2006). First, to understand the significance of action potential timing and neural integration consider the fact that a post-synaptic neuron integrates its post-synaptic potentials, and hence processes information, and if the sum of the post-synaptic potentials achieves a critical value the post-synaptic neuron initiates an action potential and propagates the flow of information through the CNS.

A single post-synaptic potential cannot initiate an action potential. This is demonstrated in Figure 1.1A where the voltage change, in response to repeated current injection, every 10 ms, is insufficient to initiate an action potential. Furthermore, because of the relatively long interval between successive current injections, the potentials cannot be integrated to achieve sufficient depolarization of the post-synaptic neuron. Figure 1.1A was generated using a modified Hodgkin-Huxley model (Hodgkin & Huxley, 1952) with the following parameters: Na^+ conductance = 30 mS/cm^2; delayed rectifier K^+ conductance = 7 mS/cm^2; Cl^- conductance = 1 mS/cm^2; A-type current K+ channel conductance = 16 mS/cm^2; Na^+ reversal potential = 45 mV; K^+ reversal potential = -90 mV; Cl^- reversal potential = -70 mV; membrane capacitance = 1.5 $\mu F/cm^2$ and injected current with conductance = 0.5 mS/cm^2.

By decreasing the interval between successive current injections, the potentials generated from each injection can sum up, or integrate, and initiate an action potential. This is demonstrated in Figure 1.1B and C with time delays between successive injections of 4 and 1 ms respectively. As the interval between the current injections decreases the potentials generated from each injection can sum up until the membrane voltage reaches a critical value at which point an action potential is generated. Note that the number of action potentials in the 50 ms interval increases from 4 to 18 (Figure 1.1B and C) as the delay between the injections are decreased. Figures 1.1A-C collectively illustrate the importance of minimizing conduction delays to allow for neural integration and the transfer of information from one neuron to the next.

The role of Na^+ currents in the generation of the action potential is obvious, however, the significance of K^+ currents in shaping the action potential and affecting neural integration maybe less obvious. Figure 1D is a simulation of the voltage trace of a neuron with parameters identical to Figure 1.1C except that the delayed rectifier K^+ conductance was increased to 20 mS/cm^2. Increasing its conductance resulted in a decrease in the number of action potentials and changed the shape of the action potentials, specifically, the interspike length of the action potential is increased. Decreasing the conductance of the delayed K^+ rectifier increases the time during which the neuron is depolarized thereby increasing the duration during which it can integrate neuronal inputs and making the neuron susceptible to fluctuations in the membrane potential thereby increasing the jitter in the action potentials.

In sum, while Na^+ currents are obviously important in the generation and propagation of action potentials, K^+ currents are also critical in shaping the action potential and ultimately contributing to the frequency with which action potentials can be generated, affecting neural integration, and in determining the precision with which action potentials are generated. Both the frequency and

the precise timing of action potentials would be expected to affect cognitive function. After having established the critical role of the delays between action potentials and the underlying mechanisms which support the action potential we will next address the structural variables which can modulate the velocity of action potentials, and hence delays.

Myelination is only one structural variable which influences conduction velocity. For both myelinated and unmyelinated axons conduction velocity increases with axonal diameter, though the functional form varies depending on the myelination status of the axon (Waxman & Bennett, 1972). There is a linear relationship between the axonal diameter, myelin thickness, and the internodal length (Walhovd, Johansen-Berg, & Karadottir, 2014; Waxman SG, 1980). This point is important because if conduction velocity is dependent on all three variables and if these variables are linearly related, the relative contribution of each variable to conduction velocity is unclear (Waxman, 1980).

However, it can be shown that for fixed axonal diameters and internodal length, conduction velocity monotonically increases with myelin thickness (Waxman, 1980). Therefore, variance in myelin thickness measurements will reflect, to some extent, variations in axonal diameter and intermodal length, each of which independently increases conduction velocity. Therefore, when we state that increasing myelin thickness increases conduction velocity, we must realize that the increased conduction velocity is a result of the "cumulative effects" of myelination, namely increased axonal diameter and internodal length.

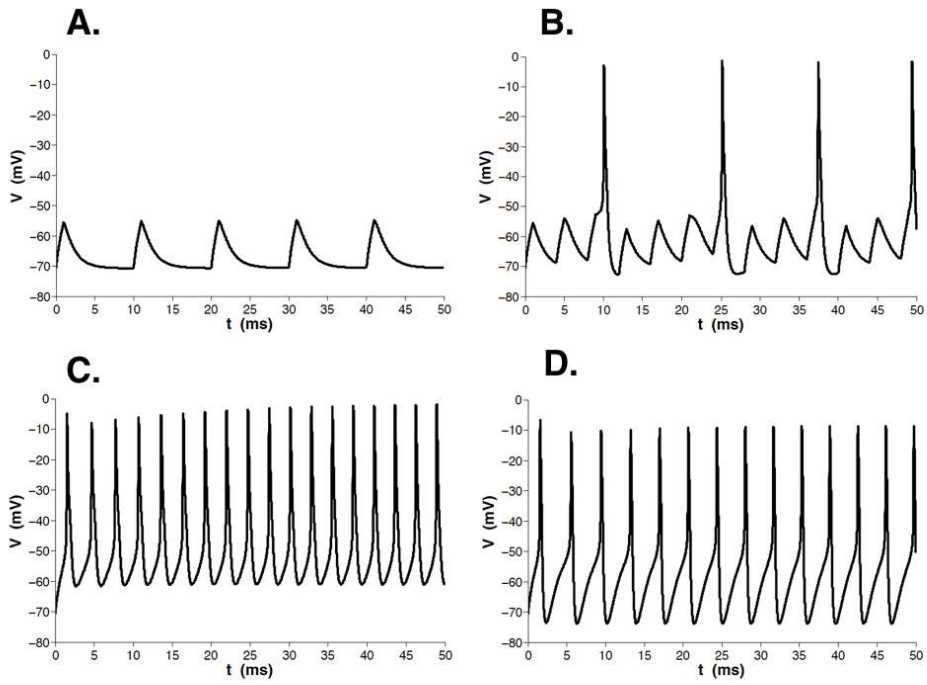

Figure 1.1: Simulations of action potentials. (A.) Simulation of voltage change over time in a neuron in response to repeated current injections in intervals of 10 ms. A single current injection is insufficient to sufficiently depolarize the neuron to generate an action potential. Additionally, because of the relatively long delays between successive current injections, the potentials decay away before the can be integrated. (B.) Simulated voltage trace with 4 ms intervals between current injections. Note that by decreasing the interval between current injections we can generate action potentials because the potentials generated by each current can be summed up. (C.) Simulated voltage trace with 1 ms intervals between current injections. By decreasing the interval to 1 ms we increase the number of action potentials generated. (D.) Voltage trace of neuron with parameters identical to Figure 1.1C except that the conductance of the K^+ delayed rectifier was increased to 20 mS/cm^2. Note that compared to Figure 1.1C increasing the conductance of the K^+ delayed rectifier the shape of the action potential as well as the number of action potentials has changed. Increasing the K^+ conductance decreased the number of action potentials.

As an example of the relative significance of increasing axonal diameter or increasing myelin thickness (along with axonal diameter and internodal length) consider that the conduction velocity of an unmyelinated axon is proportional to the square root of the diameter, therefore, to increase conduction velocity by a factor of 10 would require an increase in the diameter of the axon by a factor of 100 (this translates to an increase in the axonal volume by a factor of 10,000). For a myelinated axon, an increase in the fiber diameter of a factor of 10 would increase the conduction velocity by a factor of 10.

Myelin thickness increases conduction velocity of action potentials but why should this increased speed influence an animal's behavior? From an evolutionary perspective, it has been suggested that myelination of peripheral axons was critical to survival of large animals as faster conduction implies faster reactions to stimuli for both escape and predation maneuvers (Zalc & Colman, 2000). The evolutionary advantage of myelination to avoid predators or catch prey is reasonable, but what role could it play for processing speed of cognitive function?

Because the integration of postsynaptic potentials needs to occur within a time window, dependent on the membrane potential and the types ion channels expressed, (Koch, Rapp, & Segev 1996), and because cognitive functioning requires integration of information among distributed brain regions (Mesulam, 1990) reduced conduction velocity may impair neuronal integration and ultimately affect speed of cognitive processing. This central thesis, namely that reduced conduction velocity may impair neuronal integration across distributed brain regions and affect processing speed, is what behavioral neurologist Norman Geschwind would consider as a "disconnection syndrome". Classical disconnection syndromes, hypothesized to originate from lesions of specific white matter tracts, include conduction aphasia, associated visual agnosia, apraxia, and pure alexia (Catani & Ffytche, 2005). More generally however, reduced speed of communication between association cortices is expected to produce cognitive dysfunction including the slowing of processing speed.

Indeed, patients with MS, a demyelinating disease, have reduced processing speed compared to normal controls matched for age and education (Rao et al., 1989). When patients are given more time to perform tasks they achieve similar accuracy to that of controls, providing support for the idea that multiple sclerosis slows information processing and subsequently limits cognitive performance (Demaree, et al., 1999). While age differences in cognitive function, in healthy adults,

would not be considered a neurological disease, nonetheless, it may be possible that age related variance in myelin thickness may produce variation in cognitive performance consistent with the idea of a "disconnection syndrome" (Bennett & Madden, 2014). This agrees with studies in older non-human primates demonstrating that age is associated with degeneration of myelin sheaths and in some cases re-myelination with thinner sheaths, both of which would be expected to reduce conduction velocity and affect neuronal integration (Peters, 2009). Therefore, if a "disconnection syndrome", due to a decrease in myelin thickness, is a potential mechanism for age differences in processing speed then we expect to find that age differences in myelin content would be associated with the speed of processing.

Brain aging studies have investigated the relationship between white matter hyperintensities (WMH) and speed of processing. White matter hyperintensities are identified as abnormal signal intensity on T_2-weighted or Fluid Attenuated Inversion Recovery (FLAIR) MRI sequences and are commonly found in subcortical white matter in older individuals (Xiong & Mok, 2011). White matter hyperintensities are associated with histopathologically confirmed demyelination, however, the extent of the hyperintensities can both over and underestimate demyelination. Furthermore, hyperintensities are nonspecific markers as they also reflect changes in the interstitial fluid (Shim et al., 2015; Haller et al., 2013). Nonetheless, there is evidence that the burden of WMH is associated with slower processing speed in healthy adults (Gunning-Dixon & Raz, 2000). In a longitudinal study of 554 participants Van Den Heuvel et al. (2006) found that the change in the volume of WMH paralleled decline in processing speed providing additional support for the significance of age related changes in white matter as a potential substrate of age related slowing. However, the lack of specificity of WMH to specific neurobiological changes makes its interpretation difficult.

The supposed neurobiological specificity of Diffusion Tensor Imaging (DTI) derived indices made it an attractive tool to investigate hypothesis of the nature of age the related differences in white matter, namely myelination, and its relationship to processing speed. Diffusion tensor imaging indices reflect the directional diffusion properties of water (e.g. radial or axial diffusivity), the overall diffusion of water (e.g. mean diffusivity) and the anisotropic diffusion (e.g. fractional anisotropy). Indeed, DTI is more sensitive, though not specific, to microstructural changes in white matter than conventional MRI methods as it can detect differences in otherwise normal-appearing white matter (Moseley, 2002; O'Sullivan et al., 2001). Numerous studies have found associations between DTI indices, age, and processing speed commonly interpreting these associations as reflecting reduced "white matter integrity" (Madden et al., 2012) and suggesting that age differences in "white matter integrity" mediate age differences in processing speed (Bennett & Madden, 2014).

While DTI studies, like studies of WMH, provide support for the involvement of cerebral white matter in reduced processing speed, it also suffers from the lack of neurobiological specificity of its indices. Axonal density and caliber, intra and extracellular fluid, and organization of fibers (Beaulieu, 2002; Jeurissen et al., 2013; Jones et al., 2013; Vos et al., 2012) are a few of the variables which influence DTI indices and complicates the interpretation. The dependence of the DTI indices on crossing fibers is particularly concerning given the diverse geometry of the white matter tracts implicated in the extant literature. Given the significant limitations of DTI new methods (MacKay et al., 1994; Prasloski et al., 2011), with more specific indices, primarily to myelin as that is commonly hypothesized as a neural substrate of reduced processing speed, need to be investigated to clarify its role with age related slowing.

1.3 Addressing the limitations in the extant literature

Multi-echo T_2 imaging (see chapter 2 for more information) can overcome the limitations of DTI with respect to specific measures related to myelin. As will be discussed in chapter 2 DTI is insensitive to the myelin associated water signal. However, multi-echo T_2 imaging can detect the myelin associated water signal and through modeling of the data we can quantify the relative size of the myelin associated water signal. This measure, referred to as the Myelin Water Fraction (MWF), is proportional to myelin content. We would expect that a larger MWF would be reflective of greater myelin content (see chapter 2 for limitations) which would imply a greater number of myelin sheaths around the axon. Therefore, we expect a larger MWF to be associated with faster conduction velocity and therefore with faster processing speed.

Reaction time, operationalized as the interval between the presentation of a stimulus and the onset of a response (Pachella, 1974), is a common measure of information processing speed (Salthouse, 2000). However, older individuals tend to emphasize accuracy over speed in comparison to younger individuals (speed-accuracy tradeoff) (Salthouse,1979) therefore, the speed accuracy tradeoff confounds our interpretation of the reaction time as a measure of information processing speed. This significant limitation can be addressed using the drift diffusion model (see chapter 3). In brief the drift diffusion model accounts for accuracy and separates the reaction time into the cognitive information processing time and the non-cognitive response time (e.g., motor response). Indeed, slower reaction times in older individuals does not necessarily imply slower cognitive information processing speed (Ratcliff, Thapar, McKoon, 2006). Therefore, we used the drift diffusion model to assess information processing speed to account for the speed-accuracy tradeoff and for non-cognitive processing time.

The central thesis of this dissertation has been outlined above, however, in the latter stage of this project we also considered the possibility that age differences in axonal density may also be negatively associated with processing speed. Testing this hypothesis was not our primary aim therefore, we did not collect additional measures reflecting axonal density. As will be described in chapter 2, ME-T_2 imaging provides a putative index of axonal density, $geomT_{2\text{-}IEW}$, with longer $geomT_{2\text{-}IEW}$ suggesting a lower axonal density. Age related axonal loss has been reported in both non-human primates and humans (Marner et al., 2003; Peters, 2009) and is associated with poor cognition in macaques (Sandell & Peters, 2003). We argue that if a disconnection syndrome is possible because of myelin loss, then may be loss of axons, the structure which propagates the action potential, could be expected to produce a disconnection syndrome as well.

1.4 Project scope and aims

The central aim of this dissertation was to test the hypothesis that greater myelin content, after adjusting for age effects, would be associated with faster processing speed. However, before we could directly test this hypothesis we needed to establish a few other goals. This led to the following three aims of this dissertation plus an exploratory aim.

1) Assessing the reliability of a novel imaging method, which has been validated histologically to produce estimates of myelin content.
2) Evaluating whether MWF can reproduce the expected inverted-U pattern between age and myelin content derived from post-mortem studies.
3) Testing the hypothesis that greater myelin content is associated with faster information processing.
4) In an exploratory analysis, we tested the hypothesis that higher axonal density, indexed by shorter $geomT_{2\text{-}IEW}$, would be associated with faster information processing speed.

To convincingly answer the question of whether the slowing of processing speed is a result of myelin loss during the aging process longitudinal investigations with reliable and valid measures of myelin content are needed. The first aim addresses the question of reliability of the Multi-echo T_2 imaging indices. Valid but unreliable measures will greatly reduce the ability to detect age differences in myelin content or change in myelin content in longitudinal studies. The second aim addresses the in-vivo validity of MWF. Myelin water fraction has been extensively validated using animal models and ex-vivo tissue (see chapter 2) which makes it an ideal tool to investigate myelin in-vivo. Nonetheless, establishing the expected pattern of age myelin associations provides additional confirmation. Indeed, if MWF was unable to reproduce the expected relationships its utility as an in-vivo method to assess myelin could be questioned.

Finally, the third aim tests the substantive question which motivated this dissertation. Given the relationship between myelin thickness and conduction velocity and the reduced processing speed in MS patients, it is unsurprising that age differences in myelin thickness has been hypothesized as a substrate of slower processing speed. By measuring MWF, and inferring myelin thickness, we could test the long-standing hypothesis that greater myelin would be associated with faster processing. Elucidating such relationships is critical because it provides us with biological targets to modify and potentially reduce the effects of age on processing speed.

Chapter 2 introduces the basics of magnetic resonance imaging and a more detailed discussion of the Multi-echo T_2 imaging used in this dissertation. The discussion includes a discussion on the biological origins of multi-exponential T_2 decay, basic theory for multi-exponential T_2 decay data acquisition, data modeling, quantification and limitations. Chapter 3 introduces the use of behavioral modeling and specifically focuses on the EZ diffusion model used to generate estimates of cognitive processing speed in this dissertation.

Chapters 4 and 5 describe study design, results, conclusions and limitations for aims 1 and 2 respectively. This work has been published and the citations are included in the autobiographical statement of the dissertation. Chapter 6 provides details of the longitudinal data analysis in which we tested the hypothesis that greater myelin content would be associated with faster processing speed. Finally, chapter 7 provides a summary of the results, limitations, and future directions.

CHAPTER 2: Introduction to Multi-Echo T_2 Imaging

2.1 Brief introduction to MRI

The theoretical foundations of Magnetic Resonance Imaging and in Nuclear Magnetic Resonance (NMR) can be found elsewhere (Haacke et al., 1999; Keeler, 2005) and is beyond the scope of this dissertation. Nonetheless, a brief introduction to NMR and MRI will be provided followed by a more detailed imaging discussion relevant to the dissertation.

Atomic nuclei possess intrinsic properties, namely spin and a magnetic moment (for non-zero spin nuclei). Both the spin and magnetic moment are responsible for the precession of the spin when an external magnetic field is applied. Nuclei with spin greater than ½ may possess an electrical moment as well, however for this dissertation we will focus solely on spin ½ nuclei, specifically the hydrogen nuclei or proton. In the absence of an externally applied magnetic field the spins are oriented randomly. The vector sum of the these randomly oriented spins results in a net zero magnetization (Figure 2.1A). When the spins are placed in an external magnetic field (B_0 in Tesla; T) applied along the z axis, the z component of the magnetic moment (μ_z) can be either parallel or anti-parallel to B_0. The distribution of μ_z is slightly skewed in the direction of the externally applied magnetic field. In other words, there are more spins whose μ_z is parallel to the external field. The vector sum of the spins results in a net vector which points in the same direction as the external field and is referred to as the net magnetization (M_0) (Figure 2.1B). The spins also precess about B_0.

The precession frequency, referred to as the Larmor frequency (ν_0 in rad/s^{-1} or ω_0 in Hz) is provided by equations 2.1-2.2. The precession frequency depends on the magnitude of the external magnetic field and the nucleus specific gyromagnetic ratio (γ, in rad/s × T).

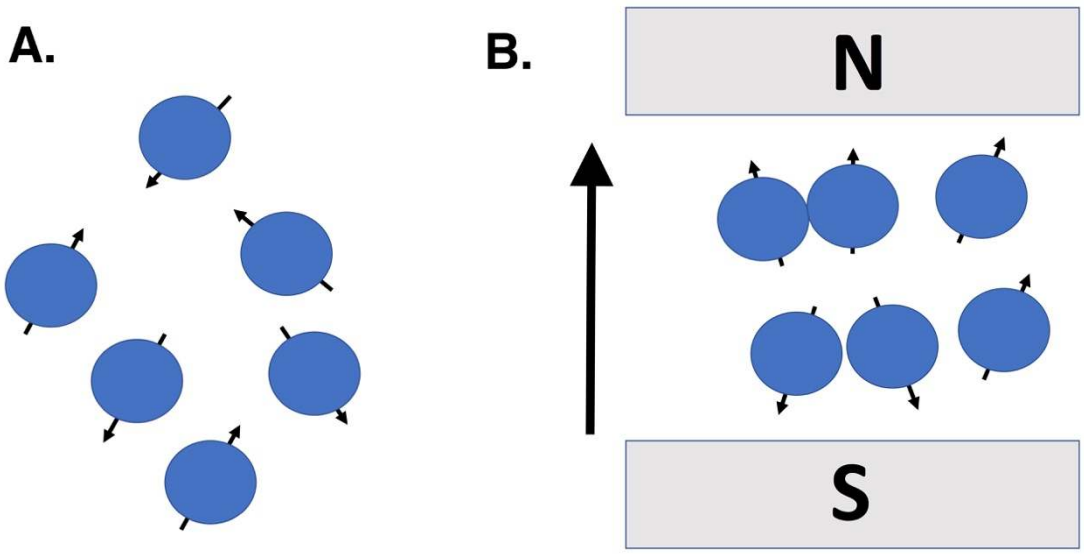

Figure 2.1: Effect of external magnetic field on spins. (A.) Protons in the absence of an external magnetic field are randomly oriented and therefore the magnetic moments of individual nuclei cancel out. (B.) In the presence of an external magnetic field most the spins align parallel to the field. The sum of the individual spins creates a net magnetization aligned parallel to the external magnetic field.

The skew in the distribution of μ_z can be manipulated by applying radio-frequency (RF) pulses, oscillating at or near the Larmor frequency perpendicular to the external field (B_1). To visualize the effect of B_1 on the net magnetization it is convenient to choose a reference frame which is oscillating at the same frequency as B_1 (referred to as a rotating frame). In this frame B_1 no longer appears to be oscillating and it net effect is to rotate the spin ensemble by an angle, referred to as the flip angle (Figure 2.2A-C). The flip angle can be found by integrating B_1 over the duration its applied.

$$\upsilon_0 = \frac{\gamma}{2\pi} B_0 \qquad \text{(Equation 2.1)}$$

$$\omega_0 = \gamma B_0 \qquad \text{(Equation 2.2)}$$

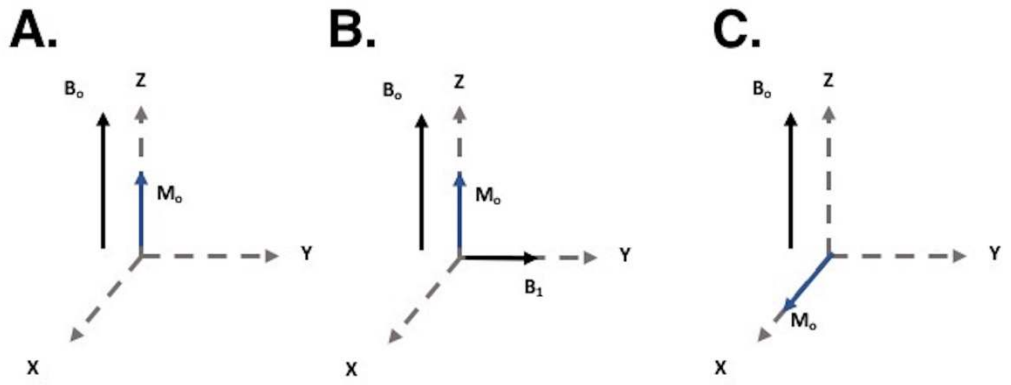

Figure 2.2: Creation of transverse magnetization. (A.) In the presence of the externally applied magnetic field (B_0) a net magnetization (M_0) parallel to the external field is generated. (B.) A radiofrequency (RF) pulse, oscillating at the Larmor frequency (ν_0), is applied perpendicular to the external field. In the rotating frame, however B_1 remains along an axis (C.) B_1 rotates the magnetization by an amount specified by the flip angle (90° in this case).

The temporal evolution of the net magnetization after the application of the RF pulse is described by the Bloch equations (Equations 2.3-2.5). The evolution of the magnetization is relatively simple to visualize and therefore we will describe it in a stationary frame of reference. The magnetization oscillates about the external field, and can be measured by the current it induces in nearby coils (referred to as Free Induction Decay, FID) (Figures 2.3A; Equations 2.3-2.5). In addition to oscillating, the spin ensemble experiences two relaxation mechanisms which return the spin ensemble to equilibrium. The first relaxation mechanism, spin-lattice relaxation (T_1 relaxation), transfers energy, which was initially provided by the RF pulse, from the spin ensemble to the lattice, and results in the re-growth of the magnetization, with a time constant referred to as T_1, along the direction of applied magnetic field (Figure 2.3B; Equation 2.5). The second mechanism, spin-spin relaxation (T_2 relaxation), occurs a result of spins exchanging their μ_z which ultimately redistributes energy among the spin ensemble, and irreversibly decreases the amplitude of the FID with a time constant referred to as T_2 (we say that the spins are dephasing).

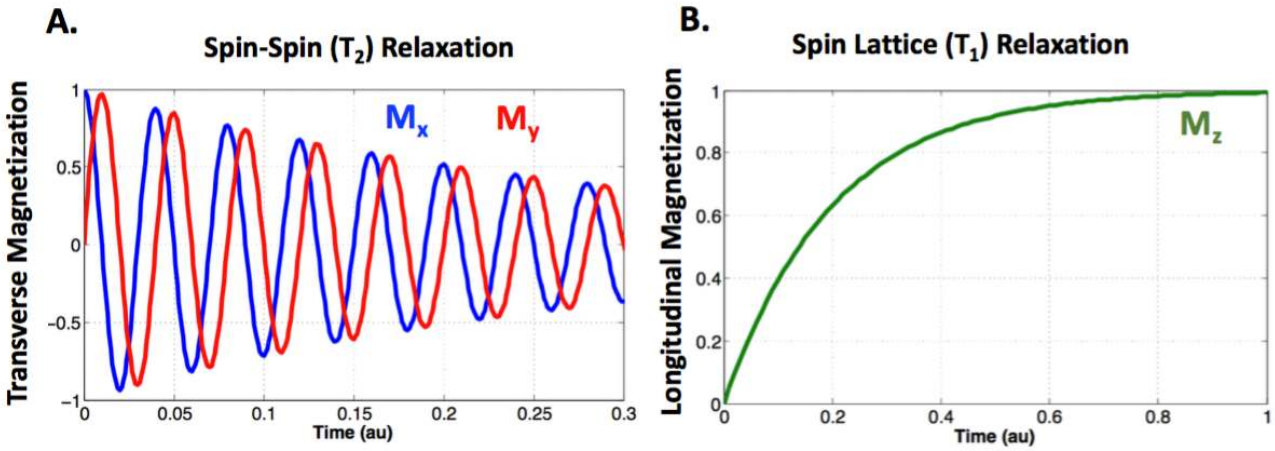

Figure 2.3: Magnetization dynamics. (A.) The net magnetization in the xy plane oscillates at the Larmor frequency while experiencing T_2 relaxation. Note the magnetization along the y axis is phase shifted by 90° with respect to the x axis. (B.) Along the z axis the magnetization returns to its equilibrium value as it experiences T_1 relaxation.

$$\frac{d}{dt}M_x(t) = \gamma M_y(t)B_0 - \frac{M_x(t)}{T_2} \qquad \text{(Equation 2.3)}$$

$$\frac{d}{dt}M_y(t) = -\gamma M_x(t)B_0 - \frac{M_y(t)}{T_2} \qquad \text{(Equation 2.4)}$$

$$\frac{d}{dt}M_z(t) = -\frac{M_z(t)-M_0}{T_1} \qquad \text{(Equation 2.5)}$$

Another source signal loss, or dephasing, is the static field inhomogeneity. The combination of the spin-spin relaxation and magnetic field inhomogeneity produces a relaxation time constant referred to as T_2^* (Equation 2.6). The relaxation effect of the magnetic field inhomogeneity is represented by the T_2' term and can be reversed using a spin echo sequence (more on this later).

$$\frac{1}{T_2^*} = \frac{1}{T_2} + \frac{1}{T_2'} \qquad \text{(Equation 2.6)}$$

Assuming a special case where the magnetization (M_0) is rotated by 90° onto the x axis (Fig 2.2B) the solution to the Bloch equations are provided in equations 2.7-2.9. Solutions to the Bloch equations describe (see Figure 2.3A-B) an oscillating magnetization in the xy plane, where the magnetization along the y axis is phase shifted by 90°, relative to the x axis, and is also decaying

exponentially with a time constant equal to the spin-spin relaxation time constant. In addition, the magnetization regrows along the +z axis with a time constant equal to the spin-lattice relaxation time constant.

$$M_x(t) = [M_0 \cos(\omega_0 t)]e^{-t/T_2} \quad \text{(Equation 2.7)}$$

$$M_y(t) = [M_0 \sin(\omega_0 t)]e^{-t/T_2} \quad \text{(Equation 2.8)}$$

$$M_z(t) = M_0[1 - e^{-t/T_1}] \quad \text{(Equation 2.9)}$$

The relaxation time constants can be measured using a variety of techniques, however, for this dissertation we will focus on measuring spin-spin relaxation using the Carr-Purcell-Meiboom-Gill (CPMG) sequence (Meiboom & Gill, 1958). The CPMG sequence is a technique which uses a series of RF pulses to generate echoes (Figure 2.4). The sequence can be written as:

$$90_y^\circ \text{ -- } \tau - (180_x^\circ \text{ -- } 2\tau)_N$$

The first 90° pulse applied along the y axis rotates the magnetization into the x axis. The magnetization then oscillates and decays exponentially with a T_2^* time constant. At time, equal to τ, a 180° RF pulse is applied along the x axis. During this interval spins will obtain different phase values (φ,θ) due to the magnetic field inhomogeneity's, which changes the local Larmor frequency. The 180° RF pulse refocuses the magnetization by removing the effects of the magnetic field inhomogeneity. Specifically, the refocusing pulse changes the phase values of the spins by 180° (+φ → - φ; + θ → - θ). Because the static field inhomogeneity is unchanged its effect on the spins is identical to what it was prior to the refocusing pulse. Therefore, during the interval between τ and 2τ spins will again accrue similar phase values (φ,θ) and we say the spins are rephasing. At time, equal to 2τ the phase of all spins will be 0, and the signal will reach its maximum with the effects of the magnetic field inhomogeneity's removed. This is depicted in Figure 2.4 where the magnetization begins to regrow and reaches its peak at 2τ. This process of refocusing the

magnetization is referred to as an echo. The magnitude of this magnetization is reduced by a factor of $e^{-2\tau/T_2}$ due to irreversible effects of spin-spin relaxation. By continually applying the 180° RF pulse, say *N* times, *N* echoes can be generated at times equal to $2N\tau$. By recording the magnitude of the magnetization at the echoes and recording the times at which the echoes occurred, an exponential function can be fit to the echoes to estimate the spin-spin relaxation time constant.

While the preceding discussion has focused on the origins of the NMR signal, how it can be manipulated by RF pulses, and relaxation mechanisms, the following paragraphs will provide a brief introduction to how magnetic field gradients can be used to spatially encode the magnetization and subsequently be used to generate images. I will limit the discussion to generating a single slice image.

When an object is placed in an external magnetic field (e.g.: brain), in the absence of any additional magnetic fields, all protons precess at the Larmor frequency. The application of a linear magnetic field gradient along the z axis (G_z, in mT/m) results in a Larmor frequency which is dependent on the position along the z axis (Equation 2.10). Because there is a one-to-one relationship between the position along the z axis and the Larmor frequency, one can choose the z position of the slice center (z') along with the slice thickness (Δz) and rotate the protons only within this region. This is accomplished by generating an RF pulse whose carrier frequency is given by Equation 2.10 with z equal to z', and a bandwidth (BW) given by Equation 2.11.

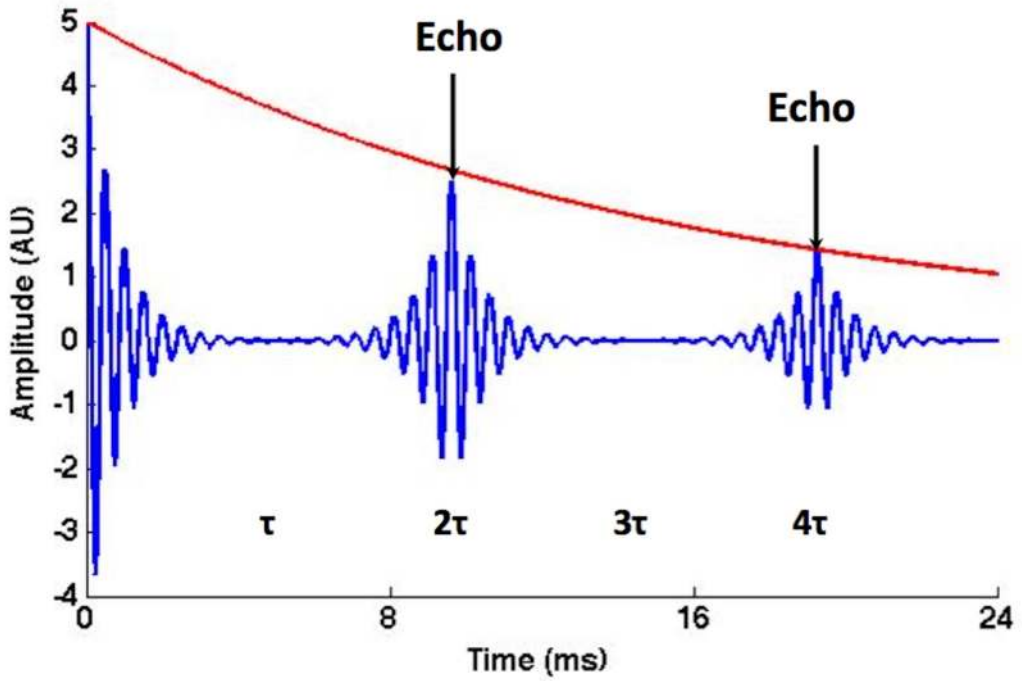

Figure 2.4: Echo train**.** A train of echoes, 2, are shown occurring at intervals of $2N\tau$. The magnetization is oscillating and experiences T_2* decay which rapidly reduces the signal amplitude. Refocusing RF pulses rephase the magnetization which results in an increase of the magnetization with the peak occurring at the echo. The amplitude of the echo is reduced due to the irreversible effects of T_2 relaxation. The red curve depicts the T_2 decay envelope. By generating multiple echoes, we can estimate the T_2 value of the T_2 decay.

$$\omega_0(z) = \gamma(B_0 + G_z z) \quad \text{(Equation 2.10)}$$

$$BW = \gamma G_z \Delta z \quad \text{(Equation 2.11)}$$

Once the protons are rotated into the xy-plane, additional magnetic field gradients (G_x,G_y) are applied to spatially encode the magnetization within this plane. To understand how these additional gradients, enable spatial encoding it is helpful to re-express the solutions of the Bloch equations using complex notation. Ignoring relaxation effects, Equations 2.12 and 2.12 can be written as:

$$M_{xy}(t) = M_x + iM_y = M_0^{xy} e^{-i\omega_0 t} \quad \text{(Equation 2.12)}$$

$$M_0^{xy} = \sqrt{(M_x)^2 + (M_y)^2}. \quad \text{(Equation 2.13)}$$

These equations can be interpreted as a vector in the xy-plane, of magnitude M_0^{xy}, rotating about the z axis at the Larmor frequency. This provides a short hand notation for describing the rotation

of the magnetization about the z axis. The angle between M_0^{xy} and the x axis, referred to as phase, increases linearly with time (Equation 2.14).

$$\varphi(t) = \omega_0 t \quad \text{(Equation 2.14)}$$

To generate an image, once the magnetization has been rotated into the xy-plane, requires that we spatially encode the phase value along both x and y axes. To spatially encode phase values along the y axis we apply a gradient along the y axis (G_y) for a brief period. This process is referred to as phase encoding and is repeated *N* times, where *N* is the number of pixels along the y axis. To accomplish *N* phase encoding steps requires that we rotate the magnetization into the xy plane *N* times and for each of the *N* steps we increase the value of G_y by a fixed amount (see 1 for more information). The application of the G_y gradient, like the G_z gradient, changes the Larmor frequency along the y axis while the gradient is on. After a short interval, δ, the magnetization along the y axis accumulates phase proportional to its position along the y axis (Equation 2.15). Because all protons along the y axis experience the main magnetic field, the B_0 term can be dropped from equation 2.15 (Equation 2.16). A new term is introduced, k_y (in 1/m; Equation 2.17), which refers to the spatial frequency along the y axis. By repeating the phase encoding steps *N* times, with a different value of G_y each time, we obtain *N* k_y values.

$$\varphi(y) = \omega_0 \delta = \gamma(B_0 + G_y y)\delta \quad \text{(Equation 2.15)}$$

$$\varphi(y) = \omega_0 \delta = \gamma G_y y \delta \quad \text{(Equation 2.16)}$$

$$k_y = \gamma G_y \delta \quad \text{(Equation 2.17)}$$

After the application of each phase encoding step the x gradient (G_x) is applied for a time *T*. The application of the x gradient is referred to as frequency encoding. As expected the application of the x gradient results in a different Larmor frequency along the x axis (Equations 2.19-2.21). Unlike the y gradient, whose magnitude changes for each phase encoding step, the magnitude of

the x gradient is the same each time. The evolution of the phase along the x axis is accomplished by allowing the magnetization to evolve over time (during the time interval *T*). During this interval $k_x$values are sampled *M* times yielding *M* k_x values.

$$\varphi(x) = \gamma G_x x t \quad \text{(Equation 2.19)}$$

$$k_x = \gamma G_x t \quad \text{(Equation 2.20)}$$

$$\varphi(x) = k_x x \quad \text{(Equation 2.21)}$$

The combination of *N* k_y and *M* k_x values make up the *N* × *M* space referred to as *K*-space. The relationship between *K*-space ($S(k_x, k_y)$) and the *N* × *M* ($m(x, y)$) image we wish to produce is described by equation 2.22. Namely, the acquired *K*-space data is the Fourier Transform (*FT*) of the image we wish to obtain. Therefore, the image can be obtained by applying the inverse Fourier Transform (*iFT*) to *K*-space (Equation 2.23). Different types of images are generated by acquiring *K*-space in various ways. For the purposes of this dissertation I will briefly describe T_2-weighted images.

$$S(k_x, k_y) = \int\int m(x, y) e^{-ik_x} e^{-ik_y} \, dx \, dy = FT[m(x, y)] \quad \text{(Equation 2.22)}$$

$$m(x, y) = iFT[S(k_x, k_y)] \quad \text{(Equation 2.23)}$$

As shown in Figure 2.4 one can generate an echo, using a spin-echo sequence, at any time so long as the time given to dephase (interval between 90 and 180° RF pulse) is identical to the given to rephrase (interval between 180° RF pulse and the peak of the echo). Images generated from this acquisition are called T_2-weighted images. The human brain can be grossly divided into 3 main tissue types: white matter (WM), gray matter (GM), and cerebrospinal fluid (CSF). These tissues have distinct T_2 relaxation values and therefore, for a fixed echo time, the magnetization of each of tissue will have different magnitudes (Figure 2.5). This allows generating contrast that enables

visualization of the different tissues. The image contrast will vary depending on the echo time (Figure 2.6).

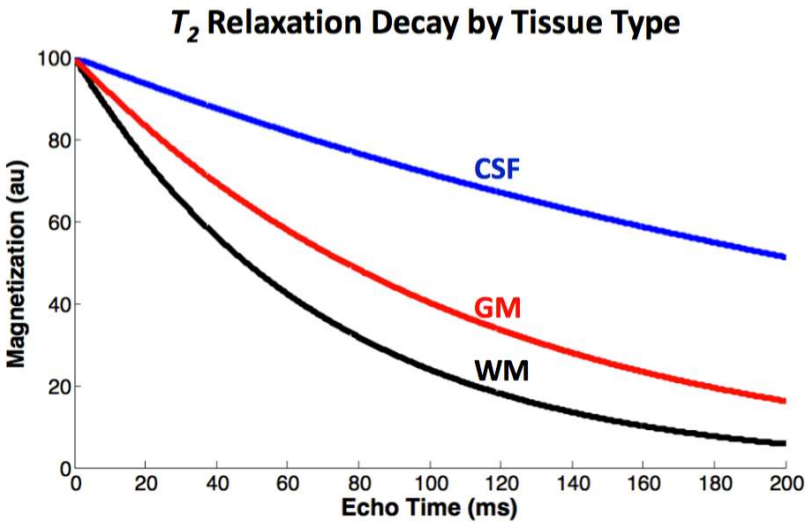

Figure 2.5: T_2 decay by tissue type. The 3 tissue types (CSF, GM, WM) have unique T_2 values and therefore, for any given echo time, the amplitude of the magnetization for each tissue will vary. Note in this example each tissue starts with the same amount of magnetization, 100 au.

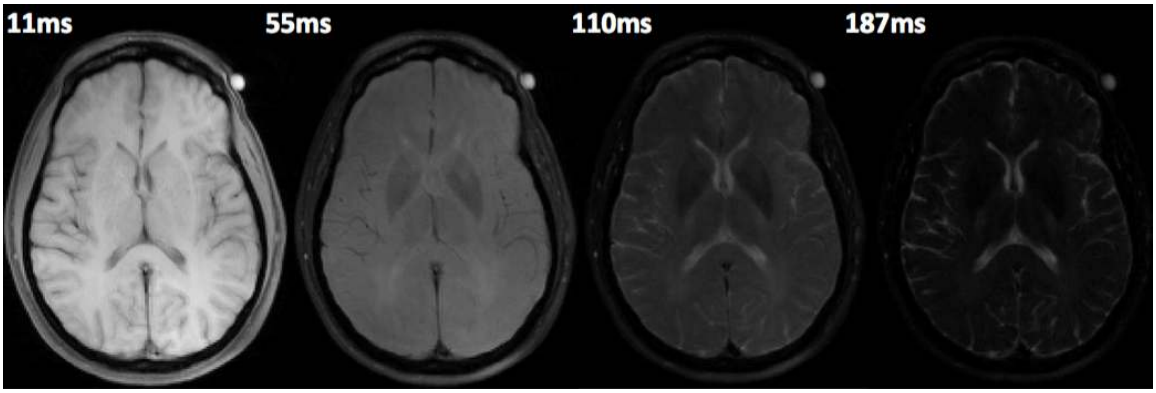

Figure 2.6: Dependence of image contrast on echo time**.** Image contrast varies as a function of the echo time because of unique T_2 values for different tissue.

2.2 Introduction to Multi-Echo T_2 (ME-T_2) Imaging

2.2.1 Correlation time and relaxation time constants

The previous section alluded to the tissue-specific T_2 relaxation time constants but did not provide a mechanism to accounts for this. This section will introduce the relationship between relaxation time constants and the environments, or compartments, in which the spins reside.

Additionally, a description of how the data are acquired and analyzed and a review of the biological sources of the multiple time constants will be provided.

A detailed discussion of the sources of nuclear relaxation is beyond the scope of this dissertation and can be found elsewhere (Sudmeier et al., 1990). We will limit the discussion to the primary source of T_2 relaxation, namely nuclear dipole-dipole relaxation mechanisms. Spins act as magnetic dipoles and, because they are tumbling (the word tumbling is used instead of rotating so not to confuse dipole-dipole relaxation with rotational relaxation), spins generate oscillating magnetic fields which affect nearby spins. The oscillating magnetic fields can be decomposed by frequency and is described by the spectral density function. The relationship between the spectral density function and T_1 & T_2 relaxation times are provided by equations 2.24 2.26 (Bloembergen, Purcell, & Pound, 1948). The characteristic timescale of spin tumbling is given by the correlation time,τ_c (sec), with short correlation times implying fast proton tumbling. In other words, if a proton is tumbling at a high rate then the time it takes to reorient by 1 radian will be short, hence a small correlation time. The remaining variables in Equations 2.24-2.26 are: magnetic permeability in vacuum (μ_0, in H/m), distance between spins (r), and the Planck's constant (h, in J×s). As shown in Figure 2.7, long correlation times are associated with a short T_2.

Protons residing within biological structures which restrict their tumbling will exhibit shorter T_2 relaxation times when compared to protons in less restrictive structures. The heterogeneity of biological tissue however results in multiple spin compartments within a typical MRI voxel. In other words, a single voxel will contain spin in highly restricted as well as relatively unrestricted compartments.

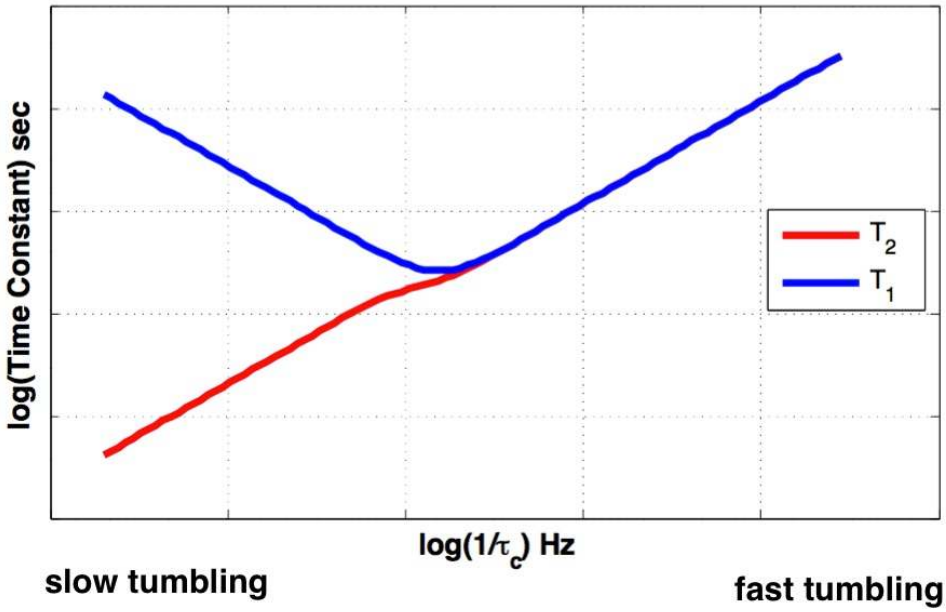

Figure 2.7: Bloembergen-Purcell-Pound (BPP) Theory**.** The relationship between the frequency of tumbling, or correlation time, with the T_1 and T_2 relaxation time constants using the BPP theory. The shorter the correlation time, or the higher the frequency, of proton tumbling the longer the T_1 and T_2 relaxation time constants.

$$\frac{1}{T_1} = k\left[\frac{\tau_c}{1+\omega_0^2\tau_c^2} + 4\frac{\tau_c}{1+4\omega_0^2\tau_c^2}\right] \quad \text{(Equation 2.24)}$$

$$\frac{1}{T_2} = \frac{k}{2}\left[3\tau_c + 5\frac{\tau_c}{1+\omega_0^2\tau_c^2} + 2\frac{\tau_c}{1+4\omega_0^2\tau_c^2}\right] \quad \text{(Equation 2.25)}$$

$$k = \frac{3\mu_0^2}{160\pi^2}\frac{h^2\gamma^4}{4\pi r^6} \quad \text{(Equation 2.26)}$$

Because each of these compartments exhibits a unique T_2 and because a single voxel contains multiple compartments the magnetization decay within a voxel is multi-exponential. Before reviewing evidence for the biological origins of the various compartments we will first review how the MRI data are collected and analyzed.

2.2.2 Biological origins of multi-compartment relaxation

In the following section, we will discuss the biological basis for the different T_2 relaxation compartments as well as the interpretation of the indices derived from the T_2 relaxation analysis. Information on data acquisition and modeling will be discussed in section 2.2.3 and 2.2.4.

Beaulieu et al (1998) demonstrated the existent of multiple proton compartments in excised garfish nerves. The Schwann cell myelinated trigeminal nerve as well as oligodendrocyte myelinated optic nerve exhibited three T_2 water compartments based on the mobility of water molecules (30-50, 150, and 500 ms). The short T_2 (30-50 ms) compartment was attributed to water protons within myelin, the intermediate T_2 (150 ms) was attributed to water protons within the axon and the long T_2 (500 ms) was attributed to the interaxonal space. Importantly, the unmyelinated olfactory nerve did not exhibit the short T_2 compartment.

Subsequent studies confirmed the short T_2 compartment as originating from water between the myelin sheaths. As the number of myelin lamella increases, the quantity of water trapped between the myelin sheathes increases. The myelin water exhibits a short T_2 and the size of this compartment is proportional to the number of myelin lamella per axon and the number of myelinated axons per unit volume. Therefore, it is assumed that MWF reflects the histologically derived estimates of myelin content (see section 2.2.4 for limitations regarding the interpretation of MWF). Using quantitative luxol fast blue staining for myelin, Laule et al (2008) found strong correlations between the histologically derived estimates of myelin content and MWF. Furthermore, using an animal model of induced demyelination and spontaneous remyelination, McCreary et al (McCreary et al., 2009) found that MWF decreased during histologically confirmed demyelination and increased during histologically confirmed remyelination. These studies provide strong support for the association of the short T_2 compartment reflecting the water trapped between the myelin sheaths and the magnitude of MWF as reflecting the amount of myelin, which is the premise of the ME-T_2 method.

The intra/extraceullar (IE) water compartment is thought to represent both water molecules from the intra and extracellular space and therefore, its interpretation is not straightforward. Recent

animal studies have yielded significant insight into the interpretation of the geometric mean T_2 (geomT_2) of the IE compartment (calculation of the *geom*T_2 is described in 2.2.3). In six white matter tracts in the rat spinal cord, Dula et al (2010) found a positive correlation between the mean axon diameter and the geom$T_{2\text{-}IEW}$. Similar results were found when comparing the mean axon diameter and T_1 relaxation (Harkins et al., 2016).

Both results are not surprising when we consider both the axonal diameter and axonal density and their relationship to the proton correlational time. In macaques and humans, axonal density declines and the axonal diameter increases along the corpus callosum, genu to splenium (Aboitz et al., 1992; De Santis et al., 2016; Lamantia & Rakic, 1990; Riise & Pakkenberg, 2011). Given the relationship between T_1 and T_2 relaxation and the correlation time, we can predict the association between the relaxation time constants and axonal diameter/density. Namely, as the mean axonal diameter increases, and axonal density decreases, the tumbling of water is less restricted in both the intra-axonal and extracellular space, that is the correlation time is smaller in both compartments, and therefore both T_1 and T_2 relaxation time constants increase. This prediction is consistent with the findings in the rat spinal cord mentioned previously.

These results also demonstrate the limitation in interpreting the geom$T_{2\text{-}IEW}$. First, it should be noted that the associations between geom$T_{2\text{-}IEW}$ and axonal density/diameter were found when looking across white matter tracts. Whether such associations exist within white matter tracts is unclear. It need not be the case that associations between indices when evaluated across white matter tracts be like within tract associations (Arshad, Stanley, & Raz 2017). Furthermore, given the relationship between axonal diameter and density, interpreting associations between the geom$T_{2\text{-}IEW}$ and some outcome of interest (e.g. speed of information processing) one can always

interpret the associations from the viewpoint that the geom$T_{2\text{-}IEW}$ reflects axonal density or axonal diameter. Therefore, additional information is needed to support one's interpretation.

For example, using speed of information processing as the outcome of interest, if one wants to interpret geom$T_{2\text{-}IEW}$ as an index of axonal diameter, then one expects a positive correlation between geom$T_{2\text{-}IEW}$ and the speed of information processing because axons with greater diameter, hence longer geom$T_{2\text{-}IEW}$, conduct action potentials faster than axons with smaller diameters. On the other hand, if the geom$T_{2\text{-}IEW}$ is considered as an index of axonal density, then the expectation is a negative correlation between the speed of information processing and geom$T_{2\text{-}IEW}$ as a loss of axons, and a subsequent increase in the geom$T_{2\text{-}IEW}$, would be expected to reduce neural signaling.

Furthermore, the population under investigation may also offer insight into the interpretation of the geom$T_{2\text{-}IEW}$. If the population consists of young individuals, infants to adolescents, in whose developing brains axons are increasing in caliber, in response to hormones for example (Pesaresi et al., 2015; Perrin et al., 2008), then interpreting the geom$T_{2\text{-}IEW}$ as a proxy for axonal diameter seems reasonable. On the other hand, in a population of older individuals, increasing axonal caliber seems unlikely, whereas axonal loss would be consistent with postmortem findings (Marner et al., 2003; Peters, 2009). In sum, while the geom$T_{2\text{-}IEW}$ provides additional characterization of white matter microstructure, namely axonal diameter or density, interpreting associations between geom$T_{2\text{-}IEW}$ and other variables of interest should be made with caution and when possible additional sources of information should be used to aid in the interpretation.

While this dissertation was initially focused on measurements specific to myelin, to test the hypothesis outlined in chapter 1, during this project we realized that characterization of age differences in myelin only, ignores the other critical feature of white matter, axons. Given the findings of axonal loss in both non-human primates and humans (Marner et al., 2003; Peters, 2009)

and the fact that MS neuropathology includes axonal loss (Haines, et al., 2011) it may be the case that age differences in processing speed could be associated with age differences in the geomT_2-$_{IE}$. Thus, we explored this possibility while acknowledging the limitations in interpreting this index and keeping in mind that studies described in this dissertation were not designed specifically to test hypothesis of axonal loss and processing speed.

2.2.3 ME-T_2 Data acquisition

As discussed previously the CPMG sequence can be used to generate a T_2 decay curve. However fitting multi-exponential data is a non-trivial task and therefore, steps should be taken to ensure high quality data acquisition. The following discussion will focus on the effects of non-ideal refocusing pulses, multi-slice vs 3D acquisition, effects of diffusion, and finally the effects of inter-echo spacing and the ability to detect short T_2 values.

2.2.3.1 Effects of non-ideal refocusing pulses

CPMG sequences use multiple 180° refocusing RF pulses to generate a train of echoes, which constitute the T_2 decay curve. However, achieving a 180° flip angle uniformly across the brain is unlikely. This non-uniformity can occur when the wavelength of the RF pulse approaches the size of the object being imaged (e.g., brain). In this situation wave effects, for example standing waves, are created in the object resulting in a spatial variation of the magnitude of the RF pulse and therefore variation in the flip angle. At 3T the wavelength of an RF pulse, in vacuum, is about 2.43 m (calculated using the speed of light = 3×10^8 m/s; frequency of the RF pulse at 3T = 1.23×10^8 /s) which is clearly much longer than the size of a brain. However, the dielectric constant and conductivity of the brain is different from that of a vacuum, which has the effect of shortening the RF wavelength. Therefore, as the RF pulse travels through the brain its wavelength shortens and approaches the size of the brain creating wave effects and variation in the flip angle across the

brain (this phenomenon is sometimes referred to as dielectric resonance). Such artifacts are worse at higher field strengths.

2.2.3.2 Crusher gradients

When the refocusing flip angle is less than ideal (α pulse), the T_2 decay curve is contaminated by unwanted echoes, namely stimulated echoes and secondary spin echoes. The net effect of an α pulse, on the magnetization in the xy plane, can be understood by considering the α pulse as behaving as a 0°, 90°, and 180° RF pulses. Because the α pulse acts as 3 different pulses we say that the α pulse produces different pathways. The equations for calculating the fraction of the magnetization in the xy plane, which experience the 0°, 90°, and 180° RF pulses, can be found elsewhere (Liang & Lauterbur, 1999). Stimulated echoes are created when, following an α pulse, a fraction of the magnetization in the xy plane is rotated into the z axis and experiences T_1 relaxation. A subsequent α pulse rotates this magnetization back into the xy plane where the magnetization generates an echo. Because the magnetization experienced T_1 relaxation the amplitude of the stimulated echo is larger than the amplitude of the fraction of the magnetization which was not rotated into the z axis. Secondary spin echoes form when a fraction of the magnetization in the xy plane is unaffected by an α pulse. Subsequent α pulse's will eventually refocus a fraction of the initial magnetization, which was unaffected by the first α pulse, and this will form the secondary spin echoes.

Figure 2.8A is a T_2 relaxation decay curve generated from a dataset with very poor refocusing RF pulses. The effects of these unwanted echoes are apparent in Figure 2.8A with the amplitude of the first echo being smaller than that of the subsequent ones. These artifacts make multi-exponential fitting very difficult and therefore must be removed by improving data acquisition. Here we will focus on the use of large amplitude gradients, crusher gradients, as a method of

removing unwanted echoes. Recall that a certain fraction of the magnetization in the xy plane, which is unaffected by the α pulse, may subsequently be influenced by later α pulses and thus contribute an echo. The application of large amplitude gradients (crusher gradients) both before and after an α pulse can prevent spurious echoes from being generated after subsequent α pulses. To understand how crusher gradients work, consider its effects on the phase distribution of the spins.

First let's consider the ideal case with a 180° flip angle. The application of a crusher gradient creates a magnetic field inhomogeneity which causes dephasing of the spins and subsequent decrease in the magnetization. Following the 180° RF pulse, which as described earlier changes the sign of the phase values, application of the crusher gradient rephases the spins. Therefore, for a 180° RF pulse, there is no net effect of the crusher gradient. For an α pulse a fraction of the magnetization will experience a 0° pulse and will be rephased after subsequent α pulses generating spurious echoes. However, when applied after the α pulse, the crusher gradient will continue to dephase the magnetization, which experienced the 0° pulse, and if the dephasing is large enough this magnetization will not be rephased after subsequent α pulses. The use of large amplitude crusher gradients along with considerations of the design of the refocusing RF pulse (time-bandwidth constant, sinc vs rectangular pulse) can significantly improve the quality of the estimated T_2 decay curve. Figure 2.8B is a T_2 decay curve from a dataset, which is successful at minimizing spurious echoes. The residual effects of stimulated echoes can be accounted for during the fitting process and will be described later.

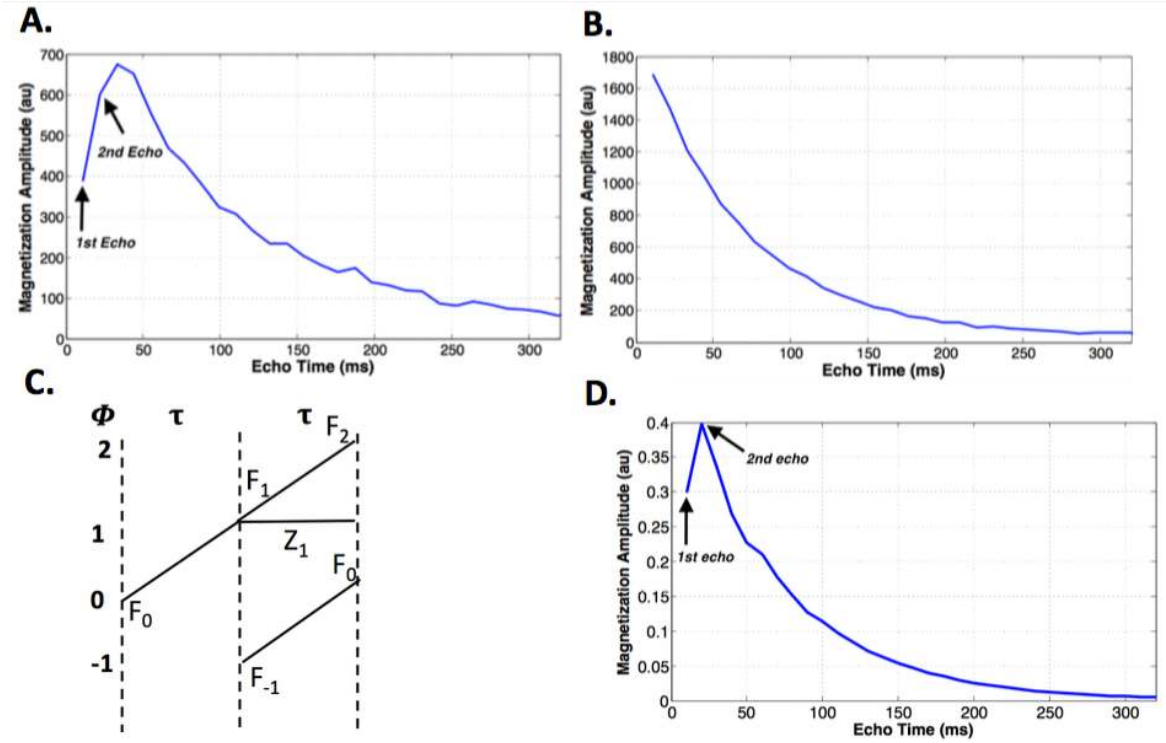

Figure 2.8: Unwanted echoes. (A) T_2 decay curve from a dataset with poor refocusing RF pulses. It's clear that the decay is corrupted with unwanted echoes. (B) T_2 decay curve from a dataset with large amplitude crusher gradients and hard refocusing RF pulses. The unwanted echoes are largely suppressed. Any residual unwanted echoes can be accounted for using the Extended Phase Graph (EPG) algorithm. (C) An extended phase diagram demonstrating how an α pulse, applied at τ, splits the magnetization (F_0) into 3 pathways (F_1,F_{-1},Z_1). The F_1 pathway continues to dephase as it experiences a 0° RF pulse, the F_{-1} pathways experiences a 180° RF pulse and will form an echo at 2τ. The Z_1 pathway experiences a 90° RF pulse and is stored along the z axis. (D) Using the EPG algorithm, a T_2 decay curve with unwanted echoes is simulated. This algorithm is used to account for residual unwanted echoes during the fitting process.

2.2.3.3 Multi-slice vs 3D Acquisition

The next consideration is the use of either 2D multi-slice or 3D imaging (phase encoding along the y and z axes). Faster data acquisition is theoretically possible with 2D multi-slice imaging, however, there are two primary limitations. First, because multi-slice imaging uses slice selective RF pulses, these pulses are off-resonance for nearby slices and act like magnetization transfer pulses (Dixon et al., 1990; Santyr, 1993). The effect of magnetization transfer pulses is greater for protons with shorter T_2 relaxation values, thus reducing the estimated size of this component (Vavasour et al., 2000). A detailed discussion on the basics of magnetization transfer (MT) can be

found elsewhere (Henkelman, Stanisz, & Graham, 2001) but a brief discussion will be provided to understand why MT effects are greater for protons with shorter T_2 relaxation values.

Protons associated with macromolecules (e.g., proteins) are restricted in their mobility and have T_2 relaxation values which are very short (less than 1ms) (Henkelman, Stanisz, & Graham, 2001). Therefore, these protons can be excited over a broad range of frequencies while protons associated with less restricted water have a relatively narrower range of frequencies over which they are excited. Thus, an RF pulse which is off-resonance with respect to the less resticted water protons, and therefore won't excite water protons, can excite protons associated with macromolecules. These excited protons can transfer their magnetization to water protons primarily through dipole-dipole interactions. Those water protons which have exchanged magnetization with the macromolecular associated protons no longer contribute to the net magnetization when an on-resonance RF pulse is applied to excite the water protons. Therefore, the net effect of MT is to reduce the magnetization of less restricted water protons.

The extent to which MT pulses affect less restricted water protons depends on the effectiveness of the magnetization transfer between macromolecular associated protons and the less restricted water protons. Dipole-dipole interactions are dependent on the distance between protons with stronger interactions occurring at shorter distances. Given that the short T_2 compartment consists of water protons near the macromolecular myelin sheaths we would expect that magnetization transfer would to be effective between the two. Vavasour et al (2000) found that when a MT pulse is followed immediately by excitation of water protons the size of the short T_2 compartment is reduced to a greater extent than the IE compartment. When the delay between an MT pulse and water proton excitation exceeded 200 ms the effect of MT was comparable between T_2 compartments. Therefore, in multi-slice imaging if slices are excited in sequential order there may

not be sufficient time for the effects of MT to have resolved (a delay of 700 ms still resulted in a detectable MT effect).

Second, multi-slice 2D imaging has a lower signal-to-noise ratio (SNR) compared to 3D imaging. Recall from a previous discussion that the images we generate are related to the data we collect through the Fourier Transform. In multi-slice 2D imaging each 2D image is generated by Fourier transforming the $N \times M$ K-space data to produce the $N \times M$ image. If we have z slices, then we have z $N \times M$ data in K-space. Thus, an image for each slice is produced using $N \times M$ data points (e.g., a 256×256 image consists of 65,536 data points). In 3D imaging, instead of having a 2D K-space we have a 3D K-space and the Fourier transform of this data set produces a 3D image. The number of data points used to generate a 3D image includes all the data points in the 3D K-space. As an example, consider a 256×256 image with 10 slices. For multi-slice 2D imaging this means we have 10 K-spaces' each of which contains 256×256 data points. An image for each slice will be generated using 65,536 data points. On the other hand, for 3D imaging we will have 1 K-space of size 256×256×10. The number of data points used to generate the 3D image will be 655,360. The greater SNR for 3D imaging is a significant advantage for quantification of the size of the short T_2 component, as this component inherently has a smaller signal.

2.2.3.4 Diffusion effects

Diffusion of water can potentially be a significant confound for the analysis of T_2 relaxation decay. Because we are interested in quantifying the different T_2 relaxation components, due primarily to the nuclear dipole-dipole interactions, any additional mechanisms which decrease the amplitude of the spin echoes, or contribute to irreversible spin dephasing, will incorrectly lead to inferences of short T_2 values. To understand how water diffusion can lead to irreversible spin dephasing lets first consider a case in which there is no water diffusion. In this case, local magnetic

field inhomogeneity's will dephase spins and reduce the magnetization. Following a 180° RF pulse the sign of the phase values will be changed. Because the spins are not diffusing they experience the same local field inhomogeneity's as they did prior to the 180° RF pulse. Therefore, the field inhomogeneity's will rephase the spins and increase the magnetization.

However, if the spins are diffusing, then they will no longer experience the same local magnetic field inhomogeneity's and will results in partial rephasing. This partial rephasing will result in a decrease in the amplitude of the echo. There are two main data acquisition parameters which can limit the effects of diffusion on the T_2 decay. The first parameter is the inter-echo spacing, τ. Equation 2.27 (Ronczka & Muller-Petke, 2012) describes the relationships between inter-echo spacing and diffusion related signal loss. $T_{2,D}$ refers to the T_2 relaxation effects related to water diffusion, D is the diffusion coefficient of water, G is the magnetic field gradient, γ is the gyromagnetic ratio and τ is the inter-echo spacing. By selecting the smallest possible value of τ the effects of diffusion on the T_2 decay are minimized.

The second parameter is the image pixel resolution. For high spatial resolution imaging the imaging gradients, which are usually considered as having negligible diffusion weighting, can contribute significant diffusion weighting and lead to estimates an underestimation of T_2 relaxation values (Oakden & Stanisz, 2014).

$$\frac{1}{T_{2,D}} = D\,\frac{(\gamma G\tau/2)^2}{3} \qquad \text{(Equation 2.27)}$$

2.2.3.5 Effects of inter-echo spacing

Finally, the choice of the inter-echo spacing has important implications for the T_2 relaxation values which can be recovered from a multi-exponential T_2 decay. Let's consider a bi-exponential decay with T_2 values of 20 ms for the fast decaying component and 60 ms for the relatively slower decaying component. If the inter-echo spacing is 20 ms then the fraction of the signal from the fast

decaying component in the first 3 echoes (20,40,60 ms) will be 36.8, 13.5, and 5%. For the slow decaying component, the fraction of the signal in the first 3 echoes are 71.7, 51.3 and 36.8%. If the inter-echo spacing is reduced to 10 ms, the fraction for the fast decaying component in the first 3 echoes (10,20,30 ms) will be 60.7, 36.8, and 22.3% (Table 2.1). It is evident from these values that the shorter the inter-echo spacing relative to the T_2 relaxation value, the greater the fraction of signal at each echo. This highlights the fact that if one wants to quantify the fast-relaxing component of a multi-exponential decay, short inter-echo times should be used so that this component contributes sufficient signal to allow for its fitting.

Inter-Echo interval	**% Signal: Echo 1**	**%Signal: Echo 2**	**%Signal: Echo 3**
20 ms	36.8	13.5	5
10 ms	60.7	36.8	22.3

Table 2.1: Effects of inter-echo spacing. The fraction of the signal for the fast decaying component for two values of the inter-echo interval are shown.

2.2.4 Multi-exponential fitting

We will define time, *t*, as the echo times (which occur at $2N\tau$ intervals as discussed previously) and the magnitude of the magnetization of the T_2 relaxation decay curve at *t* as *y(t)*. For a single T_2 compartment the T_2 relaxation decay curve is described as a mono-exponential decay (Equation 2.28). Fitting a mono-exponential function to a single compartment T_2 decay curve is trivial and the fitting provides estimates of the T_2 of the compartment as well as the magnitude or size of the compartment (M_0^{xy}).

$$y(t) = M_0^{xy} e^{-t/T_2} \qquad \text{(Equation 2.28)}$$

However, for multiple water compartments the T_2 relaxation decay curve is described as a multi-exponential decay. Multi-exponential T_2 (ME-T_2) relaxation decay curves can be modeled

as linear a superposition of exponentials (*M* exponential functions), each with a unique magnitude (M_0^i for the i[th] exponential function) and T_2 (Equation 2.29).

$$y(t) = \sum_{i=1}^{M} M_0^i \, e^{-t/T_2^i} \qquad \text{(Equation 2.29)}$$

There are two approaches to fitting multi-exponential such data, linear and non-linear. Non-linear methods require the user to provide a priori knowledge for the optimization and such methods can have difficulties converging to a global optimal solution (Hansen, 1992). Linear methods do not require a priori knowledge and converge to a global solution, but they require many exponentials, most with zero amplitudes, to solve the optimization (Lawson & Hanson, 1974). This dissertation focuses on the commonly used linear optimization method, namely the regularized Non-Negative Least Squares (rNNLS) algorithm (Kroeker & Henkelman, 1986; Lawson & Hanson, 1974; Whittall, 1989; Whittall et al., 1991; Whittal et al., 1997). The field of linear optimization is a vast research enterprise and beyond the scope of this dissertation. We will focus specifically on Tikhonov regularization (Hansen, 1992) and generalized cross validation as a method of choosing the optimal regularization parameter (Craven & Wahba, 1979; Golub et al., 1979). Using linear methods equation, 2.29 is solved for the amplitudes of the *M* exponential functions. The T_2 values are provided to the algorithm by logarithmically spacing *M* T_2 values between a specified range.

The regularized NNLS algorithm minimizes the objective function:

$$\min\{\|Ax - y\|^2 + \lambda\|\Gamma x\|^2\} \; s.t. \; x \geq 0 \qquad \text{(Equation 2.30)}$$

where λ is the regularization parameter, Γ is a $N \times M$ identity matrix, A is a $N \times M$ matrix of weights with $A_{ij} = e^{-t_i/T_{2,j}}$ (i=1,2, ..N and j = 1,2,..M) and x is the $M \times 1$ vector of amplitudes, for the M exponentials, we are solving for. Multi-exponential fitting tends to be an ill-posed problem and in the absence of regularization (λ=0) the solution to equation 2.30 either does not exist or is not

unique and tends to be sensitive to noise. Regularization produces a unique solution and is less sensitive to noise. Furthermore, regularized solutions tend to produce a continuous distribution of T_2 amplitudes, which is a more biologically plausible solution than the discrete solutions generated without regularization. The magnitude of the regularization parameter λ controls the amount of weight given to the regularization. If λ is too large the solution will contain mostly 0 amplitudes and will not adequately represent the data. If λ is too small the solution will be sensitive to noise and produce non-zero amplitudes for T_2 values which do not exist, thus overfitting the data. Generalized cross validation (GCV) is a statistical method for finding the optimal value for λ. I will describe how GCV conceptually works by describing an alternative method, cross validation, though it should be noted that the optimal value of λ can be found, using GCV, simply by minimizing equation 2.31.

$$\min\left\{\frac{(y-Ax)^T(y-Ax)}{Tr\left(I-A\left(A^TA+\lambda I\right)^{-1}A^T\right)}\right\} \qquad \text{(Equation 2.31)}$$

Generalized cross validation is like the method of cross validation however, it is computationally efficient for linear problems and is insensitive to orthogonal transformations of the data. It is not obvious from equation 2.31 how GCV works, however the cross-validation method is more straightforward and therefore I will describe this method. For a specific value of λ equation 2.30 is solved N times. During each iteration one data point is removed and equation 2.30 is solved. The value of the "missing" data is then predicted and the square of the residual is calculated. After repeating this process N times, each time removing a different data point, the sum of the squared residuals is calculated. By testing various values of λ the optimal value is the one which minimizes the sum of the squared residuals. It is obvious that this method is computationally intensive. Generalized cross validation yields the same result and is computationally simple.

In addition to the rNNLS algorithm we also use the Extended Phase Graph (EPG) algorithm (Hennig, 1988; Prasloski et al., 2011) to account for stimulated echoes. The EPG algorithm tracks how the initial transverse magnetization is divided into various pathways because of the α pulse (Figure 2.8C). Figure 2.8D is a simulation of a T_2 decay curve contaminated with unwanted echoes generated using the EPG algorithm. The application of the EPG algorithm allows for modeling stimulated echoes in the T_2 decay and enables estimation of the M exponential amplitudes.

Once an optimal solution is found it can be plotted on semi-log plot where the x axis consists of M T_2 values spaced logarithmically apart (Figure 2.9). This representation of the solution is referred to as a T_2 distribution. Figure 2.9 shows two continuous distributions one with a short T_2 value of 13.7 ms and the other with a T_2 value of 62.8 ms. The short T_2 peak defined as T_2 values between 10-40 ms and the peak between 40-200 ms are referred to as the myelin and intra/extracellular water compartments respectively.

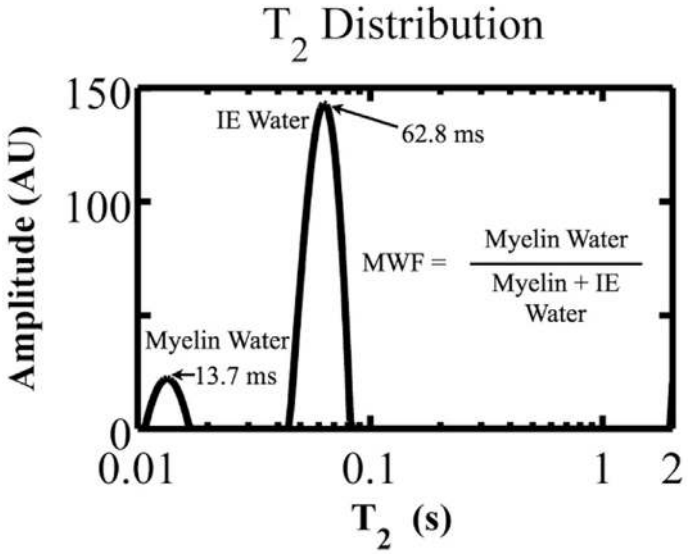

Figure 2.9: T_2 Distribution**.** The T_2 distribution is a plot of amplitudes for the exponentials. The x axis is on a logarithmic scale withT_2 values ranging from 10 to 2000 ms. The T_2 distribution clearly identifies 2 continuous peaks. The peak with the shortest T_2 value originates from water trapped between the myelin bilayer. The peak with the longer T_2 is thought to originate from water in the intra/extracellular space.

There are two indices which can be derived, for each compartment, from the T_2 distribution. The first index is the geometric mean T_2 (geomT_2). The geomT_2 is simply the mean T_2 for each compartment adjusted for the logarithmic spacing of the T_2 values. The second index is the fractional size of each compartment, referred to as the Myelin Water Fraction (MWF) or the Intra/Extracellular Water Fraction (IEWF) (Equations 2.31-2.32). As is evident from equations 2.32 and 2.33 the MWF and IEWF are not independent measures as both are normalized to the sum of the amplitudes of the entire T_2 distribution.

$$MWF = \left. \sum_{T_2=10ms}^{T_2=40ms} T_2 \right/ \sum_{T_2=10ms}^{T_2=2000ms} T_2 \qquad \text{(Equation 2.32)}$$

$$IEWF = \left. \sum_{T_2=40ms}^{T_2=200ms} T_2 \right/ \sum_{T_2=10ms}^{T_2=2000ms} T_2 \qquad \text{(Equation 2.33)}$$

While an absolute size of each compartment would potentially be a better index, the fractional size of a compartment is still a meaningful index under the correct circumstances. First, as will be discussed in later chapters, subjects in the studies in this dissertation are healthy individuals and do not have neurological disease. Diseases such as Multiple Sclerosis (MS) and Phenylketonuria (PKU) are associated with additional T_2 relaxation peaks, in the T_2 distribution, with T_2 relaxation values longer than the IE water (Laule et al., 2007; Sirrs et al., 2007). These additional proton compartments confound the interpretation of changes in MWF. An increase in the total number of protons, due to edema, could reduce MWF without any changes to the myelin water. Absolute measures of the compartment size on the other hand would be robust to such effects. However, in non-pathological cases, such as the subjects in this study, subcortical white matter consists of only the myelin and IE water compartments. In this case, an increase in one compartment necessitates a decrease in the other. An increase in MWF could occur in one of two ways. First, an increase in

total myelin, which would be accompanied with an increase in myelin water, would obviously increase the MWF. The other possibility is a decrease in the IE compartment with the myelin water compartment remaining unchanged. One possible scenario where this may occur is dehydration. While this potential confound should always be kept in mind dehydration that is severe enough to significantly affect IE fluid balance would be expected to be symptomatic. More information on hydration will be provided in the following paragraph. Conversely a decrease in MWF could also occur in two ways. First, loss of myelin, which would be associated with a decrease in myelin water, would result in a decrease in MWF. The other possibility is an increase in the IE water. However, an increase in the IE water would occur in pathological conditions associated with additional water compartments. As already stated subjects in this study are free of neurological disease. Another possibility is an increase in hydration.

Myelin water fraction is expected to depend on the total water content (TWC), reflecting hydration status, because it is defined as the myelin water content divided by the TWC. Therefore, MWF as currently expressed, is proportional to myelin content but not equal to myelin content. This limits the interpretation of MWF as a reflection of the myelin thickness. Therefore, it is critical to evaluate how sensitive MWF is to physiological changes in hydration status. Meyers et al (2016) have recently conducted a study of the effects of hydration on TWC in conditions considered routine for clinical procedures (e.g., overnight fasting). The authors collected a multi-echo T_2 dataset, multiple inversion-recovery sequence for T_1 mapping, and a structural T_1 weighted image. Imaging was collected over three days with different hydration conditions. In addition to the imaging data, body weight and urine was collected to confirm changes in hydration status (using urine specific gravity measures).

During day one, imaging, urine, and body weight data were collected. After data collection hydration was increased by having subjects consume 3L of water over 12-16 hours for scanning the following day. After data collection on day two subjects were dehydrated with overnight fasting (no fluids or food) for 9 hours for the following days scan. The authors took several steps to minimize potential confounds for the TWC calculation. TWC was calculated by summing the T_2 distribution and correcting for T_1 relaxation and RF inhomogeneity. TWC was calculated in 14 brain regions which included subcortical white matter tracts, subcortical structures and the cortex. Despite changes in bodyweight and urine specific gravity, indicating change in hydration status, the authors did not find statistically significant differences in TWC across hydration status or from baseline.

Therefore, while the use of a fractional compartment size is less than ideal it nonetheless provides a measure reflective of myelin content when the population under investigation is free of neurological disease with associated edema. Furthermore, even healthy subjects in whom it's reasonable to assume that there will be differences in hydration status, within physiological range, Meyer's et al. suggests there are no differences in TWC. These results do not imply that the fractional compartment sizes are robust to all hydration status changes. Animal models of severe changes in hydration have reported changes in TWC ranging from 5-18% (Ayus, Armstrong, & Arieff, 1996; Cserr et al., 1991; Harreveld, Collewijn, & Malhotra, 1966). However, under physiological conditions it is not surprising that water content is closely regulated considering that hypo or hypernatremia could have severe consequences for neuronal function.

CHAPTER 3: Cognitive modeling

Computational models of cognitive functions have been developed for a broad range of functions including spatial memory (Madl et al., 2015), working memory and learning (O'Reilly & Frank, 2006), visual categorization (Shen & Palmeri, 2016) and perceptual decision making (Busemeyer, 1985). Computational models explicitly describe the processes or psychological mechanisms which are hypothesized to form the basis of cognitive function, while explicating the assumptions. By modeling cognitive processes, computational models allow researchers to test hypothesis about specific process and investigate their putative neural correlates. In this dissertation, we will focus specifically on computational models of perceptual decision making.

Perceptual decision-making tasks usually involve the presentation of a stimulus and require the observer to identify stimuli embedded in arrays of alternatives (e.g., presenting a letter for a brief period and asking the subject to identify the letter among a set of other letters). When the subject is presented with two choices, one of which is the stimulus, the task is sometimes referred to as a choice reaction time task. Reaction time (RT) is usually defined as the interval between the onset of the stimulus presentation and the initiation of a response (Pachella, 1974). Reaction time data, generated from these tasks, are commonly used to assess information processing speed (Salthouse, 2000).

A significant limitation of most studies is the use of a mean or median to characterize the RT distribution. This is a serious concern specially in aging research. Compared to younger adults, older individuals tend to emphasize accuracy over speed (Salthouse, 1979). This can increase the mean or median RT for older adults, when compared to younger adults, and incorrectly suggest that older adults process information slowly. Furthermore, some component of the slow RT observed in older individuals may be due to a slowing of peripheral nerve motor conduction

(Mallik & Weir, 2005). However, cognitive modeling of the RT data can overcome these limitations. Using adult age groups ("college students", 60-74 & 75-85 years old) Ratcliff et al (2006) demonstrated that across four reaction time tasks the younger age group consistently had a shorter RT when compared to the older age groups. However, after using the diffusion model to analyze the data (the diffusion model is described in the following paragraph) they found no differences in cognitive processing in some tasks when comparing "college students" to 60-74 year olds. This demonstrates how age differences in RT may not necessarily imply age differences in cognitive processing speed.

The Ratcliff diffusion model (Ratcliff, 1978; Ratcliff & McKoon, 2008), simply referred to as the diffusion model, presumes that the reaction time data originated from a process of accumulating noisy evidence up to a threshold (Figure 2.10). Noise can be conceptualized as originating from neural circuits which process the stimuli, indeed neurons driven with identical stimuli over repeated trials will produce variability in the timing of their action potentials (Faisal, Selen, & Wolpert, 2008). Therefore, to decide one needs sufficient evidence favoring one of the alternatives over the other. The observed reaction time is decomposed into two parts, decision time and non-decision time (Ter). The non-decision time is the amount of time related to non-cognitive components, for example the time to execute a motor response once a choice is made. The decision time is the time related to cognitive processing until a choice is made. According to the described accumulator model, a choice is made when sufficient evidence is accumulated.

In Figure 2.10 the amount of evidence needed to decide is represented by the dashed lines horizontal lines (a, -a). Assuming there is no bias for a response, that is the subject has no preference for one of the two response choices, then at the beginning of the task the subject starts with no evidence and moves towards one of the two horizontal lines during the presentation of the

stimulus. The colored traces (green, black, and red) in Figure 2.10 represent the accumulation of evidence for 3 trials of the task. Note that for each of these trials the time at which each trace reaches a boundary is different. This reflects the fact that the accumulated evidence is sampled from a noisy signal and therefore, for each trial, the evidence accumulation will be stochastic, which makes it mathematically equivalent to a diffusion process. While each trial has a stochastic component, it also contains a non-stochastic component, the drift rate (*v*). Thus, for any given trial the evidence accumulation consists of both a stochastic diffusion process and a non-stochastic drift process. The drift rate is considered a more direct measure of processing speed as it reflects the cognitive process and is no longer confounded by the speed-accuracy tradeoff.

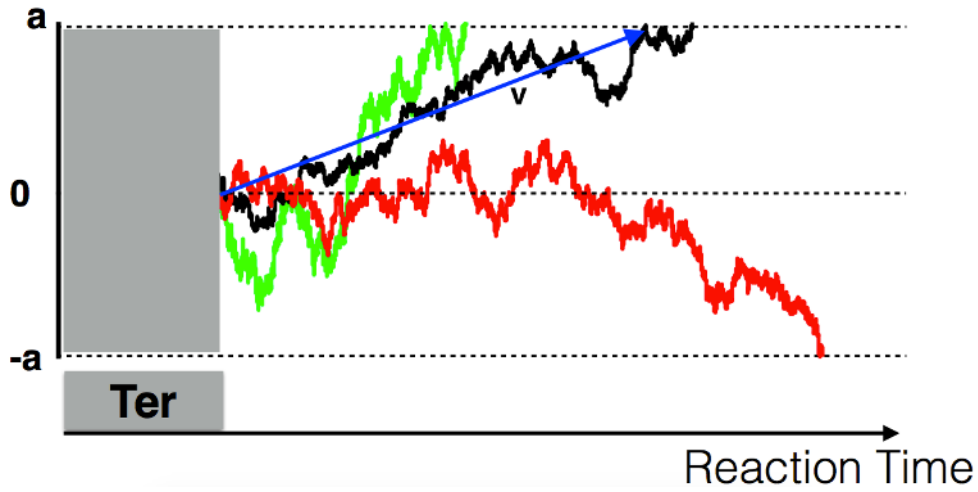

Figure 3.1: Drift diffusion model. The diffusion model separates the reaction time into a non-cognitive component, the non-decision time (Ter) and a decision time. The decision time reflects the cognitive process of accumulating noisy evidence till a sufficient amount is reached. The rate of information accumulation is represented by the drift rate (v).

Two methods of fitting the diffusion model to reaction time data are Diffusion Model Analysis Toolbox (DMAT) (Vandekerckhove & Tuerlinckx, 2008) and the EZ-diffusion model (Wagenmakers et al., 2007). DMAT implements the full diffusion model (includes across trial variability in parameters), which may be a strength of that method. However, we found that during the optimization process the Hessian matrix (matrix of second-order partial derivatives of the

models' parameters) was either non-invertible or contained 0's along the diagonal. Because DMAT uses maximum likelihood estimates, standard errors are calculated by inverting the Hessian matrix at the maximum likelihood estimate. Therefore, if the Hessian matrix is non-invertible, or contains 0's along its diagonal, the standard errors of the parameter estimates are unreliable as is it the optimal solution. While these errors are ignored and not reported in publications they should be taken seriously (Ratcliff & Childers, 2015). To overcome the limitations of DMAT we used the EZ model.

The EZ model simply computes the parameters of interest without fitting the full diffusion model to the reaction time data (the percentage of correct responses, and the mean and variance of the correct responses are transformed into the parameters of interest). The EZ model has been for not including all the parameters of the full diffusion model and therefore not accounting for specific features in the data (e.g: shifting of the leading edge of RT distribution; Ratcliff, 2008). However, these additional features, which require the full diffusion model, are usually observed in experiments designed to observe them, which was not the case for our task. Whether such patterns are found in simple experiments is unclear (Ravenzwaaij, et al., 2016). If the data do not have sufficient "features" to constrain the estimates of the model parameters the standard errors of the estimates will increase. Thus, we chose to use the EZ diffusion model to generate estimates for the drift rate as a measure of information processing speed. In doing so we accounted for the well-known speed-accuracy trade off and for the non-decision component of the reaction time.

CHAPTER 4: Test-Retest Reliability of ME-T_2 Indices

4.1 Summary

In an age-heterogeneous sample of healthy adults, we examined the test-retest reliability of multi-echo T_2 (ME-T_2) Imaging indices, namely Myelin Water Fraction (MWF) and the geometric mean T_2 of the intra/extracellular compartment (geom$T_{2\text{-IEW}}$). Assessing reliability is critical to ensure that indices are suitable for both cross-sectional and longitudinal investigations as unreliable measures will necessarily decrease the power to detect effects of interest. Test-retest reliability was assessed both with and without subject repositioning. The results revealed high reliability of both MWF and geom$T_{2\text{-IEW}}$, both with and without repositioning, and overlapping 95% confidence intervals of the intraclass correlation (ICC) coefficient across six cerebral white matter regions. We conclude that ME-T_2 indices are highly reliable and well suited for longitudinal investigations.

4.2 Introduction

In the central nervous system myelin, a lipid rich structure, plays a critical role in ensuring speed and fidelity of neural transmission and the efficiency of axonal energy metabolism (de Hoz L, & Simons, 2015; Saab et al., 2013). Structural alterations of the myelin sheath as well as the reduction of myelin content have been proposed as neuroanatomical substrates of age-related cognitive decline (Bartzokis, 2004; Lu et al., 2013). Therefore, valid in vivo methods of evaluating myelin content and changes therein is a high priority.

The multi-echo T_2 derived index, MWF, is considered a standard method for estimating myelin content (Alonso-Ortiz, 2015; Billiet et al., 2015). In addition to MWF, the geom$T_{2\text{-IEW}}$, also an ME-T_2 derived metric, provides additional characterization of white matter microstructural properties (see Chapter 2 for more information). Because of myelin's central role in theories of

cognitive aging and the importance of longitudinal studies for investigating time-dependent processes (Baltes & Nesselroade, 1979; Lindenberger et al., 2011), it is critical to ensure the test-retest reliability of MWF. Because the position of a participants head in the scanner will inevitably vary over multiple measurement occasions, sensitivity of ME-T_2 indices to repositioning is critical to assess. Finally, it is also important to determine whether ME-T_2 indices are equally reliable across multiple regions as differential reliability threatens inferences of heterochronicity of brain aging proposed in the extant literature (Fjell et al., 2014; Raz & Rodrigue, 2006).

A previous study used Pearson correlations between two scans to assess test-retest reliability and the authors concluded high test-retest reliability of MWF (Meyers et al., 2009). However, Pearson correlations, unlike intraclass correlation (ICC), is insensitive to linear changes in measures over occasions. In two small sample studies (N<10 in each) MWF was deemed less reliable than geom$T_{2\text{-IEW}}$ but no ICC values were reported (Levesque et al., 2010; Vavasour et al., 2006).

The main objective of this study, therefore, was to evaluate the test-retest reliability of ME-T_2 indices in subcortical white matter tracts chosen as representatives of commissural, associative and projection fibers. Based on previous work we hypothesized that MWF and geom$T_{2\text{-IEW}}$ would meet our criterion (ICC $\geq$ 0.80) of reliability for both participant repositioning and without repositioning.

4.3 Methods

4.3.1 Participants

Twenty healthy adult participants were recruited from the Detroit metropolitan area. They were screened via a questionnaire for history of neurological and psychiatric disorders, cardiovascular disease (other than medically treated hypertension), endocrine and metabolic disorders, head injury

accompanied by loss of consciousness for more than 5 minutes, use of antiepileptic, anxiolytic and antidepressant medications. Participants were equally divided by sex with a mean age ± SD = 45.9 ± 17.1 years and a range of 24.4-69.5 years. There was no age difference between males and females: $t(18) = -.81$, $p = 0.43$

4.3.2 Study Design

The MRI data were collected in a single session divided into two parts (Figure 4.1). The first part, part 1, was devoted to collecting structural T_1-weighted and T_2-weighted images and two ME-T_2 images. The ME-T_2 images, referred to as run 1 and run 2, were collected back-to-back, without participant repositioning. After completing part 1 the participant was removed from the scanner and given a 5-minute break, after which they were repositioned in the scanner (part 2). In part 2 we repeated the structural T_1 and T_2-weighted images along with one ME-T_2 image (run 3).

4.3.3 MRI acquisition protocol

Data were collected on a 3T Siemens MAGNETOM Verio™ MRI system using a 12-channel volume head coil. The T_1-weighed images were acquired in the axial plane with isotropic voxels (1 mm^3) using the magnetization prepared rapid gradient-echo (MPRAGE) sequence with a repetition time (TR) = 2,400 ms, echo time (TE) = 2.63 ms, flip angle (FA) = 8°, inversion time

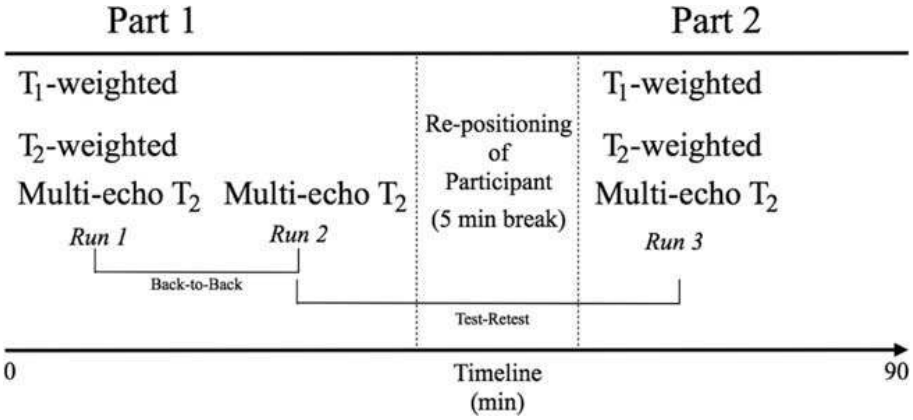

Figure 4.1: Diagram of the study design. The imaging session was a total of 90 minutes divided into two parts.

(TI) = 1,100 ms, matrix size = 256 χ 256, number of slices = 160, GRAPPA factor = 2, and acquisition time (TA) = 8:07 minutes. ME-T_2 images were also acquired in the axial plane using the 3D gradient and spin echo (GRASE) sequence, developed by Dr. Jongho Lee, Seoul National University, Republic of Korea). Acquisition parameters were as follows: TR = 1,100 ms, number of echoes = 32, first echo = 11 ms, inter-echo spacing = 11 ms, field of view (FOV) = 190 χ 220 mm^2, matrix size = 165 χ 192, in-plane resolution = 1.1 χ 1.1 mm^2, slice thickness = 5 mm, number of slices = 24, slice oversampling = 0, and TA = 17 minutes.

4.3.4 Processing of ME-T_2 data

Our processing pipeline was developed with the overall goal of generating MWF and geom$T_{2\text{-IEW}}$ values for each region of interest (ROI) in the subject space. ROIs were defined in standard space (MNI152) and mapped from standard space to subject space followed by voxel-wise ME-T_2 relaxation analysis. ME-T_2 relaxation analysis was conducted using a combination of FMRIB Software Library (FSL), in-house Linux shell scripts and MATLAB (MathWorks, Natick, MA) programs.

Each ME-T_2 dataset was interpolated to 2.5-mm thickness and co-registered to the T_1-weighted image from part 1 using the FSL FLIRT tool (Jenkinson et al., 2001, 2002) with 6 degrees of freedom (Step 1 in Figure 4.2). Procedure to generate the ROIs in the subject space will be described in the section below. ROI masks were applied to the multi-echo data followed by ME-T_2 relaxation analysis using the rNNLS algorithm along with the EPG algorithm to account for non-ideal refocusing flip angles. The optimal value for the regularization parameter was determined via Generalized Cross Validation (see Chapter 2 for more information). T_2 distributions were generated using 200 logarithmically spaced T_2 relaxation values ranging from

10 to 2,000 ms. The myelin water was defined as T_2 relaxation times between 10 to 40 ms and between 40 to 200 ms for the intracellular/extracellular water.

4.3.5 Regional parcellation

ROIs were defined in FSL (Jenkinson et al., 2002) using the Johns Hopkins University (JHU) and ICBM-DTI-81 white matter atlas (Hua et al., 2008; Wakana et al., 2007), in standard space. Step 2 in Figure 4.2 shows the 6 ROIs in the subject space. To generate the warp field for mapping from standard to subject space, we used the FSL nonlinear registration tool FNIRT to register the T_1-weighted image from part 1 to the MNI152 image in standard space. The resultant warp field was saved and inverted and used to map all ROIs from standard to subject space.

To minimize partial voluming we segmented the T_1-weighted image from part 1 into white matter, gray matter and cerebrospinal fluid using the FSL tool FAST (Zhang et al., 2001). We then applied the ROI masks to the segmented white matter and set a threshold of 0.95 followed by binarizing the masks. These steps ensured that our ROI masks consisted of white matter with a probability of 0.95 or greater. To minimize rounding errors MWF values were multiplied by 100, resulting in units of percentage. The $geomT_{2\text{-}IEW}$ was multiplied was 1,000 resulting in units of milliseconds (ms).

The selected regions included two commissural tracts: genu and splenium of the corpus callosum; two association tracts: superior longitudinal fasciculus and the inferior fronto-occipital-fasciculus; and two projection fibers: anterior and posterior internal capsules.

The ROIs were selected for both theoretical and practical considerations. First, we selected tracts which vary in their functional and ontogenetic properties. Second, we selected those regions which contain primarily white matter and would be least prone to partial voluming artifacts. Finally, three of the ROIs would also be used in the third aim of this thesis.

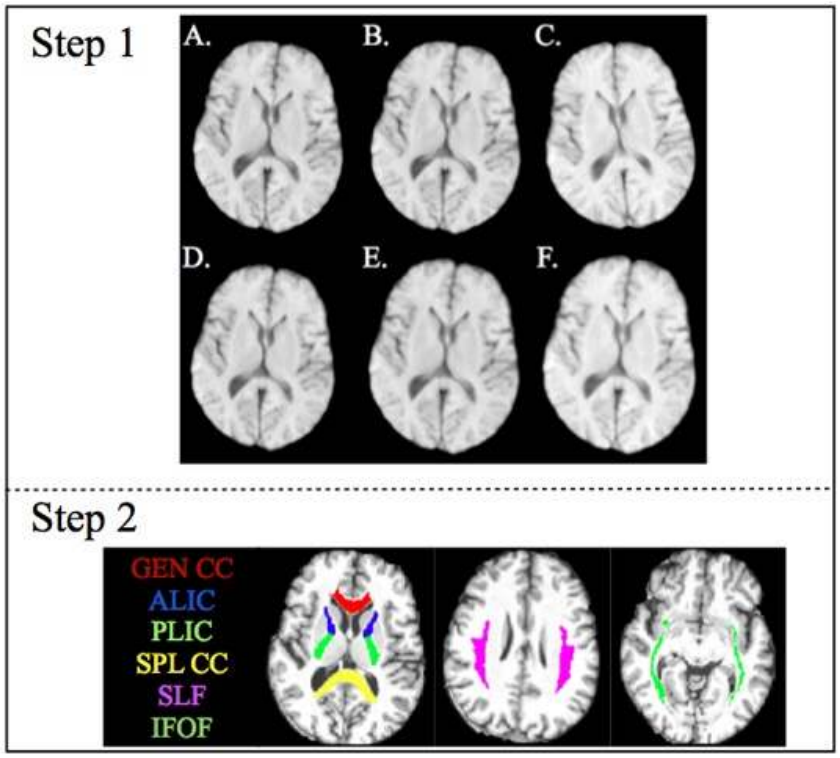

Figure 4.2: Registration steps**.** Step 1 demonstrates the 6 degree of freedom FLIRT registration of the 3 ME-T_2 runs with the T_1-weighted image from part 1. (A) Run 1 (B) Run 2 (C) Run 3. (D-F) are Runs 1-3 (A-C) after registration to the T_1-weighted image. Note the different head position in Run 3 (C), compared to Runs 1 and 2, which was collected after repositioning the participant. Step 2 demonstrates the mapping of the 6 ROIs from MNI space to subject space. ROIs include two midline commissural tracts: genu (GENU CC) and splenium (SPL CC) of the corpus callosum; two bilateral association tracts: superior longitudinal fasciculus (SLF) and the inferior fronto-occipital fasciculus (IFOF); and bilateral projection fibers: anterior (ALIC) and posterior (PLIC) limbs of the internal capsule.

4.4 Statistical Analysis

Reliability was assessed using the intraclass correlation coefficient, namely ICC(1,1) (Shrout & Fleiss, 1979). It should be noted we consider a run of the ME-T_2 acquisition as being equivalent to what Shrout and Fleiss (Shrout & Fleiss, 1979) refer to as method or rater. ICC Case 3 assumes each run is fixed and therefore the results can be generalized only to identical runs. This assumption is unrealistic because generalizing to other runs (e.g., different scanners, different days) is prevented. Case 1 assumes that each run is different, and is drawn randomly from a set of all possible runs. Each run is considered as the application of randomly selected scanner configuration/hardware state, from a set of all possible scanner configurations, at a randomly

selected time. Therefore, a run as we have defined it, rules out Case 2 and only applies to Case 1, hence our selection of ICC(1,1).

We used ICC(1,1) to assess reliability for both the back-to-back runs, namely runs 1 and 2, and to assess reliability after repositioning, using runs 2 and 3. We generated bootsrapped 95% confidence intervals, using 5,000 samples, for the ICC values. The analyses were also conducted by combing all ROIs (aggregated ROI) and for each ROI independently. ICC values $\geq$ 0.80 were considered reliable. All statistical analyses were conducted using MATLAB version 2012a (MathWorks, Natick, MA).

4.5 Results

ICC values for both ME-T_2 indices, at the level of individual ROIs, exceed our threshold of reliability, except for the SLF, whose ICC value for MWF was 0.79 (Table 4.1) after repositioning. However, dropping one observation with an extreme MWF value increased the ICC to 0.84. Additionally, the overlapping 95% confidence intervals, suggest uniform reliability across the ROIs. With all ROIs aggregated, into a global region, both indices exceed our ICC criteria for both the back-to-back run and after re-positioning.

	MWF (%)		$geomT_{2\ -\ IEW}$ (ms)	
ROI	Back-to-Back	Repositioning	Back-to-Back	Repositioning
ALIC	0.94 0.85–0.97	0.83 0.64−0.91	0.98 0.92–0.99	0.93 0.75−0.97
PLIC	0.90 0.74–0.96	0.86 0.75−0.92	0.95 0.84–0.98	0.94 0.81−0.98
Genu CC	0.94 0.87–0.97	0.83 0.64−0.93	0.99 0.98–0.99	0.99 0.96–0.99
Splenium CC	0.95 0.89–0.98	0.88 0.77, 0.94	0.98 0.94–0.99	0.97 0.92−0.98
SLF	0.95 0.90–0.97	0.79[a] 0.55, 0.93	0.98 0.90–0.99	0.96 0.75−0.99
IFOF	0.95 0.87–0.98	0.81 0.60, 0.91	0.96 0.93–0.98	0.90 0.80−0.97
Aggregated ROIs	0.97 0.96–0.98	0.93 0.90, 0.95	0.99 0.98–1.0	0.98 0.98–0.99

Table 4.1: Reliability summary. Reliability of ME-T_2 indices on back-to-back and respositioning runs. ICC with 95% confidence intervals. ALIC – anterior limb of the internal capsule; PLIC- posterior limb of the internal capsule; Genu CC- genu of the corpus callosum; Splenium CC- splenium of the corpus callosum; SLF-superior longitudinal fasciculus; IFOF- inferior fronto-occipital fasciculus; ROI – region of interest; [a]Dropping one subject increases the ICC value to 0.84.

4.6 Discussion and Limitations

The indices of myelin content (MWF) and the intra/extracellular water compartment ($geomT_{2\text{-}IEW}$) derived from ME-T_2 imaging show adequate reliability making them suitable for longitudinal studies. Of note, both indices were equally reliable across the regions investigated. This uniformity mitigates concerns of differential unreliability which could threaten the validity of conclusions based on differences among associations between regional myelin content and variables of interest such age (see Chapter 4). It should be noted however, given the wide confidence intervals, that in a larger sample small differences in reliability across regions could be detected.

In addition, due to time constraints we could not add an additional run prior to participant repositioning and compare run 3 to run 4 (participant repositioning). We had to rely on comparing run 2 with run 3 to evaluate the effects of repositioning. Because run 2 was already a part of the back-to-back analysis this introduces a dependence in the estimation of the repositioning effects. Nonetheless, our study confirms the high reliability of ME-T_2 indices (with greater reliability of $geomT_{2\text{-}IEW}$ compared to MWF) in a larger sample with a wider age range than previously reported (Levesque et al., 2010; Meyers et al., 2009; Vavasour et al., 2006).

4.7 Conclusions

Both MWF and $geomT_{2\text{-}IEW}$ are highly reliable over multiple white matter tracts, making ME-T_2 imaging suitable for in vivo longitudinal studies of regional myelin content.

CHAPTER 5: Adult age differences in subcortical myelin content

5.1 Summary

Post mortem studies suggest protracted myelination of subcortical white matter into middle age followed by a decline in late adulthood. However, establishing the proposed inverted U pattern of age-myelin association has proven difficult to investigate in vivo. The most commonly used method to investigate white matter, diffusion tensor imaging (DTI), usually reveals linear associations between age and the supposed myelin specific DTI indices. Using a novel method of estimating the myelin water fraction (MWF), based on the acquisition of multi-echo data and modeling T_2 relaxation components, we assess the relationship between age and subcortical myelin content in six white matter tracts. Myelin content evidenced a quadratic relationship with age consistent with the pattern observed in postmortem studies. Furthermore, the magnitude of age differences in MWF varied across white matter tracts. Finally, the commonly reported DTI indices, fractional anisotropy (FA) is unrelated to MWF and is related to radial diffusivity (RD) only in the splenium. These results provide in-vivo support that MWF is associated with myelin content given that the reported MWF age associations are consistent with postmortem associations between age and myelination. Finally, studies which use DTI indices to assess changes or differences in myelin content are discouraged.

5.2 Introduction

Postmortem studies in non-human primates and in humans have demonstrated life-span age differences in white matter, including regional variations in myelin content (Kaes, 1907; Peters, 2002; Yakovlev 1966). These studies suggest progressive myelination continuing into the fourth decade of life with association cortices exhibiting the greatest age difference from infancy to middle age (Kaes, 1907; Yakovlev 1966). However, the limitations of post-mortem studies include

the inability to evaluate change over time and concurrent assessment of cognition. Given the hypothesized role of age related myelin reduction as a potential neuroanatomical substrate of age related differences in cognition (Bartzokis, 2004; Lu et al., 2013) there is a need for valid and reliable in vivo measures of regional myelin content.

Early studies of age differences in white matter volume suggested non-linear age trends (Bartzokis et al., 2001; Raz et al., 2005 but see Raz et al., 1997; Raz et al., 2004), however, gross volume is a coarse measure of myelin content as it also reflects contributions from glia and axons. The development of diffusion tensor imaging (DTI) (Basser, Mattiello, & LeBihan, 1994) enabled the assessment of white matter microstructure through the examination of water diffusion. Because myelin sheaths constitute a barrier to the diffusion of water it is plausible that the degree of myelination maybe represented by the DTI indices fractional anisotropy (FA) and radial diffusivity (RD). Several studies provide support for the claim that DTI indices are sensitive to myelin content (Gulani et al., 2001; Song et al., 2003), indeed age differences in RD are frequently interpreted as evidence of differences in myelin content (Lebel et al., 2012).

To date, DTI has been the prominent tool for investigating age differences in myelin content, with RD most commonly interpreted as a measure of myelin integrity. Indeed, RD has been interpreted as reflecting myelin in training-related white matter plasticity (Mackey, Whitaker & Bunge, 2012), schizophrenia (Davis et al., 2003), and age-related cognitive decline (Davis et al., 2009). However, it is important to note that water molecules trapped between the myelin sheaths, myelin water, has a short T_2 (10-40 ms) and given that the echo times of most DTI studies exceeds 50 ms the signal from the myelin water has mostly decayed. Therefore, the reported validity of DTI indices with respect to myelin is limited not only to regions of uniform fiber directionally but is also insensitive to the diffusion of myelin water. In recent years, there is growing awareness that

although DTI measures may be sensitive to the presence of myelin, they are unlikely to serve as a specific indicator of myelin content (Jones, Knosche, & Turner 2013).

Considering the growing awareness of the lack of specificity of DTI indices it is not surprising that functional relationships between age and FA/RD vary. FA evidenced linearly declining, flat, or accelerating slope with age, while RD showed flat or accelerated age differences (Hasan et al., 2009; Michielse et al., 2010; Westlye et al., 2010). These results, when adults are considered, are inconsistent with the protracted myelination suggested by postmortem studies. DTI indices lack specificity and are influenced by multiple white matter structural properties include, axon density and caliber, intra and extracellular space, and kissing and crossing fibers (Beaulieu, 2002; Jeurissen et al., 2013; Jones, Knosche & Turner, 2013; Vos et al., 2012). Furthermore, recent longitudinal studies demonstrate differential changes in FA and other diffusivity measures in healthy adults, however, the lack of neurobiological specificity of DTI indices significantly limit the interpretation and significance of these findings (Bender & Raz, 2015; Bender et al., 2016; Sexton et al., 2014).

Alternative methods have been proposed to overcome the limitations of DTI. One commonly used method is the multi-component driven equilibrium single-component observation of T_1 and T_2 (mcDESPOT) (Deoni et al., 2008). This method produces whole brain maps of myelin fraction using a combination of balanced-steady-state- free precession (b-SSFP) and spoiled gradient echo recalled (SPGR) sequences along with fitting a three-compartment model to the data (Deoni et al., 2013). This method however may be sensitive to magnetization transfer effects (Bieri & Scheffler, 2006; Lenz, Klarhofer, & Scheffler, 2010) which tends to overestimate the myelin fraction (Deoni et al., 2008; Zhang et al., 2015). Finally, mcDESPOT has yet to be validated by quantitative comparison with histological measures of myelin content (Deoni et al., 2015).

Multi-echo T_2 (ME-T_2) relaxation analysis, (MacKay et al., 1994), overcomes the limitations mentioned above. By modeling the multi-echo T_2 data using multi-exponential decay model, ME-T_2 analysis allows for a direct measure of the myelin water fraction (MWF). In brief, the multi-echo T_2 data can be decomposed into a short T_2 component (10-40 ms), attributed to water trapped between the myelin sheaths, and a middle T_2 component (40-200 ms), attributed to the intra/extracellular components (see Chapter 2 for more information). The validity of ME-T_2 derived MWF, as an index of myelin content, is supported by histological measures of myelin obtained from optical density measurements using luxol fast blue staining (Laule et al., 2006, 2008). Furthermore, animal models of demyelination and have demonstrated the utility of MWF in monitoring demyelination and re-myelination (McCreary et al., 2009; Webb et al., 2003). Finally, ME-T_2 measures have recently been shown to be reliable across multiple white matter tracts in an age diverse sample (Arshad, Stanley, & Raz, 2017).

At present, we are only aware of one comprehensive study of white matter diffusion and ME-T_2 imaging across the adult age range (Billiet et al., 2015). This study revealed both linear and quadratic associations between age and MWF in some regions, though none survived correction for multiple comparisons. Two other studies applied MWF but those studies were not designed to investigate age differences across the entire adult age range. The age range of these studies were 15-55 years (Flynn et al., 2003) and 5-40 years (Lang et al., 2014), nonetheless they found a linear increase in MWF, and by implication myelination, into middle age. This is pattern is consistent with the postmortem findings, namely the increasing myelination into middle age. Thus, the question of age related differences in regional myelin content requires further study, namely assessing MWF/age differences across a wider age range to test for the hypothesized quadratic age effects and concurrent comparison of DTI indices.

There were two main objectives in this study. First, we wanted to characterize age differences in myelin content within selected subcortical white matter tracts in a life-span sample of healthy adults. We hypothesized that age would be quadratically related to MWF and that this relationship would vary across tracts. Second, we compared age differences in MWF with age differences in the most commonly reported DTI indices, FA and RD, which are frequently interpreted as indicators of myelination (Kumar et al., 2014; Lebel et al., 2012; Madden et al., 2012; Song et al., 2003). We hypothesized that the DTI indices, in accord with the extant literature, would exhibit linear age associations and would be unrelated to MWF.

5.3 Methods

5.3.1 Participants

Participants were volunteers from the Detroit metropolitan area. They were screened for a history of neurological/psychiatric disorders, cardiovascular disease (other than medically treated hypertension), metabolic/endocrine disorders, head injury with loss of consciousness for more than five minutes, use of antiepileptic, anxiolytic, and antidepressant medications. Participants were screened for cognitive impairment with the Mini Mental State Examination (Folstein, Folstein & McHugh, 1975; cutoff = 26) and for symptoms of depression with the Geriatric Depression Questionnaire (Radloff, 1977; CES-D, cutoff = 15).

The sample description is provided in Table 5.1. Participants were part of an ongoing longitudinal study. Men and women did not differ on age, education, MMSE, and CES-D, however more males had a history of hypertension than women. ME-T_2 data was collected on all participants, however, for DTI, data were missing for one participant, due to a technical error.

Table 5.1: Sample description

	Total	Women	Men	t or χ^2	p
N	61	36	25		
Age (years)	52.1 ± 17.9	52.1 ± 18.6	52.0 ± 17.3	0.03	0.97
Education (years)	16.0 ± 2.2	15.7 ± 2.3	16.3 ± 11.9	−1.07	0.30
MMSE	28.9 ± 0.9	29.1 ± 0.8	28.7 ± 1.1	1.92	0.06
Persons with hypertension, Number (%)	10 (16.4)	3 (8.3)	7 (28.0)	4.16	0.04
CES-D	5.4 ± 5.1	6.0 ± 5.2	4.6 ± 4.8	1.1	0.3

5.3.2 MRI acquisition protocol

Imaging was performed on a 3T Siemens MAGNETOM Verio™ using a 12-channel RF coil. The acquisition session consisted of multiple MRI sequences including: structural T_1-weighted magnetization prepared rapid acquisition gradient echo (MPRAGE), DTI and ME-T_2. A fluid attenuated inversion recovery (FLAIR) image was also collected to screen for clinically significant white matter abnormalities and space occupying lesions.

DTI images were acquired in the axial plane using a single-shot echo-plane sequence. The imaging parameters were as follows: repetition time (TR) = 12,000 ms, echo time (TE) = 124 ms, GRAPPA = 2, 20 diffusion directions, 2 averages, field of view (FOV) = 256 × 256 mm^2, matrix size = 192 × 192, slice thickness = 2 mm, number of slices = 50, b = 1000 s/mm^2, in-plane resolution = 1.3 × 1.3 mm^2. Acquisition time (TA) was 9 minutes. ME-T_2 imaging were acquired in the axial plane with a 3D gradient and spin-echo (GRASE) sequence. Acquisition parameters were previously described and I refer the reader to chapter 3. Imaging parameters for the FLAIR sequence were as follows: TR = 8,440 ms, TE = 112 ms, TI = 2,200 ms, flip angle = 150°, FOV = 256 × 256, voxel size = 1× 1× 2 mm^3, matrix size = 256 × 256, 50 axial slice and TA = 3:49 minutes. All MPRAGE and FLAIR images were inspected for potential pathology and possible

incidental findings by an experienced radiologist at the scanning facility. No incidental findings were noted in this sample.

5.3.3 Image Processing

Image processing for the ME-T_2 analysis have been previously described and I refer the reader to chapter 3. Figure 5.1 displays MWF maps from 3 representative participants across the age range. DTI data were analyzed using FSL tools. FSL Eddy Current correction was applied, using the first b_0 volume as a reference, followed by motion correction. The b-vectors were rotated following motion correction. FSL Brain Extraction Tool was used to generate a brain mask, which was passed to the FSL DTIFIT tool go generate FA images. RD images were generated by averaging the diffusion images of the two planar components of the diffusion tensor, λ_2 and λ_3. To enable comparison of MWF and FA/RD we needed to co-register the DTI and ME-T_2 data. This was accomplished in two steps. First, from the ME-T_2 data, images with an echo time = 121 ms were co-registered with the b_0 DTI image. The echo time, for the ME-T_2 data, was chosen because it had a similar echo time to the DTI, and therefore the image contrast was similar. The images were co-registered using the FLIRT tool, with six-degrees of freedom, and the registration matrix was saved. In the second step, FA images were co-registered to the first echo from the ME-T_2 dataset using the non-linear registration tool FNIRT. The registration matrix generated during the first step was used as a starting point for the FNIRT registration. The resultant warp field was then applied to the RD images to bring them into the same space as the ME-T_2 data. ROIs used in the MWF analyses were applied to the FA/RD images. Like the MWF analyses, FA/RD values were averaged over an ROI.

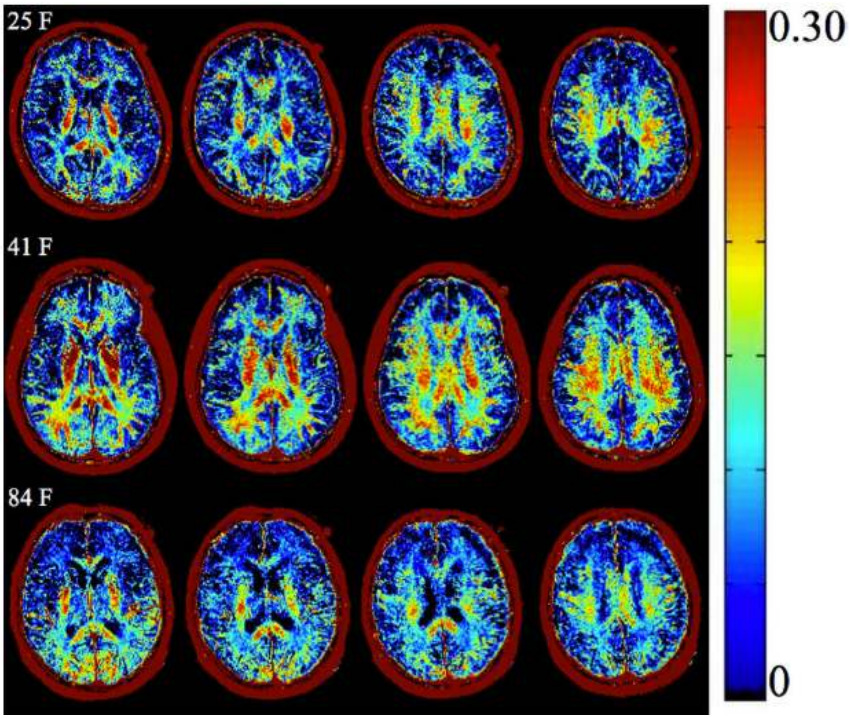

Figure 5.1: MWF maps. Representative examples of MWF maps in participants in early, mid and late adulthood. This figure depicts myelin content, expressed as MWF values, across the adult life span. Visual inspection reveals greater myelin content in middle age compared to early and late adulthood. Quantitative analyses are provided in Table 4.1.

5.3.4 Regional parcellation

The reader is referred to chapter 4 for details as the methods are identical.

5.3.5 Data conditioning

To minimize rounding errors MWF and FA values were multiplied by a factor of 100 and RD was multiplied by 10,000. To minimize effects of outliers all MRI measures were winsorized at the 90th percentiles (values about the 95th percentile was set to the 95th percentile and values below the 5th percentile was set to the 5th percentile). Because the extant literature consistently reports no age-related lateral differences (Callaghan et al., 2014; Lebel et al., 2012; Yeatman, Wandell, & Mezer, 2014), we had no reason to hypothesize such effects for any of the variables of interest. Therefore, values from bilateral ROIs (Slf, Ifof, Alic, Plic) were averaged to yield single measures, which also reduced the number of potential post-hoc comparisons.

5.4 Statistical Analysis

To assess age differences in myelin content (operationalized as MWF) and DTI indices across the sampled ROIs we used the repeated measures general linear model (RM-GLM). In each RM-GLM MWF (or DTI) values were the dependent variables, ROI was a six-level within-subject factor, sex as a between subject categorical variable, and mean centered age and age^2 terms as continuous independent variables. Within-subject interactions between sex and age and sex and age^2 were initially included in the model and were dropped if nonsignificant ($p > .05$). Reduced models were re-evaluated and significant interactions ($p < .05$) were decomposed in the post-hoc analysis using regressions for each ROI. The Huynh-Feldt correction was applied to p-values for within-subject factors to mitigate violations of the sphericity assumption. Bonferroni correction was applied for the six possible post-hoc regressions, thus the nominal $\alpha = .05$ was adjusted to $\alpha' = .008$. For each ROI, in the post-hoc analysis, only those effects which were significant in the within-subject analysis, were included. Bootstrapped, using 5000 samples, 95% confidence intervals were generated for the slope of the age^2 term and bias corrected and accelerated values are reported. Bivariate correlations between MWF and DTI indices, within each ROI, were computed and their significance values was adjusted using the Bonferroni correction. All statistical analyses were performed using SPSS Statistics (IBM Corp. IBM Statistics for Mac, Version 21.0).

5.5 Results

5.5.1 Regional age related differences in MWF

After discarding nonsignificant within-subjects interactions ROI × age × sex and ROI × age^2 × sex ($F < 1$ for both) and between-subjects interactions age × sex ($F < 1$) and age^2 × sex [$F(1,55) = 1.233$, $p = .27$], a reduced model was fitted to the data. The analysis revealed significant main effects of sex [$F(1,57) = 5.651$, $p = .021$] and age^2 [$F(1,57) = 16.521$, $p < .001$]. Women had a

higher MWF than men did, mean ± SE: 14.3 ± .3% vs 13.3 ± .3%. The main effect of age was not significant ($F < 1$). However, the ROI × age^2 interaction was significant [$F(5,285) = 4.726$, $p = .0010$], indicating that the magnitude of the quadratic effect of age differed across ROIs (Table 5.2 and Figure 5.2). For all ROIs, except the genu, the quadratic effect of age was significant at the adjusted level.

ROI	R^2	*p*	*b* (MWF/yr^2)	95% CI
ALIC	.28**	< .001	−.005	−.006, −.003
PLIC	.21**	< .001	−.003	−.004, −.001
Genu CC	.08*	.026	−.001	−.003, .000
Splenium CC	.12**	.006	−.002	−.004, −.001
SLF	.22**	< .001	−.003	−.004, −.002
IFOF	.12**	.008	−.002	−.004, −.001

Table 5.2: Summary of the post-hoc analyses. Associations between MWF and age^2 for each ROI along with bootstrapped confidence intervals.* Significant at the unadjusted α = .05 level **Significant at the Bonferroni adjusted α' = .008 level.

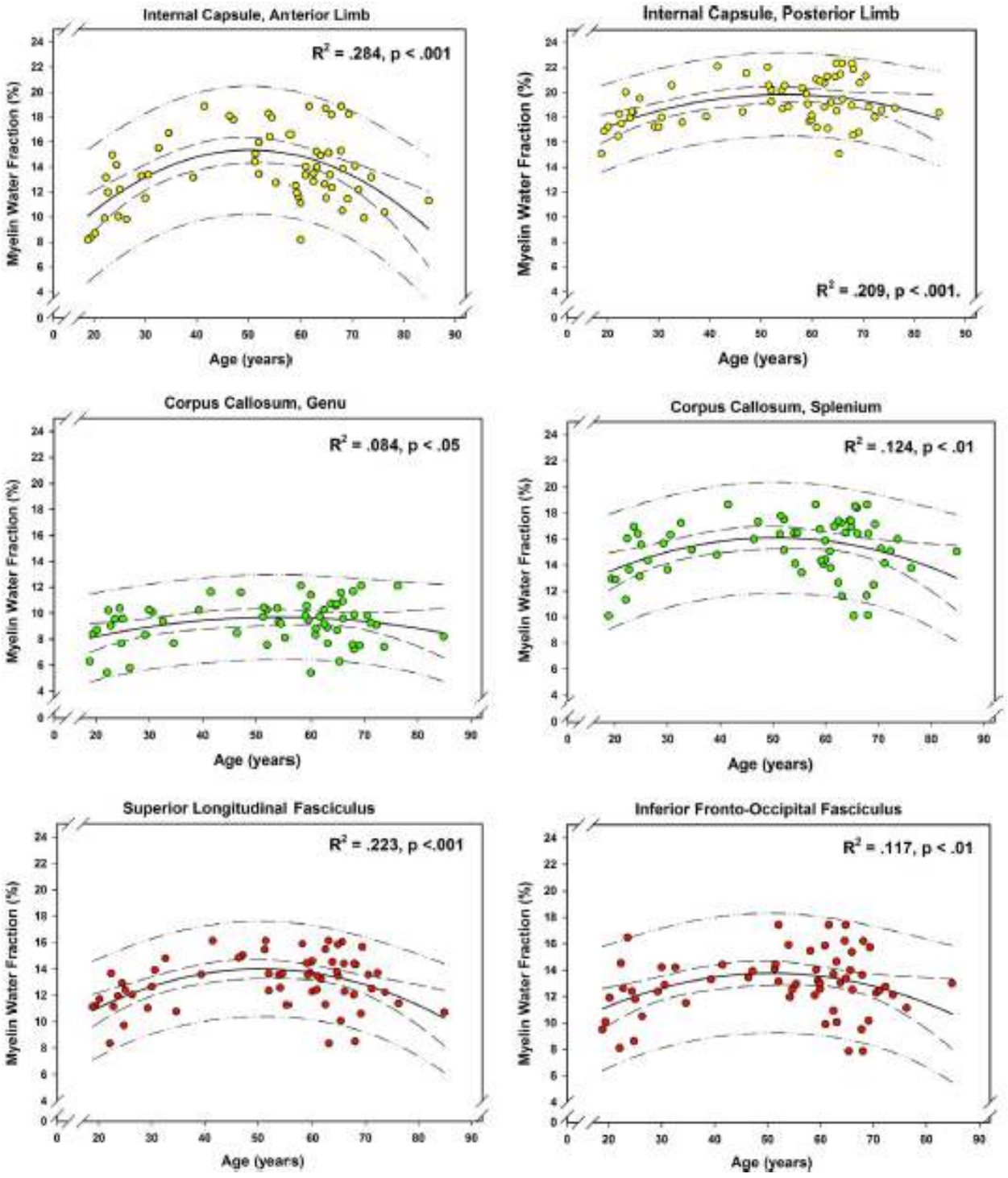

Figure 5.2: MWF age plots by ROI. Associations between MWF and age along with 95% confidence limits (dashed line) and prediction limits (dot-dash lines) lines are drawn around the regression lines for each ROI. All plots are on the same scale, making regional differences in myelin content apparent.

5.5.2 Regional age differences in DTI derived indices

Fractional Anisotropy

After discarding nonsignificant within-subjects interactions ROI × age × sex [$F(5,270) = 1.083$, $p = .36$] and ROI × age^2 × sex [$F(5,270) = 1.365$, $p = .25$] and between-subjects interactions age × sex ($F<1$) and age^2 × sex [$F(1,54) = 3.603$, $p = .063$], a reduced model was fitted to the FA data. The analysis revealed nonsignificant main effects of sex and age^2 ($F < 1$ for both). The ROI × sex [$F(5,280) = 1.832$, $p = .12$] and ROI × age^2 [$F(5,280) = 1.916$, $p = .11$] interactions were not significant, but the ROI × age interaction was [$F(5,280) = 6.297$, $p < .001$]. After the dropping the age^2 term the model was re-evaluated. The main effect of sex ($F<1$) and the ROI × sex [$F(5,285) = 1.901$, $p = .11$]interaction were not significant. The main effect of age was significant [$F(1,57)= 14.489$, $p < .001$], however this was qualified by a significant ROI × age interaction [$F(5,285) = 5.565$, $p < .001$], indicating that the linear age effects on FA varied across ROIs. Post-hoc analysis revealed significant linear age effects for the genu, splenium, and the Ifof. All other ROIs did not survive the Bonferroni-adjusted significance level (Table 5.3).

ROI	FA				RD			
	R^2	p	b (1/yr)	95% CI	R^2	p	b (mm^2/s*yr)	95% CI
ALIC	.10*	.022	−.065	−.121, −.009	.05	.074	.006	−.001, .013
PLIC	.00	.668	−.012	−.062, .040	.00	.780	.001	−.004, .006
Genu	.24**	<.001	−.109	−.163, −.052	.23**	<.001	.016	.010, .023
Splenium	.14**	.004	−.073	−.119, −.026	.18**	.001	.008	.004, .013
SLF	.01	.420	−.016	−.056, −.026	.02	.374	.002	−.003, .007
IFOF	.40**	<.001	−.116	−.149, −.082	.28**	<.001	.014	.010, .018

Table 5.3: DTI post-hoc analysis summary. A summary of post-hoc analyses of associations between DTI indices and age for each ROI. *Significant at the unadjusted α = .05 level **Significant at the Bonferroni corrected α' = .008 level.

Radial Diffusivity

After discarding nonsignificant within-subjects interactions ROI × age × sex ($F<1$) and ROI × age^2 × sex [$F(5,279) = 1.279$, $p = .28$] and between-subjects interactions age × sex ($F<1$) and age^2 × sex [$F(1,54) = 1.648$, $p = .21$] a reduced model was fit to the data. The analysis revealed

nonsignificant main effects of sex (F<1) and age^2 [F(1,56) = 2.508, p = .12]. The ROI × sex [F(5,280) = 2.114, p = .080] and ROI × age^2 [F(5,280)= 1.901, p = .11] were also not significant. After dropping the age^2 term the model was re-evaluated. The main effect of sex (F<1) and the ROI × sex interaction [F(5,285) = 2.3, p = .069] was not significant. The main effect of age was significant [F(1,57) = 14.451, p < .001], however this was qualified by the significant ROI × age interaction [F(5,285) = 14.541, p < .001]. Post-hoc analysis revealed significant effects of age for the genu, splenium and the ifof. All other ROIs did not survive Bonferroni correction (Table 5.3).

5.5.3 Regional correlations between MWF and DTI indices

Correlations between MWF and FA did not achieve Bonferroni adjusted significance level in the ROIs investigated. Similar results were found for the MWF and RD analysis, except for the splenium which achieved the Bonferroni significance level [r = .346, F(1,58) = 8.201, p = .006]. The plic and slf were significant at the unadjusted significance level (Table 5.4).

ROI	FA				RD			
	R^2	p	b (MWF)	95% CI	R^2	p	b (MWF*s/mm^2)	95% CI
ALIC	.03	.182	.132	−.055, .286	.04	.119	−1.185	−2.52, .345
PLIC	.03	.178	.083	−.043, .193	.08*	.029	−1.314	−2.386, −.014
Genu	.01	.559	.031	−.073, .126	.01	.463	−.282	−.965, .461
Splenium	.04	.114	.122	−.041, .264	.12**	.006	−2.06	−3.448, −.468
SLF	.02	.249	.109	−.082, .314	.09*	.018	−1.9	−3.407, −.359
IFOF	.00	.930	.008	−.167, .186	.01	.392	−.568	−1.886, .749

Table 5.4: DTI MWF associations summary. A summary of the post-hoc analyses of associations between the DTI indices and age for each ROI

5.6 Discussion and Limitations

5.6.1 Heterochronic associations between age and myelin content

The main finding of this study was the *in vivo* demonstration that age differences in subcortical white matter myelin content conforms to the parabolic (inverted U) relationship described in the postmortem literature. These results suggest, in the regions examined, that peak myelin content is found around the fourth-sixth decade of life. The positive linear association between MWF and

age, up to middle age, agrees with previous studies which included only that age range (Flynn et al., 2003; Lang et al., 2014).

Like Yeatman et al., who used R_1 ($1/T_1$) as a proxy for myelin content, (Yeatman, Wandell, & Mezer, 2014) we found quadratic age effects for all ROIs. Furthermore, we found that the magnitude of age differences in myelin content varied across white matter tracts. Projection fibers (alic, plic) and the slf (association fiber) exhibited the largest quadratic age effects, while ifof exhibited a weaker relationship, and the weakest association was observed in the genu. These patterns are inconsistent with the proposed "first-in-last-out" hypothesis (Raz, 2000).

We also found that women had greater myelin content than men: Cohen's d = .62. While in vivo literature on sex differences of white matter properties is very inconsistent (Salat, 2014), this finding is consistent with the reported higher levels of myelin associated proteins in female rodents (Bayless & Daniel, 2015) and may reflect the greater *g*-ratio of men compared to women (Paus & Toro, 2009). The *g*-ratio is a dimensionless index, between 0 and 1, with values closer to 1indiciating thinner myelin sheaths. Recent work has suggested that the *g*-ratio might be sensitive to sex-specific androgens, which can contribute to an increase in axonal diameter and a subsequent increase in the *g*-ratio (Pesaresi et al., 2015). Our study, however, was not designed to specifically test this hypothesis, and therefore we did not have the relevant data. Furthermore, we had a greater proportion of men with the hypertension and thus it is unclear whether disproportionally higher vascular risk among men could have contributed to the observed sex differences. In this sample, the frequency of hypertension was too low to warrant its inclusion as a covariate.

The biological mechanisms of age-related decline in myelin content remain unclear. Assuming a dynamic equilibrium between myelin production and myelin loss (Peters, 2009) and observing the continuing myelination into the fourth-sixth decade of life, it is plausible that during this period

the myelin generating process overtakes its counterpart that drives its attrition. It is plausible to hypothesize that this dynamic equilibrium shift over time and the decline in myelin content is driven by decreased myelin synthesis, increases myelin degeneration, or some combination of the two. While the mechanisms for such a shift in homeostasis is unknown, it is possible that the progressive decline in myelin is just another expression of age-related energy deficit. Indeed, the synthesis of myelin and the maintenance of the oligodendrocyte resting potential is energetically costly (Harris & Attwell, 2012).

Aging is associated with decline in mitochondrial respiration (Bratic & Trifunovic, 2010), decreased glucose and oxygen consumption, and decreased cerebral blood flow (Aanerud et al., 2012; Lin & Rothman, 2014) as well as poor vascular health (Mozaffarian et al., 2015). The age related metabolic factors would be expected to limit myelin synthesis given its energetic costs. Another potential source of myelin attrition could be the age-related reduction in the number of myelinated axons (Peters, 2002; Marner et al., 2003; Meier-Ruge, et al., 1992; Tang et al., 1997). Future investigations should assess age differences in both anabolic and catabolic aspects of myelination along with investigations of age differences in brain energetics and axonal loss.

5.6.2 Heterochronic associations between age and DTI indices: unrelated to myelin

In agreement with previous studies we found linear association between age and the DTI indices, with the magnitude of associations varying across ROIs. These associations are in stark contrast to the quadratic age effects on MWF. It should be noted that some DTI studies, which include young children and adolescents in their sample, have reported non-linear associations between age and DTI indices (Lebel et al., 2012; Westlye et al., 2010). Peak age of myelination estimated from these studies is much earlier, 24-33 years of age (Westlye et al., 2010) or 32-39

(Kochunov, et al., 2012) depending the white matter regions investigated. These estimates are earlier than those suggested by postmortem studies (Kaes, 1907).

We observed no significant associations between MWF and FA. MWF was significantly associated with RD only in ROIs containing large diameter axons (Plic and Splenium) in agreement with previously published work (Madler et al., 2008). These results are consistent with studies demonstrating that the axonal plasma membrane, fiber density, and the presence of crossing fibers contribute to diffusion anisotropy and radial diffusivity, thus complicating the biological interpretation of DTI derived indices (Beaulieu, 2002; Jones, Knosche, Turner, 2013; Vos et al., 2012).

5.6.3 Limitations

There are several limitations which should be kept in mind when interpreting the results of this study. First, inferences about change in myelin content from cross-sectional studies of age differences is inappropriate (Baltes & Nesselroade, 1979; Lindenberger, et al., 2011). Longitudinal and cross-sectional findings in brain aging research are not always in agreement with respect to mean change (Bender & Raz, 2015; Daugherty, Haacke, & Raz, 2015). Furthermore, cross-sectional studies cannot address questions about individual differences in aging trajectories. Therefore, longitudinal studies are needed to confirm the quadratic trajectory of age and to investigate individual differences therein. Furthermore, cross-sectional studies, by their design, do not reveal differences in patterns of aging across the brain, and therefore testing hypotheses such as “first-in-last-out” (Raz et al., 1997) and “gain-predicts-loss” (Yeatman, Wandell, & Mezer, 2014) can only be accomplished with longitudinal investigations.

Second, we used an ROI based analysis and therefore differences in myelin content within a tract could not be investigated. Our DTI acquisition was not optimal for tractography and therefore

we opted for the ROI based analysis. If the resolution of ME-T_2 images can be improved and made comparable to DTI, more advanced DTI acquisitions could be used to combine tractography to investigate differences in myelin content within tracts. It should be noted that the differential quadratic age effects we observed could be the result of differential reliability. However, we have shown that MWF is sufficiently reliable and we found no differences in reliability across the ROIs investigated (Arshad, Stanley, & Raz 2017).

Third, while we sampled tracts which are commonly investigated and represent major types of white matter tracts, it is possible that other regions would deviate from the inverted-U pattern. Given the 5-mm thick slices investigating other tracts of interest, which are thinner (e.g. fornix), was not feasible because of the partial voluming effect.

Fourth, we tested a quadratic relationship between age and MWF, which was motivated by postmortem data. The symmetry of the quadratic function implies a symmetry of myelination from young to middle adulthood and from middle to late adulthood. This need not be true. Higher order curves, or piece-wise fitting could have been tested if more data were available.

Fifth, it is important to note that the long component T_2 component is included in the modeling of the ME-T_2 data. However, according to our analyses, it happens to have a negligible contribution, and therefore we conclude it contributes no new water compartment. Nonetheless, it is important to acknowledge that MWF is defined as the proportion of the signal in the short T_2 component relative to the entire T_2 spectrum. A decrease in MWF is possible if there was an additional water compartment that increased the overall water content. Such a scenario is observed in pathological conditions such as multiple sclerosis (Laule et al., 2007, 2008) and phenylketonuria (Sirrs et al., 2007) is unlikely in our case as we screened our subjects for white matter abnormalities using FLAIR images.

5.7 Conclusions

Using a novel myelin specific imaging method, we observed quadratic associations between age and myelin content across all ROIs investigated, consistent with post-mortem studies. Regional differences in myelin content, as expected from postmortem studies, varied from the largest in the plic and splenium to the smallest in the genu. In agreement with the extant literature, but in contrast to MWF, we found linear age associations with DTI indices. We found no correlations between MWF and FA in any of the examined ROIs, while RD was significantly correlated with MWF in the splenium only. Thus, while DTI can provide important information regarding the state of white matter, its commonly used indices, FA and RD, do not specifically reflect myelin content and are not suitable for examining age differences therein.

CHAPTER 6: Change in processing speed and its association with white matter microstructure

6.1 Summary

Age related deterioration of white matter, and in particular, myelin, has been hypothesized as a potential neural substrate of age related slowing in processing speed. However, to date, this association has been investigated by methods that are insensitive to specific microstructural properties of the white matter, such as single-tensor DTI and WMH burden assessment. In healthy adults (18.17-83.42 years of age) we assessed processing speed at two occasions using a simple choice reaction time task and estimated the key parameter of cognitive information processing via the diffusion model. For examining white matter properties, we used a novel imaging method, Multi-Echo T_2 imaging (ME-T_2). This imaging approach yields estimates or regional myelin content, myelin water fraction (MWF), and a putative index related to axonal density/diameter, geometric mean T_2 of the intra/extracellular water ($geomT_{2\text{-}IEW}$). We tested the associations between the ME-T_2 measures and drift rate at baseline and change therein. Selecting the genu of the corpus callosum and the Slf as tracts hypothesized to be associated with drift rate, and the Plic as a control tract, we found a negative association between change in drift rate and the $geomT_{2\text{-}IEW}$ in the genu only. However, after Bonferroni correction this association was not significant. To our knowledge this study was the first to use a histologically validated in vivo index of myelin content to test the hypothesis of association between myelin and processing speed. Although the negative association between the $geomT_{2\text{-}IEW}$ in the genu and change in drift rate did not reach the Bonferroni adjusted significance level, the observation is broadly consistent with a recent report of associations between white matter R_2 ($1/T_2$) and change in a global cognitive index (Dawe et al., 2016) and suggests future research should consider the use of in vivo indices specific to axonal

density, perhaps geom$T_{2\text{-IEW}}$, to elucidate the significance of changes in axonal density with respect to drift rate as well as other cognitive functions.

6.2 Introduction

Slowing of information processing is considered one of the most reliable markers of aging (Birren & Fischer, 1995), yet the neural substrates underlying the association is unclear. Findings of reduced processing speed in patients with multiple sclerosis (Demaree et al., 1999; Rao et al., 1989), a demyelinating neurological disease accompanied by damage or loss of axons (Haines et al., 2011), led to multiple investigations of age differences in the integrity and microstructure of cerebral white matter and its association with processing speed (Gunning-Dixon & Raz 2000; Madden et al., 2012). The majority of studies have used indices derived from single-tensor DTI to characterize age differences in white matter properties along with the measures of central tendency of reaction time distributions to assess processing speed. Almost all studies used cross-sectional design, and therefore, inferences regarding aging effects on change in processing speed are not appropriate (Maxwell & Cole, 2007).

One of the limitations of DTI derived indices is the lack of clear neurobiological interpretations. Scalar indices computed from diffusion tensor eigenvalues are influenced by multiple brain properties, including axonal density and caliber, intra and extracellular fluid, and the presence of crossing and kissing fibers (Beaulieu 2002; Jeurissen, et al., 2013; Jones et al., 2013; Vos et al., 2012). This significantly limits the utility of these indices for investigating the neural mediators of age differences in speed of processing. Even the DTI measures commonly interpreted as reflecting myelination (e.g., RD) are unrelated to myelin content estimated by MWF (see chapter 2; Arshad, Stanley, & Raz 2016). For example, whereas age related deterioration of

myelin has been hypothesized as substrate of age related cognitive decline (Bartzokis, 2004) and slowing of processing speed (Lu et al., 2013) there are no direct tests of these hypotheses.

A second limitation of most studies is the use of a mean or median to characterize the RT distributions. These measures of central tendency ignore the problem of skewness that is endemic to typical RT distributions and do not account for the RT variability Intra-individual variability in RT increases with age, is associated with poor cognitive performance (Nesselroade & Salthouse, 2004), and may be a marker of compromised brain function (Hultsch et al., 2000), and therefore, it needs to be addressed. Furthermore, use of the mean or median RT is confounded by the speed-accuracy tradeoff, an age-related phenomenon. The mean and median RT of older adults is expected to be longer because, compared to younger adults, older people tend to emphasize accuracy over speed (Salthouse, 1979). These limitations can be overcome by explicitly modeling the process of information accumulation and thus accounting for the RT variability and speed-accuracy tradeoff. This approach, introduced by Roger Ratcliff (1978) also allows separating the cognitive components of the RT information processing from the motor response time. Modeling of RT data has previously demonstrated that while younger subjects may have faster RT compared to older subjects, cognitive information processing speed need not be different (Ratcliff, Thapar, & McKoon, 2006).

To overcome the limitations of DTI, a novel, histologically validated imaging technique that provides a specific index of myelin content along with a putative indicator of axonal density or diameter (see chapter 2) was used. Furthermore, application of the diffusion model (see chapter 3) to the RT distributions generated estimates of cognitive processing speed while overcoming the limitations mentioned in the previous paragraph. Finally, using latent change score models, we evaluated effects of age on change in processing speed and tested the hypothesized association

between individual differences in regional myelin content or axonal density/diameter and processing speed at baseline or with change therein.

This dissertation did not initially consider the potential role of axon diameter and density in speed of processing, and therefore did not include additional imaging techniques which could have quantified these properties and test whether axonal loss of thinning contributed to reduced processing speed. If myelin loss disrupts neural integration because of delays in conduction, it is feasible that axonal loss, which would decrease inputs into neural integrators, could also impair processing speed. Circuits in the CNS have multiple sources of noise including random fluctuations in the membrane potential (Faisal, Selen, & Wolpert, 2008). Neuronal noise can manifest as variability in the output of action potentials even when driven with identical stimulation (Faisal, Selen, & Wolpert, 2008). Therefore, axonal loss could decrease inputs into neurons, and in the presence of physiological noise may decrease processing speed and cognitive function. Indeed, in the rhesus monkey axonal density in the anterior commissure is negatively associated with cognitive impairment (Sandell & Peters, 2003).

Associations between myelin content, indexed by MWF, and axonal density or diameter, reflected by geom$T_{2\text{-IEW}}$, and processing speed, were evaluated in select white matter tracts. Tract selection was based on the extant literature and theoretical considerations of the task demands. First, because the choice reaction time task requires decision making that relies on the prefrontal circuits (Domenech & Koechlin, 2015; Rahnev et al., 2016), the DTI indices measured in the genu of the corpus callosum and the prefrontal white matter have been linked to speed of processing (Bucur et al., 2008; Kennedy & Raz, 2009; Lu et al., 2013; Madden et al., 2012). Therefore, genu was selected as a candidate region that was expected to be related to speed of processing measures obtained from the RT task.

Intra-cortical recordings in macaques performing similar tasks, have demonstrated that neurons in parietal cortex accumulate sensory information and their activity is related to reaction time (Roitman & Shadlen, 2002; Huk & Shadlen 2005). This is perhaps not surprising given the multimodal nature of the parietal cortex (Cohen, 2009). Considering that the superior longitudinal fasciculus (Slf) contains fibers connecting parts of temporal and parietal cortex to the frontal cortex (Makris et al., 2005), we expected this tract to be associated with processing speed. This is consistent with the findings that lesions involving the superior longitudinal fasciculus are associated with reduced processing speed (Turken et al., 2008). Therefore, we hypothesize that in addition to the genu of the corpus callosum, the superior longitudinal fasciculus that involve multiple higher order association cortices would be associated with processing speed and change therein.

For a control region that was not expected to show evidence of any association with the target task measures, we chose the posterior limb of the internal capsule (Plic). The Plic contains fibers projecting from the motor cortex to the spinal cord, neither of which are thought to be involved in cognitive processing and therefore should not be associated with the cognitive component of processing speed. Therefore, we hypothesized that MWF in the genu of the corpus callosum and the Slf would be positively correlated with processing speed at the first measurement occasion and with change after statistically controlling for age. Furthermore, interpreting the $geomT_{2\text{-}IEW}$ as an index of axonal density, we hypothesize that it would negatively associated with processing speed at the first measurement occasion and change therein in the genu and Slf. Finally, we expect that the neither MWF nor $geomT_{2\text{-}IEW}$ in the Plic would be associated with processing speed or change. To correct for the multiple comparisons in modeling two white matter indices in three regions, we used the Bonferroni correction and set the nominal $\alpha = .05$ to $\alpha' = .008$.

6.3 Methods

6.3.1 Participants

Participants were volunteers from the Detroit metropolitan area and were part of an ongoing longitudinal study. They were screened for a history of neurological and psychiatric disorders, cardiovascular disease (other than medically treated hypertension), metabolic and endocrine disorders, head injury with loss of consciousness for more than five minutes, use of antiepileptic, anxiolytic, and antidepressant medications. Participants were screened for cognitive impairment with the Mini Mental State Examination (MMSE, Folstein, et al., 1975 cutoff = 26) and for symptoms of depression with the Geriatric Depression Questionnaire (CES-D, Radloff, 1977;CES-D cutoff = 15). Participants had corrected visual acuity of 20/50 or better (Optec 2000 apparatus; Stereo Optical, Chicago, IL) (ICO, 1984). Cognitive testing was conducted on two occasions. Five subjects were dropped from the analysis because they did not meet our CES-D criteria. Table 6.1 describes participant characteristics, at both occasions, which made up the final sample that was analyzed. Characteristics for participants who had cognitive assessments at both occasions and imaging data, only available at occasion 2, is provided in Table 6.2. Note for these subjects there was no difference in age between males and females: t = -.80, p = .432.

Table 6.1: Sample descriptors at both measurement occasions

Time 1				
	Men Mean (SD)	**Women Mean (SD)**	***t***	***p***
N	74	138		
Age (years)	46.94 (18.8)	50.50 (18.54)	-1.32	.187
Education (years)	15.43 (1.82)	15.35 (2.12)	.291	.771
MMSE	28.47 (1.11)	28.87 (.927)		
CESD	6.11 (4.40)	4.60 (3.90)		
Time 2				
N	33	47		
Age (years)	53.41 (17.68)	60.89 (14.72)	-2.06	.043
Education (years)	15.45 (1.50)	15.98 (2.38)	-1.12	.268
MMSE	28.52 (1.20)	29.04 (.86)		
CESD	5.28 (4.03)	3.70 (3.35)		
Delay (months)	27.06 (4.06)	27.45 (5.87)	-.326	.745

Table 6.2: Sample descriptors. Summary of sample descriptors of participants with both imaging data and cognitive assessment at both occasions

	N	**Mean (SD) (years)**	**Range**
All	34	57.13 (15.07)	24.67 - 84.75
Males	13	54.43 (16.02)	24.67 - 76.17
Females	21	58.80 (14.60)	24.67 - 84.75

6.3.2 MRI acquisition protocol, Image Processing, and ROI parcellation

The acquisition protocol, image processing pipeline, the process of generating ROI masks in the subject space have been previously described. The reader is referred to section 4.3.5 for more information.

6.3.3 Choice reaction time task and diffusion modeling

Reaction data were collected in a two-choice letter discrimination task (Thapar et al., 2003). Participants were seated in a quiet room in front of a computer monitor whose height was adjusted so that the participants' eyes were at the midpoint of the monitor. Participants were asked to sit comfortably in a chair and were required to maintain their position throughout the testing period.

The task was administered in two sessions with six 108-trial blocks per session. Each session was preceded by two practice blocks. Participants were required to take brief breaks between blocks (each block was about four minutes). The total number of trials over the two sessions was 1,296, with 216 trials per stimulus duration. The letter pairs used on all decision trials were, P/R, O/Q, I/J, F/E, C/G and V/W.

Two letters are displayed, at either the left or right edge of the screen, and are displayed thought the duration of the block. A white cross appears in the middle of the screen for 500 ms, after which the target letter (one of the two letters displayed on the screen) is presented for six variable durations (13, 26, 39, 52, 66, and 80 ms), followed by a mask. The participants task is to identify the target letter and decide whether it matches the letters displayed on the left or right of the screen.

Prior to fitting the RT distributions with the EZ diffusion model, extreme RT values (below 200 ms and above 1799 ms) were removed. As stated in chapter 2 we attempted the DMAT analysis, which provides a more detailed set of RT parameters, but the ill-behaved Hessian matrix made us question the validity of the estimates. Therefore, we choose to use the simplified and more

robust EZ model. More information on the EZ model is provided in chapter 3. Drift rates were generated for both measurement occasions.

6.3.4 Data conditioning

MWF values were multiplied by 100 yielding units of percent. The geomT_2-$_{IEW}$ was multiplied by 1000 yielding units of ms. To avoid scaling issues in the latent change score model the delay period was multiplied by 12, to yield units of months, and the drift rates were multiplied by 10 (note drift rate is unit less).

6.4 Statistical Analysis

A series of latent change score models (LCSM) were used to investigate the effects of age and ME-T_2 indices on both baseline and change in processing speed. Latent change score models can be implemented within the framework of structural equation modeling (SEM). In contrast to more traditional methods of longitudinal data analysis (e.g., repeated measures general linear model), LCSM evaluates the average and individual differences in outcomes of interest. For example, we can estimate the mean change in processing speed and variance therein and test hypotheses about variables that explain variance in change. Furthermore, LCSM allows us to directly model measurement error and therefore separate the variance into measurement error variance and the variance we wish to explain (Jöreskog, 1970; Ghisletta & McCardle 2012). A detailed discussion of SEM and LCSM are beyond the scope of this dissertation and can be found elsewhere (Jöreskog, 1970; McArdle, 2009). Model fit was evaluated using multiple fit indices: non-significant χ^2 or χ^2/df<2, comparative fit index (CFI) and Tucker-Lewis Index (TLI) >.95 and root mean square error (RMSEA) <.08 (Hu & Bentler, 1999; Muller, 1996). Missing data were handled using Full Information Maximum Likelihood (FIML) estimation.

A broad overview of the analysis will be provided first, followed by a more detailed discussion of each step. We conducted the analysis in three steps. First, we established adequate model fit of the LCSM, next after verifying significant variance in both drift rate, at Time 1, and in change we added covariates to the model. Non-significant covariates were dropped. Regardless, of significance however, we always kept the age terms in the model to account for the non-random missingness of participants that was associated with that variable. Finally, while keeping the age terms in the model, ME-T_2 covariates were added, to test whether they accounted for any additional variance, and non-significant terms were dropped.

Step1: LCSM without covariates

Due to unequal number of males and females we used a multi-group analysis however we had to ensure strong factorial invariance (Gregorich, 2006; Meredith & Teresi, 2006) so that factor loadings and intercepts were invariant across both sex and measurement occasion. This was established by allowing these parameters to vary followed by fixing them and evaluating the models using the difference in χ^2. Establishing invariance is critical to interpreting the means and change in the factor scores as well as allowing us to test for potential moderating effects of sex on the covariates. Figure 6.1 illustrates the LCSM.

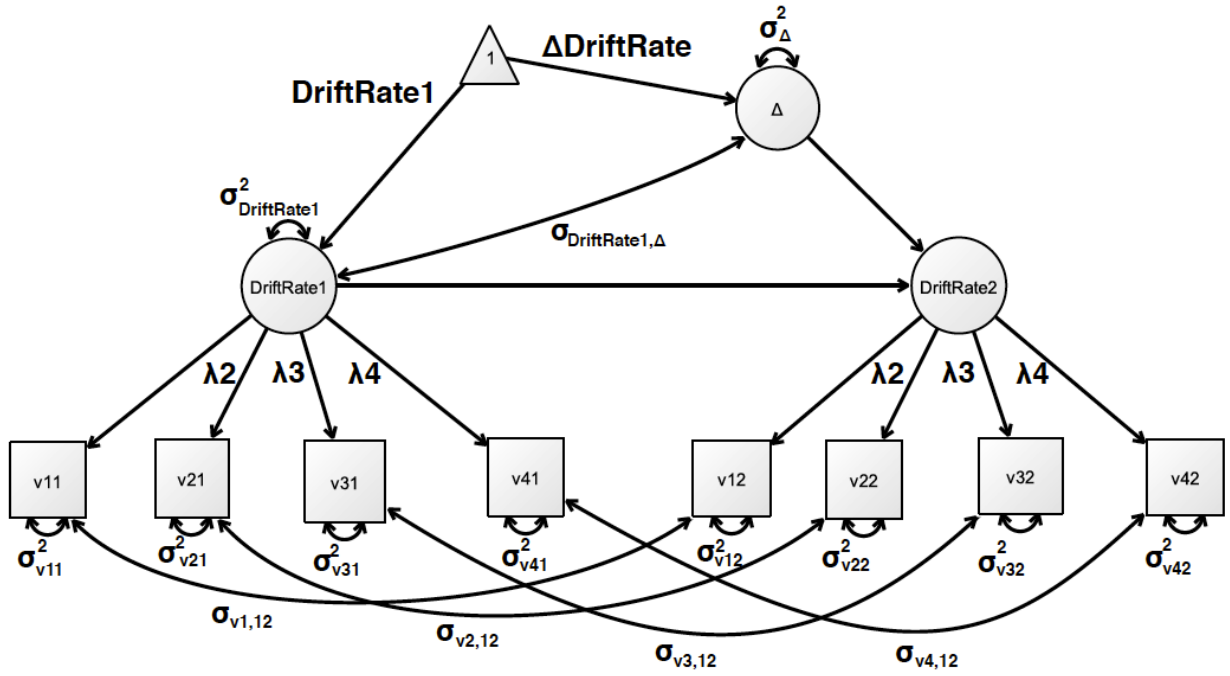

Figure 6.1: Latent change score model. Drift rate factor scores for Time 1 and 2 were generated using the drift rates for the last 4 conditions (v1, v2, v3, v4). This model simply states that the drift rate at Time 2 (DriftRate2) is equal to drift rate at Time 1 (DriftRate1) plus change (Δ).

Step 2: LCSM with age covariates

After establishing adequate fit for the LCSM, strong invariance, and significant variance in both change (Δ) and drift rate at occasion 1 (DriftRate1) we then added covariates. Age (centered at the sample mean) at Time 1 was added as a predictor of DriftRate1 and Δ. We also added delay as a predictor of Δ to account for potential effects of the variability in the delay period. Age terms were always kept in the model; however, delay could be dropped if non-significant. We initially allowed the slope of the covariates to vary by sex, then fixed them and evaluated the change in χ^2 to test for potential moderating effects.

Step 3: LCSM with age and ME-T_2 covariates

Finally, we tested if the ME-T_2 covariates were associated with either DriftRate1 or Δ while accounting for the effects of age. In other words, after statistically controlling for age do the ME-T_2 indices account for any additional variance. For both ME-T_2 variables we first added MWF or

geom$T_{2\text{-}IEW}$ as covariates, allowing slopes to differ by sex, to both DriftRate1 and Δ. Next, we fixed the slopes and using the change in χ^2 evaluated whether sex moderated the slopes of the covariates. Finally, non-significant covariates were dropped and the model was re-evaluated. Statistical analysis was conducted in R (version 3.3.2) using the package *lavaan* (version 0.5-22) (Rosseel, 2012). Onyx (von Oertzen, Brandmaier, & Tsang, 2015) was used to generate the path diagrams.

6.5 Results

6.5.1 LCSM no covariates

Using six or fivedrift rates as indicators produced poor model fit: ($\chi^2(96) = 513.265$, $p < .001$, $\chi^2/df = 5.34$, CFI = .857, TLI = .803, RMSEA =.202; $\chi^2(58) = 170.705$, $p < .001$, $\chi^2/df = 2.94$, CFI = .956, TLI = .932, RMSEA =.135, respectively. Using drift rates for the last 4 task conditions (referred to as v1, v2, v3 and v4) we could establish strong metric invariance and adequate model fit: ($\chi^2(48) = 53.020$, $p = .287$, $\chi^2/df = 1.10$, CFI = .997, TLI = .997, RMSEA =.031). Furthermore, we found significant variability in both DriftRate1 and Δ in sexes (see Table 6.3). Given the statistically significant variance in both DriftRate1 and Δ, we proceeded to the next level of the analysis.

Table 6.3: LCSM variance and mean estimates. Summary of variance and mean estimates for DriftRate1 and Δ by sex.

Parameter Estimates	**Females**	**Males**
Variance in DriftRate1 (SE)	85.369 (11.062)	100.929 (17.380)
Variance in Δ (SE)	19.566 (4.935)	18.582 (5.240)
DriftRate1 (SE)	22.145 (.820)	24.363 (1.195)
Δ (SE)	3.350 (.718)	3.211 (.763)

All significant at $p < .001$.

6.5.2 LCSM with age covariates

In the first model, we included age as a covariate of DriftRate1 and Δ, as well as delay as a predictor of Δ. There was no statistically significant difference when the slopes of the covariates were fixed across sex ($\Delta\chi^2(3) = .57$, $p = .903$), indicating that sex did not have a moderating effect. Furthermore, delay was not a statistically significant ($p = .295$) predictor of Δ and therefore was removed in the final model. The fit indices for the final model were: $\chi^2(62) = 68.663$, $p = .262$, $\chi^2/df = 1.10$, CFI = .997, TLI = .996, RMSEA =.032. Figure 6.2 depicts the final model. Age at Time 1 was negatively associated with DriftRate1 ($p < .001$) but was not a statistically significant predictor of Δ ($p = .308$).

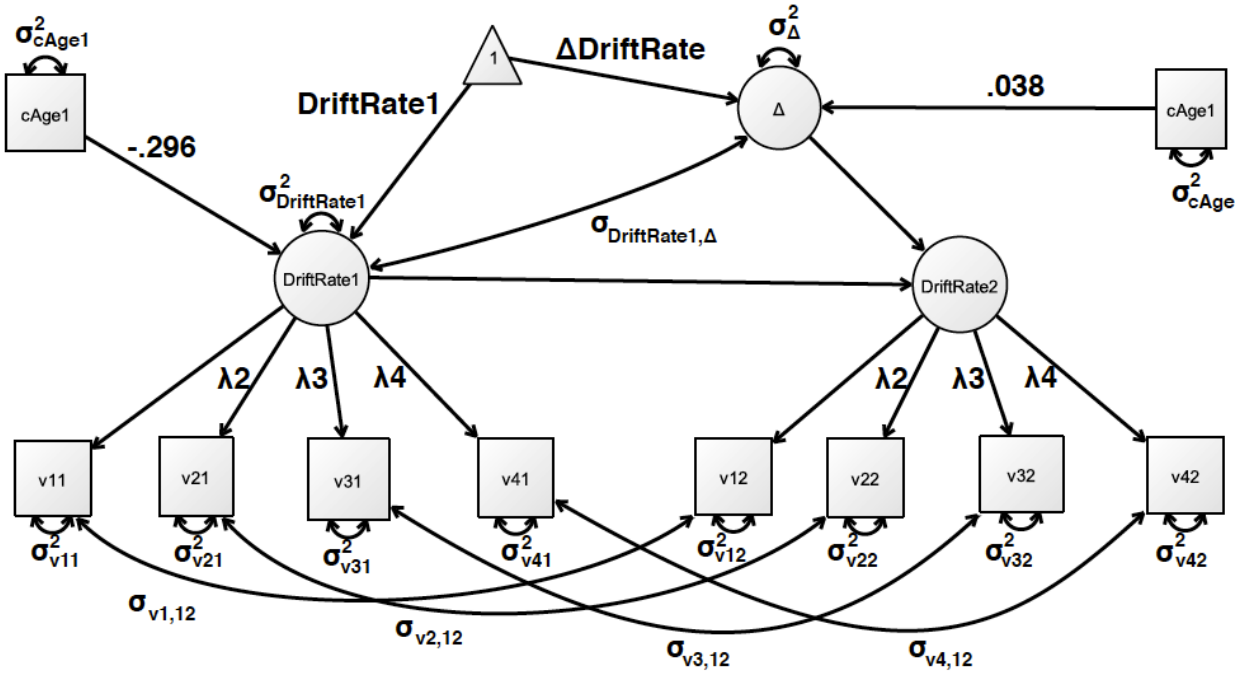

Figure 6.2: LCSM with age covariate. The final model with age covariates. Parameter estimates are only shown for the covariates. Age is negatively correlated with DriftRate1.

6.5.3LCSM with age and ME-T_2 covariates

MWF

Starting with the Slf, we found that fixing the slopes of the covariates across sexes did not significantly affect the model fit ($\Delta\chi^2(2) = 2.941$, $p = .229$). Furthermore, we found that the association between MWF and DriftRate1, as well with Δ, was not statistically significant: $p = .815$; $p = .089$, respectively. For the genu, fixing the slopes of the covariates across sex did not significantly affect the model fit ($\Delta\chi^2(2) = 2.13$, $p = .345$). The association between MWF and DriftRate1, as well with Δ, was not statistically significant ($p = .549$; $p = .520$, respectively). Finally, for the Plic, we also found that fixing the slopes of the covariates across sex did not significantly affect the model fit ($\Delta\chi^2(2) = 1.76$, $p = .414$). The association between MWF and DriftRate1, as well with Δ, was not statistically significant ($p = .743$; $p = .178$, respectively).

$\underline{\text{geomT}_{2\text{-IEW}}}$

Starting with Slf, we found that fixing the slopes of the covariates across sex did not significantly affect the model fit ($\Delta\chi^2(2) = .59$, $p = .744$). Furthermore, we found that the association between $\text{geomT}_{2\text{-IEW}}$ and DriftRate1, as well with Δ, was not statistically significant ($p = .875$; $p = .622$, respectively).

For the genu, fixing the slopes of the covariates across sex did not significantly affect the model fit ($\Delta\chi^2(2) = .32$, $p = .852$). Furthermore, we found that the association between $\text{geomT}_{2\text{-IEW}}$ and DriftRate1 was not statically significant ($p = .179$), however, the $\text{geomT}_{2\text{-IEW}}$ was significantly associated with Δ at the unadjusted $\alpha = .05$ level ($p = .012$). The model was re-evaluated after dropping $\text{geomT}_{2\text{-IEW}}$ as a covariate of DriftRate1. The $\text{geomT}_{2\text{-IEW}}$ was significantly associated with Δ ($\beta = -.887$, $p = .016$) at the unadjusted $\alpha = .05$ level. Fit indices for the final model were: $\chi^2(77) = 105.993$, $p = .016$, $\chi^2/df = 1.37$, CFI = .986, TLI = .984, RMSEA =.06. It should be noted that age was positively associated with Δ ($\beta = .092$, $p = .022$), at the unadjusted $\alpha = .05$ level, after including the $\text{geomT}_{2\text{-IEW}}$ of the genu. Figure 6.3 depicts the final model. Figure 6.4 depicts the association between Δ and the $\text{geomT}_{2\text{-IEW}}$ of the genu.

Figure 6.3: LCSM genu model. Age is negatively associated with DriftRate1 while the geomT$_{2\text{-IEW}}$ in the genu is negatively associated with Δ.

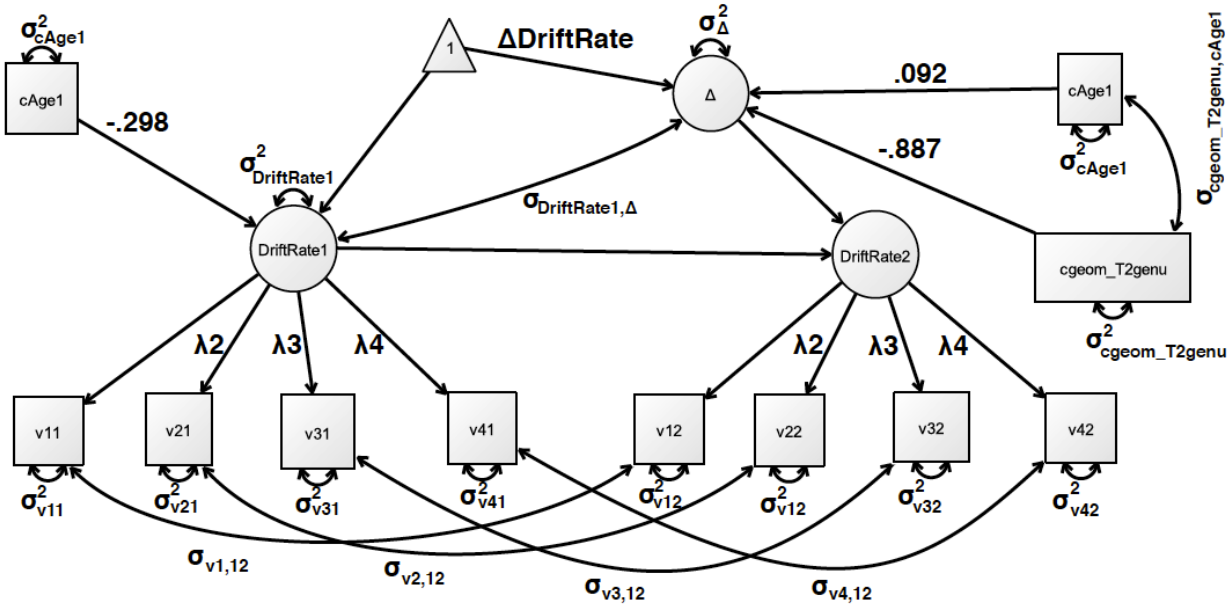

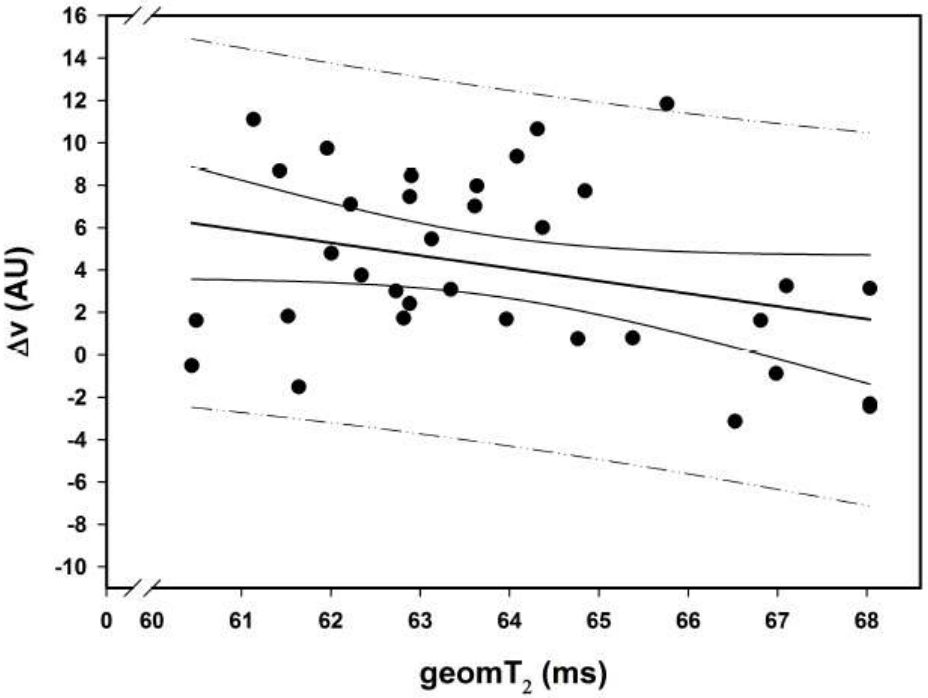

Figure 6.4: Genu geomT$_{2\text{-IEW}}$ and Δ association. The geomT$_{2\text{-IEW}}$ in the genu is negatively associated with change in drift rate. In other words, persons with longer geomT$_{2\text{-IEW}}$ exhibited smaller positive gains or negative change in drift rate. Note this association did not reach the Bonferroni adjusted significance level. Dashed lines are 95% prediction lines while the solid lines around the regression line are the 95% confidence lines.

For the Plic, fixing the slopes of the covariates across sex did not significantly affect the model fit: $\Delta\chi^2(2)= .502$, $p = .778$. Furthermore, we found that the association between $geomT_{2\text{-}IEW}$ and DriftRate1, as well with Δ, was not statistically significant ($p = .978$; $p = .172$, respectively).

6.6 Discussion and Limitations

Effects of Age on drift rate and change therein

Age was negatively associated with drift rate at the first measurement occasion (DriftRate1), in line with a previous study, using a similar task and extreme age groups, which demonstrated that older individuals had lower drift rates (Thapar, Ratcliff, & McKoon, 2003). Age did not, however, predict change in processing speed. The absence of age differences in change implies that the observed change in drift rate are related to other factors, that may include increased familiarity with the task due to repeated exposure.

Effects of ME-T_2 indices on drift rate and change therein

After statistically controlling for age effects, for all tracts investigated, MWF was associated with neither baseline drift rate, nor with change therein. Thus, within the limitations of the study, we could not find support for the hypothesis positing that greater myelin content, in the hypothesized tracts, would be associated with faster drift rate or greater change in drift rate.

We found a negative association between the $geomT_{2\text{-}IEW}$ in the genu and change in drift rate, while statistically controlling for age effects. This association, however, did not achieve the Bonferroni-adjusted significance level. Nonetheless, considering the relatively small sample size, which limited our power, and the similarity of our results with that of a recent study (Dawe et al., 2016) we will consider an interpretation of the results. While on average drift rate was greater at the second measurement occasion, as reflected by a positive change value (Table 6.3), the significant variance in change indicates that some individuals improved by more than three units

while others performance decreased (negative change). The negative association between change in drift rate and the $geomT_{2\text{-}IEW}$ of the genu suggests that the shorter the $geomT_{2\text{-}IEW}$ the larger, more positive, the change in drift rate (Figure 6.4). As discussed in chapter 2, interpreting the $geomT_{2\text{-}IEW}$ is not straightforward because it can reflect both axonal density and diameter. However, given the negative association it seems more plausible to interpret the $geomT_{2\text{-}IEW}$ as reflecting axonal density. Let's first consider what we would expect if the $geomT_{2\text{-}IEW}$ was reflective of axonal diameter.

After statistically controlling for age effects, we would expect a positive association between change in speed and the $geomT_{2\text{-}IEW}$. This is because larger diameter axons have larger $geomT_{2\text{-}IEW}$ values and would therefore be expected to conduct action potentials faster. This is not what we find however. It should also be noted that such a finding would be inconsistent, with our lack of MWF findings because increasing myelination has a greater effect on conduction velocity than simply increasing axonal diameter. On the other hand, if the $geomT_{2\text{-}IEW}$ is viewed as reflecting axonal density, then the negative association is expected. A higher density of axons, and therefore a smaller $geomT_{2\text{-}IEW}$, would be expected to be associated with a more positive change in processing speed. A recent study provides some evidence in support of our interpretation, though we acknowledge the limitations of our findings considering the limited sample size.

In a study of 425 deceased older adults consisting of persons from the Longitudinal Rush Memory and Aging Project and the Religious Orders Study Dawe et al (2016) used a mixed-effects analysis to estimate between subject variance in longitudinal change, slope, in various memory domains as well as processing speed. Upon death, subjects' brains underwent ex-vivo MRI using a fast spin echo sequence to generate T_2 relaxation images (note that the authors report R_2 but $R_2 = 1/T_2$). The authors found that between-subject differences in the slope of cognitive decline,

across the cognitive domains investigated, was associated with T_2 relaxation time constants in frontal and temporal white matter. Longer T_2 values were associated with a greater slope of decline in cognitive function. The authors speculate shorter T_2 relaxation time constants may reflect a greater number of axons and therefore persons with shorter T_2 exhibited smaller slopes of decline. While there are clear differences between Dawe et al. and our study, including our use of multi-exponential T_2 modeling and subject characteristics, nonetheless this study does suggest that individual differences in T_2 relaxation may be associated with individual differences in change in processing speed, consistent with our findings.

It should be noted that this dissertation was not initially designed to explore the role of axonal density or the $geomT_{2\text{-}IEW}$ and therefore we did not have additional, independent measures, of axonal density which would have helped in the interpretation of our results and provided additional evidence. Indeed prior to this work the $geomT_{2\text{-}IEW}$ was relatively unexplored. These results demonstrate that further work needs to be conducted to fully appreciate the significance of the $geomT_{2\text{-}IEW}$. Just as MWF has received extensive validation using ex-vivo tissue and animal models (Beaulieu et al., 1998; Laule et al., 2008; McCreary et al., 2009), the $geomT_{2\text{-}IEW}$ needs to be investigated using similar methods to clarify its interpretation.

Limitations

There were several limitations to this study. First, we assessed processing speed at only two occasions. Repeated testing effects are well known and are the largest between the first and second measurement occasions (Collie et al., 2003; Salthouse, Schroeder, & Ferrer, 2004). Therefore, if the effects of MWF or $geomT_{2\text{-}IEW}$ are smaller than the retest effects it is possible that we may not have been able to detect them. Salthouse et al. (Salthouse, Schroeder, & Ferrer, 2004) has estimated

that at least seven years is needed before retest effects are no longer detectable and given that on average we had a two year delay we should expect retest effects to be a confound.

Second, not only did we have a relatively small sample of participants who had both ME-T_2 imaging and longitudinal behavioral data, the imaging was collected at the second measurement occasion. This precluded inferences about the predictive nature of the ME-T_2 indices. Future studies should collect both imaging and behavioral data concurrently, and at multiple occasions. This would allow us to investigate whether changes in imaging indices parallel changes in behavior.

Third, because this study was not initially designed to test hypothesis involving axonal density caution should be taken when interpreting results. Given the age-heterogeneous sample and the relatively small number of subjects who also had imaging, we could not divide our participants into narrow age bins. This would minimize age effects on processing speed and imaging measures, allowing us to investigate the relationship between the two and to see whether the associations vary by age group.

Fourth, we selected only a few tracts to investigate. While the tract selection was motivated by considering the literature and to minimize multiple comparisons given the novelty of the imaging measures and the lack of studies investigating their relationship to behavior it may be worthwhile to consider alternative analysis in the future. For example, one could conduct an "unbiased" search by doing a voxel-wise analysis of the relationship between the imaging measures and behavior. These results, after correcting for multiple comparison, could then be compared with tractography to see if they overlap with defined tracts.

With regards to the lack of associations between MWF and drift rate and change therein there are a few points to consider. First, we used an atlas-based method to define our hypothesized tracts.

Atlas-based tracts are probabilistic in nature and do not capture variation in tract anatomy. For example, the Slf as defined in the John's Hopkins University (JHU) atlas is a single tract, whereas the actual Slf is composed of at least four tracts with different cortical points of origin and termination (Makris et al., 2005) in the cerebral cortex. Use of high angular resolution DTI to define tracts, within the subjects' space, can mitigate the limitations of atlas based methods by allowing us to follow tracts from one association cortex to another and to evaluate myelination differences along the tract. With such an approach, we could select specific regions of the association cortices, identify tracts connecting them, and assess myelin content only in select tracts. Second, cohort effects cannot be avoided in an age heterogeneous sample when comparing baseline processing speed. In brief when we compare processing speed of a 20-year-old compared to an 80-year-old (who was 20 in the year 1937) we are assuming, on average, the 80-year old's processing speed was like that of 20-year old's today. Furthermore, we assume that our 20-year old's performance will, on average, be comparable to our 80 year olds sixty years from now. In other words, we assume that there is no difference in mean performance as a function of the birth cohort. However, this assumption is not supported as longitudinal studies of aging with, various birth cohorts, have demonstrated that baseline performance on processing speed, along with other cognitive functions, depends on the birth cohort with later born cohorts exhibiting better performance (Brailean, et al., 2016; Gerstorf & Ram, 2011). Therefore, a lack of associations between MWF, or the $geomT_{2\text{-}IEW}$, with the drift rate does not suggest that either variable is not important at predicting cognitive processing speed, only longitudinal studies of change in drift rate and change in MWF or $geomT_{2\text{-}IEW}$ will provide us with that information.

6.7 Conclusions

In a longitudinal study design across the adult lifespan we investigated associations between processing speed, indexed by the drift rate, and myelin content as well as a putative measure of axonal density. Within the framework of latent change score modeling we found that individual differences in $geomT_{2\text{-}IEW}$, in the genu of the corpus callosum, was associated with change in drift rate, while accounting for age effects, though this finding did not reach the Bonferroni adjusted significance level. While these results are interesting given the limitations of the study longitudinal investigations need to be conducted to clarify the role of myelin content and axonal density as mediators of aging related change in drift rate. Furthermore, animal research needs to be conducted to examine the hypothesis that the $geomT_{2\text{-}IEW}$ is an index of axonal density.

CHAPTER 7: Discussion and Future Directions

7.1 Discussion

Advancements in quantitative in-vivo imaging has made it possible to study the human brain from development to old age. We can ask how development and aging are modified by genetic or environmental factors and how these variables are related to behavioral change over the lifespan. Imaging methods which provide indices reflective of microstructural neuroanatomy allow us to infer the biological mechanisms which may be responsible for the changes in cognitive function. Without such tools, we would be limited to studying the human brain postmortem. Furthermore, imaging is one of the few tools that can be used in both humans and animals which makes it an excellent tool to conduct translational research.

One of the main goals of cognitive aging research has been to use these tools to investigate how the aging process affects the brain and the relationship between brain and behavior. The long-term goal of such work is to identify the neural mechanisms responsible for cognitive aging with the hopes that we could someday develop targeted interventions to mitigate cognitive aging.

To this end, using a novel quantitative imaging method with histologically confirmed interpretation of one of its indices, MWF, we investigated age differences in myelin content and its relationship with information processing speed and change therein. We also explored another imaging metric, $geomT_{2\text{-}IEW}$, which is thought to reflect axonal density/diameter, and its association with processing speed. Given the central role processing speed plays in hypothesis of cognitive aging, identifying its potential neural substrates is critical to understanding the neurobiology of age related slowing.

First, we established the reliability of both indices (ICC $\geq$ .80) across multiple white matter tracts and demonstrated that there was no differential unreliability. We also achieved sufficient

reliability after repositioning participants in the scanner. These results were very promising and suggested that both indices are of sufficient reliability to be used in longitudinal investigations. After establishing reliability, we investigated age differences in myelin content. Myelin loss has been hypothesized as potential substrate of age related slowing, to date however testing this hypothesis has been difficult due to the lack of valid in-vivo imaging indices. In fact, the commonly used imaging indices are unable to reproduce the protracted myelin of subcortical white matter suggested by postmortem work. Given the substantial histological validation of MWF, as a measure of myelin content, we expected this measure should be able to demonstrate the quadratic age effects suggested in postmortem studies.

The study in chapter 5 provided in-vivo demonstration of the quadratic effects of age on myelin content, consistent with postmortem investigations. Many studies have attempted to investigate age differences in myelin using diffusion imaging techniques, yet most studies in adults produced linear age effects which were inconsistent with postmortem studies. As mentioned in chapter 5, the reported nonlinear age effects in the literature tend to include young children and adolescence and the peak values are reached in early adulthood. This is clearly inconsistent with the peak ages suggested in postmortem work. Given the histological and experimental validation of MWF we expected that unlike the diffusion based indices, MWF would produce quadratic age effects consistent with the postmortem studies. As hypothesized, we demonstrated quadratic age effects across multiple white matter tracts and found that the pattern of myelin content between the tracts was consistent with postmortem studies as well. Had MWF not shown quadratic age effects it would raise the possibility that perhaps in-vivo it is not a good proxy for myelin content and would require further exploration. Once we established the quadratic effect of age on MWF, providing

more evidence for interpretation of MWF as reflecting myelin content, we then proceeded to the main goal of this thesis.

As stated in the introduction many studies have hypothesized that age differences in myelin content are associated with age differences in speed of processing. However, the commonly used diffusion indices are not associated with MWF and therefore these studies were unable to test hypothesis related to myelin. We measured speed of processing at two occasions, allowing us to investigate associations between MWF and change in speed of processing. In two hypothesized white matter tracts, Slf and the genu of the corpus callosum, we tested whether myelin content was associated with processing speed or change in speed after adjusting for age. We did not find any statistically significant associations. We also explored the associations between the $geomT_{2\text{-}IEW}$, an index thought to represent axonal diameter/density and with processing speed. We found a negative association between change in processing speed and the $geomT_{2\text{-}IEW}$ in the genu, however this was not significant at the Bonferroni adjusted level. Given the sign of the association, we speculate that this finding is plausible with the interpretation of the $geomT_{2\text{-}IEW}$ as an index of axonal density, suggesting that a higher axonal density, smaller $geomT_{2\text{-}IEW}$, is associated with a more positive change in processing speed.

Whereas the first two studies produced findings that are relatively easy and straightforward to interpret, the final study results are more complex. Nonetheless, this study was the first to directly test hypothesis linking myelin content and processing speed, as previous studies have relied on more global and nonspecific indices of the white matter. Furthermore, to the best of our knowledge, this study was also the first to explore the potential significance of the $geomT_{2\text{-}IEW}$ in characterizing putative brain substrates of age-related cognitive change. Although the results should be interpreted with caution, they are nonetheless informative and open a new line of investigation.

Namely, they point to the loss of axons, rather than myelin loss as potential substrate of age-related slowing.

The results of this dissertation are significant for several reasons. First, we established reliability of the ME-T_2 indices of white matter properties, which is a necessary condition for conducting valid longitudinal investigations. In particular, it was important to establish uniform reliability of white-matter measures across diverse tracts as a foundation for a valid discourse of differential effects. Second, by confirming quadratic associations between chronological age and MWF that mirrors the histological findings, we contributed to in-vivo validation of MWF, as a measure of myelin content. Finally, although we could not confirm the link between myelin content and processing speed, our results brought attention to the possible role of axon density as reflected in geom$T_{2\text{-IEW}}$ and at the very least we have identified a new path of investigation in the future.

7.2 Limitations

The findings reported here should be interpreted in the context of several limitations. First, our demonstration of quadratic associations between age and MWF was based on cross-sectional data. In cross-sectional designs, many sources of individual differences are confounded with age and elucidation of individual temporal dynamics of aging is impossible. Second, our ROI-based analysis precluded assessment of variation in myelin content along the tracts. The assumption of myelin content uniformity may not hold, especially when age-related shifts in demyelination-remyelination equilibrium are considered. Third, due to limitations of the current technique we could not investigate myelin in important but narrow white matter tracts (e.g.: fornix) nor could we investigate intra-cortical myelination. Fourth, while we used a longitudinal dataset to evaluate change in processing speed, we only had two occasions which is insufficient to define a trajectory

and examine possible nonlinear changes. Furthermore, because we only had two measurement occasions, we could not model the effects of repeated exposure on age-related change in drift rate. Fifth, we did not have longitudinal measures of MWF or geom$T_{2\text{-IEW}}$, and therefore we could not investigate whether changes in these measures precedes, follows or mirrors changes in processing speed. Sixth, the original focus of this project was on assessing myelin content and therefore did not include neuroimaging means that would be necessary for validating the geom$T_{2\text{-IEW}}$ as an index of axonal density. Finally, given the novelty of ME-T_2 imaging very little work has been done to investigating associations between its neurobiologically relevant indices and behavior. While this study used a hypothesis based selection of tracts, we could not rule out the possibility that other tracts maybe involved. Future studies may use more inclusive methods of white matter evaluation to explore these associations.

7.3 Future Directions

The results of this thesis offer exciting directions for future investigations. First, after its utility has been demonstrated, the ME-T_2 sequence should be further developed to allow faster acquisition and better spatial resolution. This will make it compatible with DTI-based tractography, which will allow defining tracts within the subject space and investigating within-tract variations. Furthermore, by reducing the echo times we would increase the SNR and if the gain was significant we could perhaps investigate intra-cortical myelin.

Because myelination is a life-long process, future studies should include participants across the lifespan and assess MWF at multiple occasions. This would provide significant insight into both development and aging as well as characterize individual variation therein. As the results of this thesis have demonstrated, proper characterization of cerebral white matter should also include an investigation into changes in axonal density. While much of the literature has focused on the

relationship between myelin and cognitive function, investigations into the relationship between measures of axonal density and cognitive function has been relatively unexplored.

Longitudinal investigations of myelin content and axonal properties should be accompanied with multiple measurements of speed of processing along with other cognitive functions. Such studies would allow us to investigate whether changes in myelin or axonal density predict changes in processing speed differentially with respect to cognitive operations involved in decision making. Considering the complex relationships between age, cognition, and in vivo measures of myelin or axon density and diameter, it may be worthwhile to consider multiple age bins along the lifespan. Within each bin the effects of age on cognition and imaging measures should be small and therefore allow for investigations of individual differences in the imaging measures and its association with cognition. Comparing cognition and imaging associations across the bins could offer insight into how age effects these relationships.

An interesting trend observed in this project, albeit not at a stringent level of statistical significance, was the association between the change in processing speed and the $geomT_{2\text{-}IEW}$. Shorter $geomT_{2\text{-}IEW}$ was associated with a more positive change in drift rate. We speculate that the $geomT_{2\text{-}IEW}$ may be interpreted as reflecting axonal density, with shorter $geomT_{2\text{-}IEW}$ values suggesting greater axonal density. Within this framework, we hypothesize that higher axonal density maybe associated with a greater magnitude change or improvement in processing speed. This is consistent with a recent study reporting that shorter T_2 relaxation times are associated with a smaller slope of decline in cognition. While our finding needs to be replicated in a larger sample perhaps more importantly this project has revealed the potential significance of the $geomT_{2\text{-}IEW}$. This index has been relatively unexplored with very little work done in animals to provide insight into its interpretation. Given our findings we believe animal models ranging with a wide variety

of neuropathology, from axonal degeneration to loss of dendrites, should be used to provide insight into the interpretation of the $geomT_{2\text{-}IEW}$ in both white and gray matter.

Finally, while this dissertation focused on healthy adults exploring the utility of ME-T_2 indices in a variety of neurological or psychiatric conditions may prove fruitful. Among the strengths of ME-T_2 imaging include the relatively straightforward interpretations of its indices which would be highly relevant for clinical applications (e.g.: multiple sclerosis or post- radiation therapy). Finally, its quantitative nature should make the method more robust to across scanner and site variation which is critical for multi-site clinical trials.

REFERENCES

Aanerud, J., Borghammer, P., Chakravarty, M.M., Vang, K., Rodell, A.B., Jonsdottir, K.Y., Moller, A., Ashkanian, M., Vafaee, M.S., Iversen, P., Johannsen, P., & Gjedde, A. (2012). Brain energy metabolism and blood flow differences in healthy aging. *J Cereb Blood Flow Metab*, *32*(7), 1177-1187.

Aboitz, F., Scheibel, A.B., Fisher, R.S., & Zaidel, E. (1992). Fiber composition of the human corpus callosum. *Brain Res*, *589*(1-2),143-153.

Alonso-Ortiz, E., Levesque, I.R., & Pike, G.B. (2015). MRI-based myelin water imaging: A technical review. *Magn Reson Med*, *73*(1), 70-81.

Arshad, M., Stanley, J.A., & Raz N. (2016). Adult age differences in subcortical myelin content are consistent with protracted myelination and unrelated to diffusion tensor imaging indices. *Neuroimage, 143*, 26-39.

Arshad, M., Stanley, J.A., & Raz N. (2017). Test-retest reliability and concurrent validity of in vivo myelin content indices: Myelin water fraction and calibrated T1w/T2w image ratio. *Hum Brain Mapp*, *38*(4), 1780-1790.

Ayus, J.C., Armstrong, D.L., & Arieff, A.I. (1996). Effects of hypernatremia in the central nervous system and its therapy in rats and rabbits. *J Physol, 492*(1), 243-255.

Ball, K., Ross, L.A., Roth, D.L., & Edwards, J.D. (2013). Speed of processing training in the ACTIVE study: Who Benefits?. *J Aging Health*, *25*(8), 65S-84S.

Baltes, P.B., & Nesselroade, J.R. (1979). History and rational of longitudinal research. In: Nesselroade JR, Baltes PB, editors. Longitudinal research in the study of behavior and development. New York: Academic Press. pp 1-39.

Bartzokis, G., Beckson, M., Po, H.L., Nuechterlein, K.H., Edwards, N., Mintz, J. (2001). Age-related changes in frontal and temporal lobe volumes in men: A magnetic resonance imaging study. *JAMA Psychiatry*, *58*(5), 461-465.

Bartzokis, G. (2004). Age-related myelin breakdown: A developmental model of cognitive decline and Alzheimer's disease. *Neurobiol Aging*, *25*(1), 5-18.

Basser, P.J., Mattiello, J., & LeBihan, D. (1994). Estimation of the effective self-diffusion tensor from the NMR spin echo. *J Magn Reson Series B*, *103*(3), 247-254.

Bayless, D.W., & Daniel, J.M. (2015). Sex differences in myelin-associated protein levels within and density of projections between the orbital frontal cortex and dorsal striatum of adult rats: implications for inhibitory control. *Neuroscience*, *300*, 286-296.

Beaulieu, C., Fenrich, F.R., & Allen, P.S. (1998). Multicomponent water proton transverse relaxation and T2-discriminated water diffusion in myelinated and nonmyelinated nerve. *Magn Reson Imaging*, *16*(10), 1201-1210.

Beaulieu, C. (2002). The basics of anisotropic water diffusion in the nervous system-technical review. *NMR in Biomedicine, 15*(7-8), 435-455.

Bender, A.R., & Raz, N. (2015). Normal-appearing cereberal white matter in healthy adults: mean change over 2 years and individual differences in change. *Neurobiol. Aging*, *36*(5), 1834-1848.

Bender, A.R., Volkle, M.C., & Raz, N. (2016). Differential aging of cerebral white matter in middle-aged and older adults: a seven-year followup. *Neuroimage*, *125*, 74-83.

Bennett, I.J., & Madden D.J. (2014). Disconnected aging: Cerebral white matter integrity and age related differences in cognition. *Neuroscience, 276*, 187-205.

Bieri, O., & Scheffler, K. (2006). On the origin of apparent low tissue signals in balanced SSFP. *Mag Reson Med*, *56*(5), 1067-1074.

Billiet, T., Vandenbulcke, M., Madler, B., Peeters, R., Dhollander, T., Zhang, H., Deprez, S., Van den Bergh, B.R., Sunaert, S., & Emsell, L. (2015). Age-related microstructural differences quantified using myelin water imaging and advanced diffusion MRI. *Neurobiol Aging*, *36*(6),2107-2121.

Birren, J.E., & Fisher, L.M. (1995). Aging and slowing of behavior: Possible consequences for psychological functioning. *Annual Review of Psychology, 46*(1), 329-353.

Bloembergen, N., Purcell, E.M., & Pound, R.V. (1948). Relaxation effects in Nuclear Magnetic Resonance Absorption. *Physical Review*, *73*(7), 679-716.

Bratic, I., & Trifunovic, A. (2010). Mitochondrial energy metabolism and ageing. *Biochim Biophys. ACTA-Bioenergetics*, *1797*(6-7), 961-967.

Brailean, A., Huisman M., Prince, M., Prina, A.M., Deeg D.J., & Comijs, H. (2016). Cohort differences in cognitive aging in the longitudinal aging study Amsterdam. *J Gerontol B Psychol Soc Sci,* gbw129.

Bucur, B., Madden D.J., Spaniol J., Provenzale J.M., Cabeza, R., White, L.E., & Huettel, S.A. (2008). Age-related slowing of memory retrieval: Contributions of perceptual speed and cerebral white matter integrity. *Neurobiol Aging, 29*(7), 1070-1079.

Busemeyer, J.R. (1985). Decision making under uncertainty: a comparison of simple scalability, fixed-sample, and sequential-sampling models. *J Exp Psychol Learn Mem Cogn*, *11*(3), 538-564.

Callaghan, M.F., Freund, P., Draganski, B., Anderson, E., Cappelletti, M., Chowdhury, R., Diedrichsen, J., FitzGerald, T.H.B, Smittenaar, P., Helms, G., Lutti, A., & Weiskopi, N.

(2014). Widespread age-related differences in the human brain microstructure revealed by quantitative magnetic resonance imaging. *Neurobiol Aging*, *35*(8),1862-1872.

Chevalier, N., Kurth, S., Doucette M.R., Wiseheart, M., Deoni S.CL., Dean, D.C., O'Muircheartaigh, J., Blackwell K.A., Munakata, Y., & LeBourgeois M.K. (2015). Myelination is associated with processing speed in early childhood: preliminary insights. *Plos One, 10*(10), e0139897.

Cohen, Y.E. (2009). Multimodal activity in the parietal cortex. *Hear Res, 258*(1-2), 100-105.

Collie, A., Maruff, P., Darby D.G., & McStephen M. (2003). The effects of practice on the cognitive test performance of neurologically normal individuals assessed at the brief test-retest intervals. *J Int Neuropsychol Soc, 9*(3). 419-428.

Craven, P., & Wahba, G. (1979). Smoothing noisy data with spline functions. Estimating the correct degree of smoothing by the method of Generalized Cross Validation. *Numerische Mathematik*, *31*, 377-403.

Crawley, A.P., & Henkelman, R.M. (1987). Errors in T2 estimation using multislice multiple-echo imaging. *Magnetic Resonance in Medicine*, *4*(1), 34-47.

Cserr, H.F., DePasquale M., Nicholson, C., Patlak, C.S., Pettigrew, K.D., & Rice, M.E. (1991). Extracellular volume decreases while cell volume is maintained by ion uptake in rate brain during acute hypernatremia. *J Physiol, 442*, 277-295.

Daffner, K.R. (2010). Promoting successful cognitive aging: A comprehensive review. *J Alzheimers Dis, 19*(4), 1101-1122.

Daugherty, A.M., Haacke, E.M., & Raz N. (2015). Striatal iron content predicts its shrinkage and changes in verbal working memory after two years in healthy adults. *J Neurosci*, *35*(17), 6731-6743.

Davis, S.W., Dennis, N.A., Buchler, N.G., White, L.E., Madden, D.J., & Cabeza, R. (2009). Assessing the effects of age on long white matter tracts using diffusion tensor tractography. *Neuroimage*, *46*(2), 530-541.

Davis, K.L., Stewart, D.G., Friedman, J.I., Buchsbaum, M., Harvey, P.D., Hof, P.R., Buxbaum, J., & Haroutunian, V. (2003). White matter changes in schizophrenia: evidence for myelin-related dysfunction. *Arch Gen Psychiatry*, *60*(5), 443-456.

Dawe, R.J., Yu, L., Leurgans, S.E., Schneider, J.A., Buchman, A.S., Arfanakis, K., Bennett, D.A., & Boyle, P.A. (2016). Postmortem MRI: a novel window into the neurobiology of late life cognitive decline. *Neurobiology of Aging, 45*, 169-177.

Deary, I.J., Corley, J., Gow, A.J., Harris S.E., Houlihan, L.M., Marioni, R.I., Penke, L., Rafnsson, S.B., & Starr J.M. (2009). Age-associated cognitive decline. *Br Med Bull, 92*, 135-152.

de Hoz, L., & Simons, M. (2015). The emerging functions of oligodendrocytes in regulating neuronal network behavior. *Bioessays*, *37*, 60-69.

Demaree, H.A., DeLuca, J., Gaudino, E.A., & Diamond, B.J. (1999). Speed of information processing as a key deficit in multiple sclerosis: Implications for rehabilitation. *Journal of Neurology Neurosurgery and Psychiatry*, *67*(5), 661-663.

Deoni, S.C.L., Dean, D.C.D., Remer, J., Holly, D., & O'Muircheartaigh, J. (2015). Cortical maturation and myelination in healthy toddlers and young children. *Neuroimage*, *115*, 147-161.

Deoni, S.C.L., Matthews, L., & Kolind, S.H. (2013). One component? Two components? Three? The effects of including a non-exchanging free water component in multicomponent

driven equilibrium single pulse observation of T1 and T2 (mcDESPOT). *Mag Reson Med*, *70*(1), 147-154.

Deoni, S.C.L., Rutt, B.K., Arun, T., Pierpaoli, C., & Jones, D.K. (2008). Gleaning multicomponent T1 and T2 information from steady-state imaging data. *Magn Reson Med*, *60*(6), 1372- 1387.

De Santis, S., Jones, D.K., & Roebroeck, A. (2016). Including diffusion time dependence in the extra-axonal space improves in vivo estimates of axonal diameter and density in human white matter. *Neuroimage*, *130*, 91-103.

Dixon, W.T., Engels, H., Castillo, M., & Sardashti, M. (1990). Incidental magnetization transfer contrast in standard multislice imaging. *Magn Reson Imaging*, *8*, 417-422.

Dodge, H.H., Kadowaki, T., Hayakawa, T., Yamakawa, M., Sekikawa, A., Ueshima, H. (2005). Cognitive impairment as a strong predictor of incident disability in specific ADL-IADL tasks among community-dwelling elders: The Azuchi Study. *Gerontologist, 45*(2), 222-230.

Domenech, P., & Koechlin, E. (2015). Executive control and decision-making in the prefrontal cortex. *Current Opinion in Behavioral Sciences, 1,* 101-106.

Dula, A.N., Gochberg, D.F., Valentine, H.L., Valentine, W.M., & Does, M.D. (2010). Multi-exponential T2, Magnetization Transfer, and Quantitative Histology in White Matter Tracts of Rat Spinal Cord. *Magn Reson Med*, *63*(4), 902-909.

Faisal, A.A., Selen, L.P.J., & Wolpert, D.M. (2008). Noise in the nervous system. *Nat Rev Neurosci, 9*(4). 292-303.

Finkel, D., Reynolds, C.A., McArdle, J.J., & Pedersen, N.L. (2005). The longitudinal relationship between processing speed and cognitive ability: genetic and environmental influences. *Behav Genet., 35*(5), 535-549.

Fjell, A.M., McEvoy, L., Holland, D., Dale, A.M., Walhovd, K,B., & Alzheimer's Disease Neuroimaging Initiative. (2014). What is normal in normal aging? Effects of aging, amyloid and Alzheimer's disease on the cerebral cortex and the hippocampus. *Prog Neurobiol*, *117*, 20-40.

Flynn, S.W., Lang, D.J., MacKay, A.L., Goghari, V., Vavasour, I.M., Whittall, K.P., Smith, G.N., Arango, V., Mann, J.J., Dwork, A.J., Falkai. P., & Honer, W.G. (2003). Abnormalities of myelination in schizophrenia detected in vivo with MRI, and postmortem analysis of oligodendrocyte proteins. *Mol Psychiatry*. *8*(9), 811-820.

Folstein, M.F., Folstein, S.E., & McHugh P.R. (1975). "Mini-mental state". A practical method for grading the cognitive state of patients for the clinician. *J Psychiatric Res*, *12*(3), 189-198.

Gerstorf, D., & Ram N. (2011). Cohort differences in cognitive aging and terminal decline in the Seattle Longitudinal Study. *Dev Psychol, 47*(4), 1026-1041.

Ghisletta, P., & McArdle, J.J. (2012). Teacher's corner: Latent curve models and latent change score models estimated in R. *Struct Equ Modelling, 19*(4), 651-682.

Gittelman, J.X., & Tempel B.L. (2006). Kv1.1-Containing channels are critical for temporal precision during spike initiation. *J. Neurophysiol, 96*, 1203-1214.

Golub, G.H., Heath, M., & Wahba, G. (1979). Generalized cross-validation as a method for choosing a good ridge parameter. *Technometrics*, *21*(2), 215-223.

Gregorich, S.E. (2006). Do self-report instruments allow meaningful comparisons across diverse population groups? Testing measurement invariance using confirmatory analysis framework. *Med. Care, (11 Suppl 3)*, S78-S94.

Gunning-Dixon, F.M. & Raz N. (2000). The cognitive correlates of white matter abnormalities in normal aging: A quantitative review. *Neuropsychology*, *14*(2), 224-232.

Gulani, V., Webb, A.G., Duncan, I.D., & Lauterbur, P.C. (2001). Apparent diffusion tensor measurements in myelin-deficient rat spinal cords. *Mag Reson Med*, *45*(2), 191-195.

Haacke, E.M., Brown B.M., Thompson, M.R., Venkatesan R. (1999). *Magnetic Resonance Imaging: Physical Principles and Sequence Design.* John Wiley & Sons.

Haines, J.D., Inglese, M., & Casaccia, P. (2011). Axonal damage in multiple sclerosis. *Mt Sinai J Med. 78*(2), 231-243.

Haller, S., Kovari, E., Herrmann, F.R., Cuvinciuc, V., Tomm, A.M., Zulian, G.B., Lovblad, K.O., Giannakopoulos, P., & Bouras, C. (2013). Do brain T2/FLAIR white matter hyperintensities correspond to myelin loss in normal aging? A radiologic-neuropathologic correlation study. *Acta Neuropathol Commun*, *9*, 1-14.

Hansen, P.C. (1992). Analysis of discrete ill-posed problems by means of the l-curve. *SIAM Review*, *34*(4), 561-580.

Hansen, P.C. (1992). Numerical tools for analysis and solution of Fredholm integral equations of the first kind. *Inverse Problems*, *8*(6), 849-872.

Harkins, K.D., Xu, J., Li, K., Valentine, W.M., Gochberg, D.F., Gore, J.C., & Does, M.D. (2016). The microstructural correlates of T1 in white matter. *Magn Reson Med*, *75*(3), 1341-1345.

Harreveld, A.V., Collewijn, H., & Malhotra, S.K. (1966). Water, electrolytes, and extracellular space in hydrated and dehydrated brains. *Am J Physiol, 210*(2), 251-266.

Harris, J.J., & Attwell, D. (2012). The energetics of the central nervous system white matter. *J Neurosci, 32*(1), 356-371.

Hasan, K.M., Kamali, A., Iftikhar, A., Kramer, L.A., Papanicolaou, A.C., Fletcher, J.M., & Ewing-Cobbs, L. (2009). Diffusion tensor tractography quantification of the human corpus callosum fiber pathways across the lifespan. *Brain Res*, *1249*, 91-100.

Henkelman R.M., Stanisz, G.J., & Graham, S.J. (2001). Magnetization transfer in MRI: a review. *NMR Biomed, 14*, 57-64.

Hennig J. (1988). Multiecho imaging sequences with low refocusing flip angles. *Journal of Magnetic Resonance*, *78*(3), 397-407.

Hertzog, C. (1989). Influences of cognitive slowing on age differences in intelligence. *Developmental Psychology*, *25*(4), 636-651.

Hodgkin, A.L., & Huxley, A.F. (1952). A quantitative description of membrane current and its application to conduction and excitation in nerve. *The Journal of Physiology, 117*(4), 500-544.

Hu, L.T., & Bentler, P.M. (1999). Cutoff criteria for fit indexes in covariance structure analysis: Conventional criteria versus new alternatives. *Structural Equation Modeling, 6*(1), 1-55.

Hua, K., Zhang, J., Wakana, S., Jiang, H., Li, X., Reich, D.S., Calabresi, P.A., Pekar, J.J., van Zijl, P.C., & Mori, S. (2008). Tract probability maps in stereotaxic spaces: Analyses of white matter anatomy and tract-specific quantification. *Neuroimage*, *39*(1), 336-347.

Huk, A.C., & Shadlen, M.N. (2005). Neural activity in macaque parietal cortex reflects temporal integration of visual motion signals during perceptual decision making. *J Neurosci, 25*(45), 10420-1036.

Hultsch, D.F., MacDonald, S.W., Hunter, M.A., Levy-Bencheton, J., & Strauss, E. (2000). Intraindividual variability in cognitive performance in older adults: comparison of adults with mild dementia, adults with arthritis, and healthy adults. *Neuropsychology, 14*(4), 588-598.

ICO. (1984). Visual Acuity Measurement Standard.

Jenkinson, M., Bannister, P., Brady, M., & Smith, S. (2002). Improved optimization for the robust and accurate linear registration and motion correction of brain images. *Neuroimage*, *17*(2), 825-841.

Jenkinson, M., Beckmann, C.F., Behrens, T.E., Woolrich, M.W.F, & Smith, S.M. (2012). FSL. *Neuroimage*, *62*(2), 782-790.

Jenkinson, M., & Smith, S. (2001). A global optimization method for robust affine registration of brain images. *Med Image Anal*, *5*(2), 143-156.

Jeurissen, B., Leeman A., Tournier, J.D., Jones D.K., & Sijbers, J. (2013). Investigating the prevalence of complex fiber configurations in white matter tissue with diffusion magnetic resonance imaging. *Hum Brain Mapp, 34*(11), 2747-2766.

Jones, D.K., Knosche, T.R., & Turner, R. (2013). White matter integrity, fiber count, and other fallacies: the do's and don't's of diffusion MRI. *Neuroimage, 73*, 239-254.

Joreskog, K.G. (1970). A general method for analysis of covariance structures. *Biometrika, 57*(2), 239-251.

Kaes T. (1907). Die Grosshirnrinde des Menschen in ihren Massen und in ihrem Fasergehalt Ein Gehirnanatomischer Atlas. Gustav Fischer, Jena.

Keeler J. (2005). *Understanding NMR Spectroscopy.* Chichester, England; Hoboken, NJ: Wiley.

Kennedy, K.M., & Raz, Naftali. (2009). Aging white matter and cognition: Differential effects of regional variations in diffusion properties on memory, executive functions, and speed. *Neuropsychologia, 47*(3), 916-927.

Knickman, J.R., & Snell, E.K. (2002). The 2030 problem: Caring for aging baby boomers. *Health Serv Res, 37*(4), 849-884.

Koch, C., Rapp, M., & Segev I. (1996). A Brief History of Time (Constants). *Cerebral Cortex, 6,* 93-101.

Kochunov, P., Williamson, D.E., Lancaster, J., Fox, P., Cornell, J., Blangero, J., & Glahn, D.C. (2012). Fractional anisotropy of water diffusion in cerebral white matter across the lifespan. *Neurobiol Aging*, *33*(1), 9-20.

Kroeker, R.M., & Henkelman, R.M. (1986). Analysis of biological NMR relaxation data with continuous distributions of relaxation times. *Journal of Magnetic Resonance*, *69*(2), 218-235.

Kumar, R., Pham, T.T., Macey, P.M., Woo, M.A., Yan-Go, F.L., & Harper, R.M. (2014). Abnormal myelin and axonal integrity in recently diagnosed patients with obstructive sleep apnea. *Sleep*, *37*(4), 723-732.

Lamantia, A.S., & Rakic, P. (1990). Cytological and quantitative characteristics of four cerebral commisures in the rhesus monkey. *J Comp Neurol*, 291, 520-537.

Lang, D.J.M., Yip, E., MacKay, AL., Thornton, A.E., Rodriguez, F.V., MacEwan, G.W., Kopala, L.C., Smith, G.N., Laule, C., MacRae, C.B., & Honer, W.G. (2014). 48 echo T2 myelin

imaging of white matter in first-episode schizophrenia: Evidence for aberrant myelination. *Neuroimage Clin*, *6*, 408-414.

Laule, C., Kozlowski, P., Leung, E., Li, D.K.B., MacKay, A.L., & Moore, G.R.W. (2008). Myelin water imaging of multiple sclerosis at 7T: correlations with histopathology. *Neuroimage*, *40*(4), 1575-1580.

Laule, C., Leung, E., Li, D.K.B., Traboulsee, A.L., Paty, D.W., MacKay, A.L., & Moore G.R.W. (2006). Myelin water imaging in multiple sclerosis: quantitative correlations with histopathology. *Mult Scler*, *12*(6), 747-753.

Laule, C., Vavasour, I.M., Moore, G.R.W., Oger J., Li, D.K.B, Paty, D.W., & MacKay, A.L. (2004). Water content and myelin water fraction in multiple sclerosis. A T2 Relaxation study. *J Neurol, 25*(3), 284-293.

Laule, C., Vavasour, I.M., Kolind, S.H., Traboulsee, A.L., Moore, G.R., Li, D.K., & MacKay, A.L. (2007). Long T2 water in multiple sclerosis: what else can we learn from multi-echo T2 relaxation. *Journal of Neurology*, *254*(11), 1579-1587.

Laule, C., Kozlowski, P., Leung, E., Li, D.K., Mackay, A.L., & Moore, G.R. (2008). Myelin water imaging of multiple sclerosis at 7T: correlations with histopathology. *Neuroimage*, *40*(4), 1575-1580.

Lawson, C.L., & Hanson, R.J. (1974). *Solving least square problems*. Prentice Hall, Englewood Cliffs NJ, 1974.

Lebel, C., Gee, M., Camicoli, R., Wieler, M., Martin, W., & Beaulieu, C. (2012). Diffusion tensor imaging of white matter tract evolution over the lifespan. *Neuroimage*, *60*(1), 340-352.

Lenz, C., Klarhofer, M., & Scheffler, K. (2010). Limitations of rapid myelin water quantification using 3D bSSFP. *MAGMA*, *23*(3), 139-151.

Levesque, I.R., Chia, C.L., & Pike, G.B. (2010). Reproducibility of in vivo magnetic resonance imaging-based measurement of myelin water. *J Magn Reson Imaging*, *32*(1), 60-68.

Liang, Z.P., & Lauterbur, P.C. (1999). *Principles of Magnetic Resonance Imaging. A Signal Processing Perspective.* Wiley-IEEE Press.

Lin, A.L., & Rothman, D.I. (2014). Review: what have novel imaging techniques revealed about metabolism in the aging brain? *Future Neurol*, *9*(3), 341-354.

Lindenberger, U., von Oertzen, T., Ghisletta, P., & Hertzog, C. (2011). Cross-sectional age variance extraction: What's change got to do with it?. *Psychol Aging*, *26*(1), 34-47.

Lu, P.H., Lee, G.J., Raven, E.P., Tingus K., Khoo T., Thompson P.M., & Bartzokis G. (2011). Age related slowing in cognitive processing speed is associated with myelin integrity in a very healthy elderly sample. *J Clin Exp Neuropsychol, 33*(10), 1059-1068.

Lu, P.H., Lee, G.J., Tishler, T.A., Meghpara, M., Thompson, P.M., & Bartzokis, G. (2013). Myelin breakdown mediates age-related slowing in cognitive processing speed in healthy elderly men. *Brain Cogn*, *81*, 131-138.

MacKay, A.L., Whittall, K., Adler, J., Li, D., Paty, D., & Graeb, D. (1994). In vivo visualization of myelin water in brain by magnetic resonance. *Mag Reson Med*, *31*(6), 673-677.

Mackey, A.P., Whitaker, K.J., & Bunge, S.A. (2012). Experience-dependent plasticity in white matter microstructure: reasoning training alters structural connectivity. *Front. Neuroanat*, *6*, 1-9.

Madden, D.J., Bennett, I.J., Burzynska, A., Potter, G.G., Chen, N.K., & Song, AW. (2012). Diffusion tensor imaging of cerebral white matter integrity in cognitive aging. *Biochim Biophys Acta*, *1822*(3), 386-400.

Madl, T., Chen, Ke., Montaldi, D., & Trappl, R. (2015). Computational cognitive models of spatial memory in navigation space: A review. *Neural Networks*, *65*,18-43.

Madler, B., Drabycz, S.A., Kolind, S.H., Whittal, K.P., & MacKay, A.L. (2008). Is diffusion anisotropy an accurate monitor of myelination? Correlation of multicomponent T2 relaxation and diffusion tensor anisotropy in human brain. *Mag Reson Imaging*, *26*(7), 874-888.

Makris, N., Kennedy, D.N., McInerney, S., Sorensen, A.G., Wang, R., Caviness, V.S. Jr., & Pandya, D.N. (2005). Segmentation of subcomponents within the superior longitudinal fascicle in humans: a quantitative, in vivo, DT-MRI study. *Cereb Cortex, 15*(6), 854-869.

Mallik, A., & Weir, A.I. (2005). Nerve conduction studies: Essential and pitfall in practice. *J Neurol Neurosurg Psychiatry, 76*(Suppl II), 23-31.

Marner, L., Nyengaard, J.R., Tang, Y., Pakkenberg, B. (2003). Marked loss of myelinated nerve fibers in the human brain with age. *J Comp Neurol*, *462*(2), 144-152.

Maxwell, S.E., & Cole, D.A. (2007). Bias in cross-sectional analyses of longitudinal mediation. *Psychological Methods, 12*(1), 23-44.

McArdle, J.J. (2009). Latent variable modeling of differences and changes with longitudinal data. *Annual Review of Psychology, 60,* 577-605.

McCreary, C.R., Bjarnason, T.A., Skihar, V., Mitchell, J.R., Yong, V.W., & Dunn, J.F. (2009). Multiexponential T2 and Magnetization Transfer MRI of demyelination and remyelination in murine spinal cord. *Neuroimage*, *45*(4), 1173-1182.

Meiboom, S., & Gill, D. (1958). Modified spin-echo method for measuring nuclear relaxation times. *Rev Sci Instr*, *29*, 688-691.

Meier-Ruge, A., Ulrich, J., Bruhlmann, M., Meier, E. (1992). Age-related white matter atrophy in the human brain. *Ann NY Acad Sci*, *673*, 260-269.

Meredith, W., & Teresi, J.A. (2006). An essay on measurement and factorial invariance. *Med. Care, 44*(1), S69-S77.

Meyers, S.M., Laule, C., Vavasour, I.M., Kolind, S.H., Madler, B., Tam, R., Traboulsee, A.L., Lee, J., Li, D.K., & MacKay, A.L. (2009). Reproducibility of myelin water fraction analysis: A comparison of region of interest and voxel-based analysis methods. *Magn Reson Imaging*, *27*(8), 1096-1103.

Meyers, S.M., Tam, R., Lee J.S., Kolind, S.H., Vavasour I.M., Mackie, E., Zhao Y., Laule, C., Madler, Burkhard., Li, D.K.B., MacKay, A.L., & Traboulsee, A.L. (2016). Does hydration status affect MRI measures of brain volume or water content? *J Magn Reson Imaging, 44*, 296-304.

Michielse, S., Coupland, N., Camicioli, R., Carter, R., Seres, P., Sabino, J., & Malykhin, N. (2010). Selective effects of aging on brain white matter microstructure: a diffusion tensor imaging tractography study. *Neuroimage*, *52*(4), 1190-1201.

Moseley, M. (2002). Diffusion tensor imaging and aging – A review. *NMR in Biomedicine*, *15*(7-8), 553-560.

Mozaffarian, D., Benjamin, E.J., Go, A.S., Arnett, D.K., Blaha, M.J., Cushman, M., de Ferranti, S., Despres. J.P., Fullerton, H.J., … Turner MB. (2015). American Heart Association Statistics Committee and Stroke Statistics Subcommittee. Heart disease and stroke statistics-2015 update: a report from the American Heart Association. *Circulation*, *131*, E29 322.

Mesulam, MM. (1990). Large-scale neurocognitive networks and distributed processing for attention, language, and memory. *Ann Neurol, 28*(5), 597-613.

Muller, R.O. (1996). Basic principles of structural equation modeling: An introduction to LISREL and EQS. Springer Verlag; New York.

Nesselroade, J.R., & Salthouse, T.A. (2004). Methodological and theoretical implications of intraindividual variability in perceptual-motor performance. *Journals of Gerontology-Series B Psychological Sciences and Social Sciences, 59*(2), 49-55.

Oakden, W., & Stanisz, G.J. (2014). Effects of diffusion on high-resolution quantitative T2 MRI. *NMR Biomedicine*, *27*(6), 672-680.

O'Reilly, R.C, & Frank, M.J. (2006). Making working memory work: A computational model of learning in the prefrontal cortex and basal ganglia. *Neural Computation*, 18, 283-328.

O'Sullivan, M., Summers, P.E., Jones, D.K., Jarosz, J.M., Williams, S.C.R., & Markus, H.S. (2001). Normal-appearing white matter in ischemic leukoaraiosis: A diffusion tensor MRI study. *Neurology*, *57*(12), 2307-2310.

Pachella, R.G. (1974). The interpretation of reaction time in information processing research. In BH Kantowitz (Ed.), *Human information processing: tutorial in performance and cognition.* Pp 41-82. Hillsdale, NJ: Lawrence Erlbaum.

Paus, T., & Toro, R. (2009). Could sex differences in white matter be explained by g ratio? *Front Neuroanaomy*, *3*, 107.

Perrin, J.S., Herve, P.Y., Leonard, G., Perron, M., Pike, G.B., Pitiot, A., Richer, L., Veillette, S., Pausova, Z., & Paus T. (2008). Role of Testosterone and Androgen Receptor. *Journal of Neuroscience, 28*(38), 9519-9524.

Pesaresi, M., Shiong-Soon, R., French, L., Kaplan, D.R., Miller, F.D., & Paus, T. (2015). Axon diameter and axonal transport: In vivo and in vitro effects of androgens. *Neuroimage*, *115*, 191-201.

Peters, A. (2002). The effects of normal aging on myelin and nerve fibers: A review. *J. Neurocytol*, *31*(8-9), 581-593.

Peters, A. (2009). The effects of normal aging on myelinated nerve fibers in monkey central nervous system. *Front Neuroant*, 3-11.

Poon, C.S., & Henkelman, R.M. (1992). Practical T2 quantitation for clinical applications. *J. Magn. Reson. Imag*, *2*, 541-553.

Prasloski, T., Madler, B., Xiang, Q.S., MacKay, A., & Jones, C. (2011). Applications of stimulated echo correction to multicomponent T2 analysis. *Magnetic Resonance in Medicine*, *67*(6), 1803-1814.

Radloff, L.S. (1977). The CES-D scale: A self report depression scale for research in the general population. *Appl Psychol Meas*, *1*(3), 385-401.

Rahnev, D., Nee, D.E., Riddle, J., Larson, A.S., & D'Esposito, M. (2016). Causal evidence for frontal cortex organization for perceptual decision making. *Proc Natl Acad Sci, 113,* 6059-6064.

Rao, S.M., St Aubin-Faubert, P., & Leo, G.J. (1989). Information processing speed in patients with multiple sclerosis. *Journal of Clinical and Experimental Neuropsychology*, *11*(4). 471-477.

Ratcliff, R. (1978). A theory of memory retrieval. *Psychological Review, 85*(2), 59-108.

Ratcliff, R. (2008). The EZ diffusion method: Too EZ? *Psychonomic Bulletin & Review*, *15*(6), 1218-1228.

Ratcliff, R., & Childers, R. (2015). Individual differences and fitting methods for the two-choice diffusion model of decision making. *Decision*, *2*(4), 237-279.

Ratcliff, R., & McKoon, G. (2008). The Diffusion Decision Model: Theory and Data for Two-Choice Decision Tasks. *Neural Computation*, *20*(4), 873-922.

Ratcliff, R., Thapar A., & McKoon G. (2006). Aging and individual differences in rapid two choice decisions. *Psychon Bull Rev, 13*(4), 626-635.

Raz N. Aging of the Brain and its Impact on Cognitive Performance: Integration of Structural and Functional Findings. In: Craik FIM, Salthouse TA, editors. The Handbook of Aging and Cognition. London: Lawrence Erlbaum. 2000.

Raz, N., Gunning-Dixon, F.M., Head, D., Dupuis, J.H., McQuain, J.M., Briggs, S.D., Thornton, A.E., Loken, W.J., & Acker, J.D. (1997). Selective aging of human cerebral cortex observed in vivo: Differential vulnerability of the prefrontal gray matter. *Cereb Cortex*, *7*(3), 268-282.

Raz, N., Gunning-Dixon. F.M., Head, D., Williamson, A., Rodrigue, K., & Acker, J.D. (2004). Aging, sexual dimorphism, and hemispheric asymmetry of the cerebral cortex: Replicability of regional differences in volume. *Neurobiol Aging*, *25*(3), 377-396.

Raz, N., Lindenberger, U., Rodrigue, KM., Kennedy, K.M., Head, D., Williamson, A., Dahle, C., Gerstorf, D., & Acker, J.D. (2005). Regional brain changes in aging healthy adults: general trends, individual differences and modifiers. *Cereb Cortex*, *15*(11), 1676-1689.

Raz, N., & Rodrigue, K.M. (2006). Differential aging of the brain: Patterns, cognitive correlates and modifiers. *Neurosci Biobehav Rev*, *30*(6), 730-748.

Riise, J., & Pakkenberg, B. (2011). Stereological estimation of the total number of myelinated callosal fibers in human subjects. *J Anat*, *218*, 277-284.

Robitaille, A., Piccinin, A.M., Muniz, G., Hoffman, L., Johansson, B., Deeg, D.J.H., Aartsen, M.J., Comijs, H.C., & Hofer, S.M. (2013). Longitudinal mediation of processing speed on age related change in memory and fluid intelligence. *Psychol Aging, 28*(4), 887-901.

Roitman, J.D., & Shadlen, M.N. (2002). Response of neurons in the lateral intraparietal area during a combined visual discrimination reaction time task. *J Neurosci, 22*(21), 9475-9489.

Ronczka, M., & Muller-Petke, M. (2012). Optimization of CPMG sequences to measure NMR transverse relaxation time T_2 in borehole applications. *Geosci, Instrum. Method. Data Syst, 1*, 197-208.

Rosseel, Yves. (2012). lavaan: An R Package for Structural Equation Modeling. *Journal of Statistical Software, 48*(2), 1-36. URL http://www.jstatsoft.org/v48/i02/.

Saab, A.S., Tzvetanova, I.D., & Nave, K.A. (2013). The role of myelin and oligodendrocytes in axonal energy metabolism. *Curr Opion Neurobiol*, *23*, 1065-1072.

Sandell, J.H., & Peters A. (2003). Disrupted myelin and axon loss in the anterior commisure of the aged rhesus monkey. *J Comp Neurol, 466*(1), 14-30.

Santyr, G.E. (1993). Magnetization transfer effects in multislice mr imaging. *Magn Reson Imaging*, *11*, 521-532.

Salat, D.H. (2014). Diffusion Tensor Imaging in the study of aging and age-associated neural disease. In: Johansen-Berg, H Behrens, TEJ, (Eds), Diffusion MRI: From Quantitative Measurement to in-vivo Neuroanatomy. pp. 257-281.

Salthouse, T.A. (1992). Influence of processing speed on adult age differences in working memory. *Acta Psychologica, 79*(2), 39-61.

Salthouse, T.A. (1993). Speed mediation of adult age differences in cognition. *Developmental Psychology, 29*(4), 722-738.

Salthouse, T.A. (1996). The processing speed theory of adult age differences in cognition. *Psychological Review, 103*(3), 403-428.

Salthouse, T.A. (1997). Adult age and the speed-accuracy trade-off. *Ergonomics, 22*(7), 811-821.

Salthouse, T.A. (2000). Aging and measures of processing speed. *Biological Psychology*, *54*, 35-54.

Salthouse, T.A., Schroeder, D.H., & Ferrer, E. (2004). Estimating retest effects in longitudinal assessments of cognitive functioning in adults between 18 and 60 years of age. *Dev Psychol, 40*(5), 813-822.

Sexton, C.E., Walhovd, K.B., Storsve, A.B., Tamnes, C.K., Westlye, L.T., Johansen-Berg, H., & Fjell, A.M. (2014). Accelerated changes in white matter microstructure during aging: A longitudinal diffusion tensor imaging study. *J Neurosci*, *34*(46), 15425-15436.

Sing-Manoux, A., & Kivimaki, M. (2010). The importance of cognitive ageing for understanding dementia, *Age, 32*(4), 509-512.

Sirrs, S.M., Laule, C., Madler, B., Brief, E.E., Tahir, S.A., Bishop, C., & MacKay, A. (2007). Normal appearing white matter in patients with phenylketonuria: Water content, myelin water fraction, and metabolite concentrations. *Radiology*, *242*(1), 236-243

Shen, J., & Palmeri, T.J. (2016). Modeling individual differences in visual categorization. *Visual Cognition*, *24*(3), 260-283.

Shim, Y.S., Yang, D.W., Roe, C.M., Coats, M.A., Benzinger, T.L., Xiong, C., Galvin, J.E., Cairns, N.J., & Morris, J.C. (2015). Pathological correlates of white matter hyperintensities on magnetic resonance imaging. *Dement Geriatr Cogn Disord*, *39*(1-2), 92-104.

Shrout, P.E., & Fleiss, J.L. (1979). Intraclass correlations: Uses in assessing rater reliability. *Psychol Bull*, *86*(2), 420-428.

Song, S.K., Sun, S.W., Ju, W.K., Lin, S.J., Cross, A.H., & Neufeld, A.H. (2003). Diffusion tensor imaging detects and differenciates axon and myelin degeneration in mouse optic nerve after retinal ischemia. *Neuroimage*, *20*(3), 1714-1722.

Sudmeier, J.L., Anderson S.E., & Frye JS. (1990). Calculation of nuclear spin relaxation times. *Concepts in Magnetic Resonance*, *2*, 197-212.

Tang, Y., Nyengaard, J.R., Pakkenberg, B., Gundersen, H.J.G. (1997). Age-induced white matter changes in the human brain: a stereological investigation. *Neurobiol. Aging*, *18*(6), 609-615.

Thapar, A., Ratcliff, R., & McKoon, G. (2003). A diffusion model analysis of the effects of aging on letter discrimination. *Psychology and Aging, 18*(3), 415-429.

Turken, A.U., Gabrieli, SW., Bammer R., Baldo J., Dronkers N.F., & Gabrieli, D.E. (2008). Cognitive processing speed and the structure of white matter pathways: Convergent evidence from normal variation and lesion studies. *Neuroimage, 42*(2), 1032-1044.

Vandekerckhove, J., & Tuerlinckx, F. (2008). Diffusion model analysis with MATLAB: A DMAT primer. *Behavior Research Methods*, *40*, 61-72.

Van Den Heuvel, D.M.J, Ten Dam, V.H., De Craen, A.J.M., Admiraal-Behloul, F., Olofsen, H., Bollen, E.L., Jolles, J., Murray, H.M., Blauw, G.J., Westendrop, R.G., & van Buchem, M.A. (2006). Increase in periventricular white matter hyperintensities parallels decline in mental processing speed in a non-demented elderly population. *Journal of Neurology, Neurosurgery and Psychiatry*, *77*(2), 149-153.

van Ravenzwaaij, D., Donkin, C., & Vandekerckhove, J. (2016). The EZ diffusion model provides a powerful test of simple empirical effects. *Psychon Bull Rev,* 1-10.

Vavasour, I.M., Clark, C.M., Li, D.K., & MacKay, A.L. (2006). Reproducibility and reliability of MR measurements in white matter. Clinical implications. *Neuroimage*, *32*(2), 637-642.

Vavasour, I.M., Whittall, K.P., Li, D.K., & MacKay, A.L. (2000). Different magnetization transfer effects exhibited by the short and long T2 components in human brain. *Magn Reson Med*, *44*(6),860-866.

Verhaeghen, P., & Salthouse, T.A. (1997). Meta-analyses of age-cognition relations in adulthood: Estimates of linear and nonlinear age effects and structural models. *Psychological Bulletin*, *122*(3), 231-249.

von Oertzen, T., Brandmaier, A.M., & Tsang, S. (2015). Structural Equation Modeling with **Ω**nyx. *Structural Equation Modeling: A Multidisciplinary Journal, 22*(1), 148-161.

Vos, S.B., Jones D.K., Jeurissen, B., Viergever, M.A., & Leemans, A. (2012). The influence of complex white matter architecture on the mean diffusivity in diffusion tensor MRI of the human brain. *Neuroimage, 59*(3), 2208-2216.

Wagenmakers, E.J., van der Maas, H.L.J, Grasman, R.P. (2007). An EZ-diffusion model for response time and accuracy. *Psychon Bull Rev, 14*(1), 3-22.

Wakana, S., Caprihan, A., Panzenboeck, M.M., Fallon, J.H., Perry, M., Gollub, R.L., Hua, K., Zhang, J., Jiang, H., Dubey, P., Blitz, A., van Zijl, P., & Mori, S. (2007). Reproducibility of quantitative tractography methods applied to cerebral white matter. *Neuroimage*, *36*(3), 630-644.

Waxman, S.G., & Bennett, M.V.L. (1972). Relative conduction velocities of small myelinated and non-myelinated fibres in the central nervous system. *Nature New Biol., 238*(85), 193-224.

Waxman, S.G. (1980). Determinants of conduction velocity in myelinated nerve fibers. *Muscle & Nerve, 3*(2), 141-150.

Webb, S., Munro, C.A., Midha, R., Stanisz, G.J. (2003). Is multicomponent T2 a good measure of myelin content in periphernal nerve? *Magn Reson Med*, *49*(4), 638-645.

Westlye, L.T., Walhovd, K.B., Dale, A.M., Bjornerud, A., Due-Tonnessen, P., Engvig, A., Grydeland, H., Tamnes, C.K., Ostby, Y., & Fjell, A.M. (2010). Life-span changes of the human brain white matter: diffusion tensor imaging (DTI) and volumetry. *Cereb Cortex*, *20*(9), 2055-2068.

Whittall, K.P. (1989). Quantitative interpretation of NMR relaxation data. *Journal of Magnetic Resonance*, *84*(1), 134-152.

Whittall, K.P., Bronskill, M.J., & Henkelman, R.M. (1991). Investigation of analysis techniques for complicated NMR relaxation data. *Journal of Magnetic Resonance*, *95*(2), 221-234.

Whittall, K.P., MacKay, A.L., Graeb, D.A., Nugent, R.A., Li, D.K., & Paty, D.W. (1997). In vivo measurements of T2 distributions and water contents in normal human brain. *Magn Reson Med*, *37*(1), 34-43.

Williams, K., & Kemper, S. (2010). Exploring interventions to reduce cognitive decline in aging. *J Psychosoc Neurs Mentl Health Serv, 48*(5), 42-51.

Xiong, Y.Y., & Mok, V. (2011). Age-related white matter changes. *J Aging Res,* 617927.

Yakovlev PI, Lecours AR. (1966). The myelogenetic cycles of regional maturation of the brain. In : Minkowski, A. (Ed.), Regional Development of the Brain Early in Life. Blackwell Scientific Publications Inc, Oxford, UK, pp. 3-70.

Yeatman, J.D., Wandell, B.A., & Mezer, A.A. (2014). Lifespan maturation and degeneration of human brain white matter. *Nat. Commun*, *5*, 4932.

Zalc, B., & Colman, D.R. (2000). Origins of vertebrate success. *Science*, *288*(5464), 271-272.

Zhang, Y., Brady, M., & Smith, S. (2001). Segmentation of brain MR images through a hidden Markov random field model and the expectation-maximization algorithm. *IEEE Trans Med Imaging*, *20*(1), 45-57.

Zhang, J., Kolind, S.H., Laule, C., & MacKay, A.L. (2015). Comparison of myelin water fraction from multiecho T2 decay curve and steady-state methods. *Magn Reson Med*, *73*(1), 223-232.

Zimprich, D., & Martin, M. (2002). Can longitudinal changes in processing speed explain longitudinal age changes in fluid intelligence? *Psychol Aging*, *17*(4), 690-695.

ABSTRACT

CHANGE IN PROCESSING SPEED AND ITS ASSOCIATIONS WITH CEREBERAL WHITE MATTER MICROSTRUCTURE

by

MUZAMIL ARSHAD

August 2017

Advisors: Dr. Naftali Raz, Dr. Jeffrey Stanley

Major: Translational Neuroscience

Degree: Doctor of Philosophy

The decline of cognition with age is one of the most feared aspects of aging, while the slowing of responses, or reduced processing speed, is one of the most reliable aspects of aging. Slowing of processing has been hypothesized to affect other domains of cognition as well. Despite the well-known slowing-age relationship and central position processing speed plays in theories of cognitive aging the neurobiological mechanisms which underpin slowing is unclear. If we could identify the biology associated with processing speed we could then attempt to develop interventions to mitigate the effects of age on those variables. In turn we could test whether "preventing" or reducing the decline of processing speed helps alleviate the decline in other cognitive domains. Not only would this provide basic knowledge about aging, cognition, and their relationship but it may also have a broader societal impact.

In this project, we tested whether the amount of myelin content, indexed by MWF, in white matter tracts hypothesized to be important for performing a choice reaction time task, could explain the variance in processing speed or in change of processing speed after controlling for age effects. While MWF did not explain any additional variance in our variables of interest we did found that the geom$T_{2\text{-IEW}}$, a measure thought to be related to axonal density, in the genu was negatively

associated with change in processing speed. These results suggest that axons maybe an important structure supporting processing speed and that future investigations should look at both myelin and axonal changes as potential substrates sub serving processing speed.

AUTOBIOGRAPHICAL STATEMENT

I have always been curious about how things work in the real world. My mom has told me that from a young age I would constantly ask why questions. This drive to understand the world led me to pursue an undergraduate degree in physics at Benedictine University. What could be better than studying mathematics and physics to understand the world we live in. However, in my studies as an undergraduate I became amazed by the complexity of biology and found it hard to believe that we could understand the subatomic world of quarks and the vastness of the universe but had relatively little understanding of biology. During my time as an undergraduate I also became interested in medicine and ultimately chose to pursue an MD/PhD.

As a graduate student in the MD/PhD program at Wayne State University I get to pursue my interest in both medicine and learn how to do science from my mentors. It has certainly been both exciting and stressful and I am grateful for this opportunity. As I look forward to the future I'm confident that I want a career in medicine and I hope to use the skills I have developed to address questions which I hope will improve the practice of medicine.

Publications relevant to the dissertation:

Arshad, M., Stanley J.A., Raz N. (2016). Adult age differences in subcortical myelin content are consistent with protracted myelination and unrelated to diffusion tensor imaging indices. *Neuroimage, 143*, 26-39.

Arshad, M., Stanley J.A., Raz N. (2017). Test-Retest reliability and concurrent validity of in vivo myelin content indices: Myelin water fraction and calibrated T1w/T2w image ratio. *Hum Brain Mapp, 38,* 1780-1790.